T-4028

Alloy Phase Analysis from Measurements of Bulk Electronic and Magnetic Properties

by

Kirk Arthur Lindahl

A thesis submitted to the Faculty and the Board of Trustees of the Colorado School of Mines in partial fulfillment of the requirements for the degree of Master of Science (Metallurgical and Materials Engineering).

Golden, Colorado

Date November 5, 1993

Signed: Kirk Arthur Lindahl

Kirk Arthur Lindahl

Approved: David L Olson

Dr. David L. Olson
Thesis Advisor

Golden, Colorado

Date November 5, 1993

Glen Edwards for JJM

Dr. John Moore
Department Head, Metallurgical and Materials Engineering

ABSTRACT

This research investigates whether measurements of bulk electronic and magnetic properties can be used to reveal the microstructure and phase stability of alloys. The ability to characterize alloy properties and phase stability through correlation with electronic measurements may allow significant improvements in the non-destructive evaluation of advanced alloy properties and the prediction of service life. There is a sound fundamental basis to expect that the electronic state of an alloy can be correlated to metallurgical properties. The metallurgical stability of intermetallic phases as well as some of the mechanical properties in certain alloys have been successfully predicted by correlating to electron concentration. In addition, bulk electronic and magnetic properties are also a result of the electron state. Therefore, measurements of these properties should correlate to the microstructure and phases present in metal alloys. Because the aluminum-copper alloy phase and microstructure has been thoroughly studied and documented, it was selected as a model system and an alloy of aluminum with 4 wt. pct. copper was used. The magnetic susceptibility was selected as the measured property, based on its known relationship to the electron concentration and the electronic nature of a metal. The magnetic susceptibility measurement exhibited three regions that correspond to the aluminum-copper alloy microstructure. The regions identified include: 1) metastable GP1 phase refinement, 2) formation of metastable GP2 and θ' phases, and 3) θ' phase refinement and θ phase formation. Based on these findings, it appears possible to non-destructively determine the microstructure and phase stability of an alloy by making electronic and magnetic measurements.

TABLE OF CONTENT

TABLE OF CONTENT (CONTINUED)

LIST OF FIGURES

LIST OF TABLES

ACKNOWLEDGMENTS

I want to express my sincere gratitude to my thesis advisor, Dr. David Olson, for his guidance on the project. I also want to thank the committee members, Dr. Brajendra Mishra, Dr. John Moore, Dr. John Trefny. Mr. Robert McGrew provided the guidance and instruction needed to produce the quality Transmission Electron Microscopy. I am grateful for the assistance of Mr. Steve Donelson in machining the samples needed for measurement. Mr. Alcides Raraz assisted with vacuum furnace operations for alloying the aluminum and copper.

It is a pleasure to acknowledge the assistance of Mr. Robert Cross at the National Institute of Standard and Technologies, who provided the equipment and materials needed to complete the magnetic susceptibility measurements. Mr. Cross provided training on equipment operations and insight on technique for obtaining accurate results.

The EG&G Rocky Flats Materials and Surface Technology department, managed by Ms. Wendy Sticka, provided financial support for this project in the form of tuition reimbursement. The cooperation and assistance of my coworkers, in particular the adjustment of work schedule to attend classes, has enabled me to earn this degree.

Gratitude is extended to my parents, Bruce and Dorothy, for instilling curiosity and the desire to learn from an early age. Finally, I would like to thank my wife, Diane, for her encouragement, and more importantly, her understanding of time spent pursuing this degree.

CHAPTER 1

INTRODUCTION

1.1 Objectives Of Research

The objective of this research is to determine whether bulk electronic and magnetic properties can be used to evaluate the microstructure and phase stability of an alloy. The ability to characterize alloy properties and phase stability through correlation with electronic measurements may allow significant improvements in the non-destructive evaluation of advanced alloy properties and the prediction of service life. For example, the aluminum industry would benefit from improved methods of phase determination to assure desired microstructure and resulting strength exists within the alloy [1].

The metallurgical stability of intermetallic phases as well as some of the mechanical properties in certain alloys have been successfully predicted by correlating to electron concentration. Hume-Rothery [2] has identified that intermetallic phases occur at specific electron to atom ratios and has called these phases electron compounds. Brewer [3-5] has established a relationship between electron concentration and the compositional range for a specific crystal structure or phase. Cho [6] connected many mechanical properties, including bulk modules, shear modulus, and Young's modules to the electron concentration and thus the Fermi energy.

There is a sound fundamental basis to expect that the electronic state of an alloy can be correlated to metallurgical properties [7-10]. For example, in a simple free electron gas theory, the isothermal bulk modules, B, can be expressed as:

$$B = \tfrac{2}{3} E_F n_e \tag{1}$$

where E_F is the Fermi energy and n_e is the carrier density, which for conductivity by electrons is equivalent to electron concentration. The Fermi Energy at 0 K, $E_F(0\text{ K})$, is also related to the electronic concentration by the following relationship.

$$E_F\,(0\text{ K}) = (\hbar^2/2m)(3\,\pi^2 n_e)^{2/3} \tag{2}$$

where $2\pi\,\hbar = h$, h is the Planck's constant, and m is the effective mass of the electron. These relationships imply that a change in the Fermi energy or electron concentration could effectively influence the mechanical properties of metals.

The concept of using calculated electron concentrations to predict, from known alloy composition, the susceptibility of an alloy to form topological close packed intermetallic phases has been developed and is named Phacomp. Phacomp involves a calculation of an electron number which is compared with a criteria value. Whether the electron number is greater or smaller than this criteria value allows prediction of phase stability. The Phacomp calculation method and the more recent improved New Phacomp method have been successfully used to evaluate the susceptibility of forming sigma phases in superalloys. These analytical techniques do suggest that the electronic state is important to the phase state of the alloy.

If the mechanical properties are fundamentally a function of electron concentration, and there has been success correlating calculated electronic states to mechanical properties and alloy phases, could the electron concentration be measured with advanced bulk electronic or magnetic methods? Can these measurements provide insight into the condition of the alloy, and its structural properties? In an attempt to non-destructively determine the properties of materials, electronic and magnetic measurements have been conducted on several alloy systems. The correlation between magnetic susceptibility and the precipitation of solute in heat-treatable aluminum alloys has been investigated [11]. Magnetic phase analysis has been used for alloys with no more than two phases, which have known and widely differing susceptibilities. One application is the measurement of the amounts of the body-centered cubic and face-centered cubic phases in iron-rich binary alloys at high temperatures [12]. Hall coefficient and electrical resistance measurements have been performed on alloys (Bismuth alloys, Fe-Co, Pd-Fe, Pb-Ni, Pd-Co) to investigate the dependence on structural modifications, composition, and temperature. [13-21]. Magnetic Barkhausen Noise signals have been used to characterize the microstructures in aged 17-4-PH stainless steel, and tempered 2.25Cr-1Mo bainitic steel [22, 23].

1.2 Scope Of Research

To evaluate the use of electronic and/or magnetic measurements requires the selection of an alloy system which has been thoroughly studied as to its phase stability. The binary aluminum-copper system, with its well investigated phase transitions during annealing, which include GP1, GP 2, θ', and θ phases, makes a model system for this investigation. The phase transitions go from pre-precipitation conditions with coherent interfaces to non-coherent precipitates. Samples of Aluminum - 4 wt. pct. Copper with varying microstructure were prepared through a series of designed thermal treatments, and fully characterized. Two practiced electronic and magnetic measurements, magnetic susceptibility and Hall coefficient, were examined to determine the physical nature of these measurements, their dependence on electron concentration, and a relationship to phase stability. Because of its known relationship to the electron concentration and the electronic nature of a metal, the magnetic susceptibility was selected as the measured property. Magnetic susceptibility measurements were made on the prepared samples, and results were compared with microstructural information. The magnetic susceptibility was found to correlate with various phase conditions. Based on the correlation, the magnetic susceptibility can assist with nondestructively measuring alloy phase stability or the service life of a precipitation strengthened alloy.

1.3 Thesis Organization

Chapter 2 presents the literature review conducted for this thesis. The relevant electronic physics describing the behavior of metals is developed so that the relationship between electron concentration and material properties is understood. To discern both magnetic susceptibility and Hall coefficient and the information each represents, a summary on the magnetism and Hall effect is presented. The details of the Al-Cu alloy system are also discussed.

Chapter 3 presents the experimental procedures used in preparing samples, measuring the magnetic susceptibility, and characterizing sample microstructure. Chapter 4 examines the correlation between magnetic susceptibility and alloy properties. Conclusions drawn from the investigation are presented in Chapter 5. The cited references and appendices are included at the end of the Thesis.

CHAPTER 2

LITERATURE REVIEW

2.1 Physics Of Metals

In the simplest view, atoms in metallic crystals are ionized and a metal is an assemblage of positive ions in a periodic lattice, immersed in a cloud of electrons. Metallic crystals are held together by the electrostatic attraction between the negative electrons and the positively charged ions. The electronic potential in the interior of the metal varies periodically as a result of the presence of the positive ions arranged on a space lattice. The motion of a conduction electron in this periodic potential is described by a system of waves. The use of wave mechanics to characterize the velocities that a wavelike electron can have as it moves around in a metal with a periodic potential has been classified as the *band theory of solids*. However, many of the important relationships can be derived by ignoring the periodic potential, and considering what is called the *free electron theory*.

The wavelength that describes the motion of the electron depends on the velocity of the electron according to the relation:

$$\lambda = 2\pi\hbar/mv \tag{3}$$

where $2\pi\hbar = h$, h is the Planck's constant, m is the effective mass of the electron, and v is its velocity.

A much used quantity in electron theories is the *wave number k*, which is the inverse wavelength multiplied by 2π. Thus,

$$k = 2\pi/\lambda = mv/\hbar \tag{4}$$

which shows that the wave number of a free electron is proportional to its momentum *mv*.

Since the kinetic energy of a free electron, E_k, with wave number k is

$$E_k = \frac{mv^2}{2} \tag{5}$$

it can be expressed as

$$E_k = (\hbar^2 2m)k^2 \tag{6}$$

in which form it is clear that the kinetic energy is proportional to k^2. In the free electron theory of solids, the relation between kinetic energy and wave number is parabolic, and the curve is symmetrical about $k = 0$ because electrons moving in opposite directions with the same velocity would have the same energy.

It is convenient to indicate both the magnitude and the direction of the momentum of an electron in a crystal by plotting a vector in **k** space. As suggested by equation 3, the **k** space is actually a reciprocal lattice space with symmetries determined by the symmetry of the unit cell in real space.

2.1.1 Fermi Surfaces

At 0 K, all electrons reside in the lowest possible energy states. By the Pauli exclusion principle, only two electrons can occupy any state, one with spin "up" and one with spin "down." As a consequence of this principle, at absolute zero the electrons fill all the states up to a certain maximum energy level and none have energies above this state. The level which divides the filled and vacant levels is known as the *Fermi level* at absolute zero and is denoted by $E_F(0)$. At higher temperatures some electrons are excited to higher energy levels. The energy level at which the probability of occupation by an electron is ½ is defined as the *Fermi level* E_F [24].

In the free electron theory, the Fermi level, expressed as an energy [25], is given by:

$$E_F = (\hbar^2/2m)(3\,\pi^2 n_e)^{2/3} \tag{7}$$

It is clear from this equation that the maximum energy of the electrons is a function of n_e, the number of electrons per unit volume or electron concentration, and not of the size or shape of the whole crystal. While this observation is made by considering the free electron case, it suggests a relation that should hold similar for electrons in a periodic potential

In **k** space, the **k** vectors of electrons that have energies at the Fermi level terminate upon a surface, the *Fermi surface*. At absolute zero this surface separates the occupied from the "empty" quantum states. At higher temperatures, even though there is a slight spread of vacant and occupied states near E_F, the Fermi surface still essentially provides all the electron states that can play any significant part in the properties of metals.

2.1.2 Brillouin Zones

The interaction of electrons with the periodic lattice of the solid will cause Bragg reflection to occur for electron waves in crystals. The Bragg reflection leads to an energy gap in the distribution of the conducting electron states.

Any electron will be reflected from a set of atomic planes in a crystal if Bragg's law, $n\lambda = 2d \sin\theta$, is satisfied. For an electron moving exactly along the x axis of a crystal, reflection from (100) planes, of spacing a, will occur when $n\lambda = 2a$, since $\theta = 90^0$. Since the wavelength of the electron is $\lambda = 2\pi/k$, the reflecting condition can be written $2\pi n = 2ak \cos(90 - \theta)$, which in vector notation can be rewritten as $\mathbf{k}\cdot\mathbf{x} = k_x = \pi n/a$.

In general for the three dimensional **k** space, any planes will reflect when k_d, the component normal to them, is given by:

$$k_d = n\pi/\mathrm{d} \tag{8}$$

where d is the spacing of the planes, and n is an integer that describes order of reflection. The energy gaps occur when the **k** vector ends on one of the planes normal to **k** and at distances $n\pi/d_{hkl}$ from the origin. The allowed ranges of the wave vector **k** are called *Brillouin zones*.

The wave equation describing the motion of electrons is known as the Schrödinger equation. Many periodic functions can be used to model the potential field that the lattice ions exert on the conducting electrons. For whatever potential function used to describe the ionic atoms arrangement, the solutions of the Schrödinger equation have the following characteristic. For certain ranges of energy, there exist traveling-wave-type solutions of the Schrödinger equation. These energy ranges, called *bands*, are separated by an energy gap in which no traveling wave can exist. That is, there may arise a substantial region of energy in which solutions of the wave equation do not exist.

2.1.3 Density of States

The interaction of the Fermi surface with the Brillouin zone boundaries is an important phenomenon in understanding the properties solids exhibit. A critical parameter in the interaction is the number of states available to an electron near a given energy, which is termed the *density of states*.

If the Fermi surface lies well within the Brillouin zone, the relationship between the energy E and the density of states $N(E)$ in the band is parabolic and is given by:

$$N(E) = m^{3/2}(E - E_o)^{1/2} / (2^{1/2}\pi^2\hbar^3) \qquad (9)$$

where E is the energy at the state of interest, and E_o is the energy of the lowest states in the band.

Contact between the Fermi surface and the Brillouin zone will correspond to a peak in the density of states as the Fermi surface first overlaps the boundary. The peak in the density of states results because any deviation from sphericity for a given volume increases the surface area. Following contact, the density of states rapidly decreases because the total area of the Fermi surface decreases as the corners of the zone are filled. For the energy states near the top of a band, the energy is measured down from the top of the band (E_{max}) to give an expression for the Density of States as:

$$N(E) = m^{3/2}(E_{max} - E)^{1/2} / (2^{1/2}\pi^2\hbar^3) \quad (10)$$

Since **k** space is a reciprocal lattice spacing, the shape of the Brillouin zone is determined by the crystal planes most widely spaced. Crystal structures with the widest spaced planes will have the smallest Brillouin zones. When the density of states decreases following contact between the Fermi surface and the Brillouin zone, it may become favorable for a crystal to transform to closer planes, smaller lattice spacing, which would enlarge the zones, and make more states available to electrons.

2.1.4 Alloy Phase Stability

To obtain the best properties and performance, the major alloy systems depend upon control of the solid-state phase equilibria. In certain cases, segregation can alter the phase equilibria and degrade the alloy, even without the appearance of a second phase. In other circumstances, the material may degrade because of an undesirable second phase.

Paradoxically, in other alloy systems, adequate performance is dependent on the type, concentration, morphology, and size distribution of second phase particles. The use of second phase in the form of precipitates is fundamental to the successful use of superalloys, aluminum alloys, chrolloys and stainless steels. The material composition, thermo-mechanical processing sequences and the service life of the alloy part will influence the nature of precipitation. The second phase formation and growth are a strong function of both time and temperature. Numerous different precipitates are involved in many of these alloys. Each precipitate appears at a given time and temperature, in a very characteristic state of development, as seen by the carbide precipitation in 2.25Cr-1Mo steel (Figure 2.1). Each characteristic state of precipitation produces a specific condition of alloy performance, with definite limits to the alloy's chemical, physical, and mechanical behavior. For most of the commercial alloys, special practices for mechanical working and heat treatment help produce the correct state of precipitation consistent with optimal mechanical and corrosion performance [26].

Empirical studies have shown that in many alloy systems the electron concentration is the important parameter that influences such factors as the extent of primary solid solubility, the presence or absence of a particular crystallographic structure, the range and stability of intermediate phases, the formation of long-period superlattices, trends in lattice spacings, the number of vacant sites in defect structures, the magnetic susceptibility, and many others [2]. The stability of electron phases, like the stability of the primary solid solutions, appears to be the consequence of interactions between the Fermi surface and the

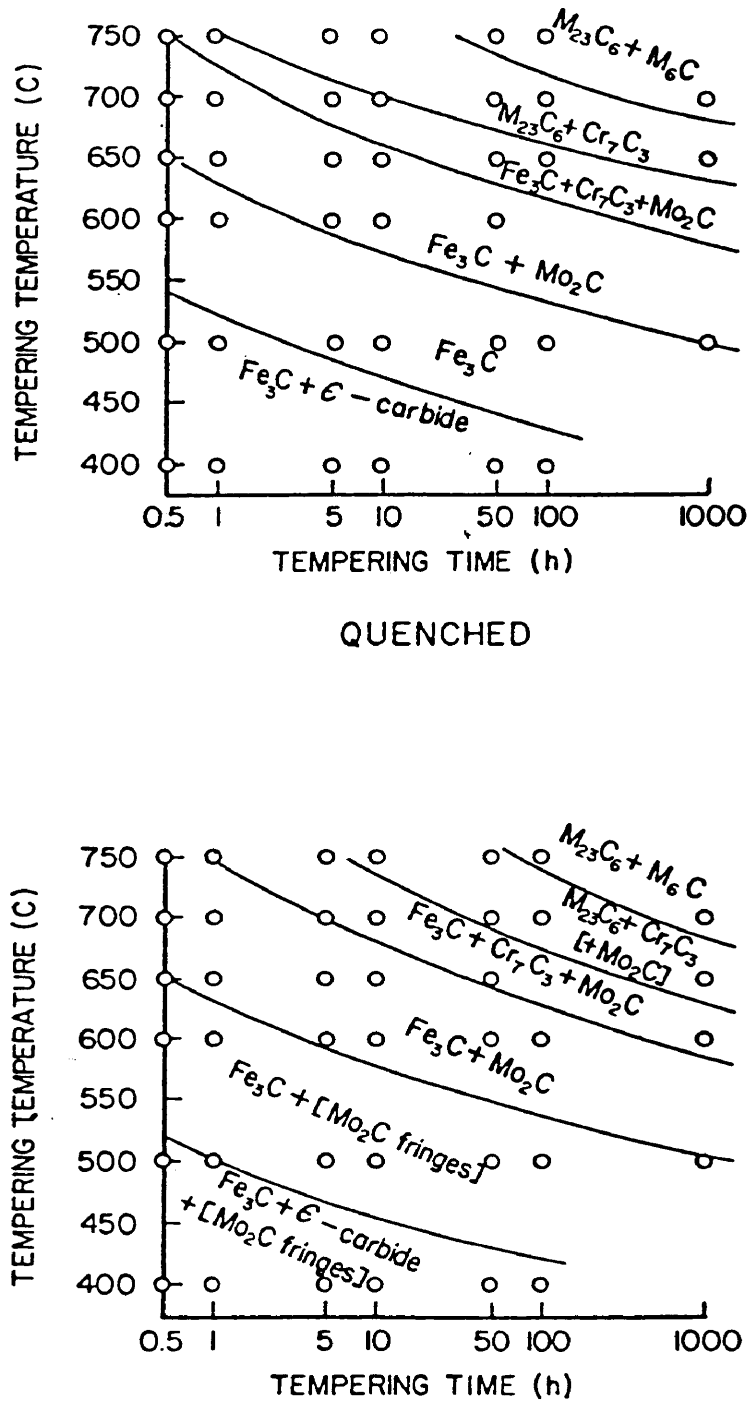

Figure 2.1: Baker-Nutting Diagram which shows time-temperature dependence of carbide stability for 2.25 Cr- 1 Mo steel a) quenched and tempered b) normalized and tempered [27].

Brillouin zones of these structures, with emphasis on the influence of such interactions upon the density of states N(E_F) at the Fermi surface. As the number of conduction electrons is varied by the alloying constituents of a different valence from that of the solute matrix, the relative positions of the Fermi surface and zone boundaries are altered. It is not certain whether or not, on alloying, all the valence electrons of a solute atom enter into the conduction band of the alloy, since some of them may fill in d-levels and produce more localized and directional electronic interactions in the metal.

It is apparent that there is an intimate connection between the electron concentration at which a new phase appears and the electron concentration at which the Fermi surface makes contact with the Brillouin zone boundary and a peak in the density of states. The general explanation of the association is that it is expensive energetically to add further electrons once the filled states contact the zone boundary. Additional electrons can be accommodated only in states above the energy gap characterizing the boundary or in the states near the corners of the first zone. The number of states near the corners falls off markedly as a function of energy. In this circumstance it is often energetically favorable for the crystal structure to change, the final structure being one which contains a larger Fermi surface. In this way the sequence α (1.36 e/a), β (1.48 e/a), γ (1.54 e/a), ε (1.69 e/a) is made plausible, where the numbers in parentheses refer to the electron concentration per atom at which contact between the Fermi level and the Brillouin zones occurs and the density of states is maximized.

2.2 Electronic Measurements

In an attempt to nondestructively determine the properties of materials, electronic and magnetic measurements have been conducted on several alloy systems. The correlation between magnetic susceptibility and the precipitation of solute in heat-treatable aluminum alloys has been investigated [11]. The Aluminum-Copper, Aluminum-Zinc, and Aluminum-Magnesium alloy systems were studied. For both the Aluminum-Copper and Aluminum-Magnesium alloy systems, varying solute compositions were measured in two extreme tempers, completely annealed and as-quenched. Measurements on the Aluminum-Zinc alloy were carried out at temperatures high enough to assure complete solid solution. This investigation compared the measured magnetic susceptibilities to calculated magnetic susceptibilities based on a mixture of components not alloyed, but simply mixed together in their pure states without producing a new phase. The data indicate that the difference between the magnetic susceptibility of a mixture of pure components and an alloy of the same bulk composition is equivalent to the Pauli paramagnetism of the aluminum metal associated with the alloy phases. The study calculated the number of aluminum atoms affected by solute such that their Pauli paramagnetism was not measured. The calculations supported the existence of short-range order in dilute solid solutions. In the quenched solid solutions, the solute atoms tend to avoid being nearest neighbors to an extent greater than that which would result from a purely random arrangement, supporting the Hume-Rothery prediction of short-range order. Calculation for the fully aged samples showed excellent agreement with predicted equilibrium phases. For example, in the alumimum-copper alloy, roughly two aluminum atoms were associated with each copper atom which corresponds to the predicted $CuAl_2$ phase.

Magnetic phase analysis has been used for the Iron-Carbon and Iron-Silicon systems [12, 28]. These alloy systems have ferromagnetic phases with established magnetic characteristics. A series of samples covering the composition range was annealed. The spontaneous magnetizations were measured for the annealed samples at a several temperatures. The overall sample magnetization is known to be the sum of the magnetization for individual phases times the respective fractions of these phases in the alloy. It is therefore possible to solve for the fraction each phase occupies in the total sample. For the Iron-Carbon system, these investigations were able to determine what composition of the alloy was precipitated as cementite (Fe_3C) and what fraction contained carbon in solid solution as ferrite. Analysis of the Iron-Silicon system was able to map the phases present across the phase diagram at various temperatures. The study was able to chart the change in weight fraction of α, α'', and η phases during annealing.

Hall coefficient measurements have been performed on Palladium-Iron alloys [17]. The dependence on temperature and concentration were investigated for alloys ranging from 0.5 to 99.5 at. pct. iron in the range of 2-300 K. The alloys provided a continuous series of disordered solid solutions. Alloys with less than 77 at. pct. iron have an face-centered cubic structure, and those with iron above 93 at. pct. have body-centered cubic structure. The changes in the crystal structure were found to alter the temperature dependence and the sign of the Hall coefficient.

The Hall effect and electrical resistance throughout the entire Iron-Cobalt alloy system has been investigated in a temperature range from liquid nitrogen to 800 K [14]. The composition dependence of Hall effect and resistivity was found to be analogous at all temperatures. Both values reached peaks at compositions with 10 and 80 at. pct. cobalt. The lowest values were found for alloys containing approximately the same amount of both components. These minimum values were apparently due to the formation of superstructure known to form in that compositional range.

Magnetic Barkhausen Noise (MBN) signals have been used to characterize the microstructures in aged 17-4-PH stainless steel, and tempered 2.25Cr-1Mo bainitic steel [22, 23]. This method of analysis tracks a signal generated by sweeping a ferromagnetic material through a magnetic hysteresis loop. A plot is obtained in which the X-axis denotes the scan between maximum magnetization field strength (80,000 A/m) and minimum magnetization field strength (full reversal of the maximum field), and the Y-axis denotes the variation in MBN rms voltage. The MBN signals are generated at the steep portion of the hysteresis loop. The peak height of the plot is taken as a parameter to assess the microstructure. In the aged 17-4-PH stainless steel material, the MBN plot was able to track the coherency strains associated with the copper precipitates that provide peak hardness, as well as the precipitation of austenite along the lath boundaries. In the tempered 2.25Cr-1Mo bainitic steel, the linearity in the plot showed that MBN peak height can be used as a nondestructive parameter for assessing the tempering process. The decrease in hardness with increase in tempering temperature was due to the removal of the internal quenching strains and the precipitation of carbides which corresponded to an increase in MBN peak heights.

This Literature Review presents two practiced electronic measurements, magnetic susceptibility and Hall coefficient. The physical nature of these measurements is examined and a relationship to phase stability is developed.

2.2.1 Magnetic Susceptibility

If a substance is placed in a magnetic field it becomes a source of a measurable magnetic field. The magnetic field within the substance will be either greater or smaller than the applied magnetic field. The different types of magnetic materials are usually classified on the basis of their permeability or susceptibility. The permeability is defined as

$$\mu = B/H \tag{11}$$

and the susceptibility is defined as

$$\chi = M/H \tag{12}$$

where H is the magnetic field, B is the magnetic induction, and M is the magnetization [29].

The magnetic induction, B, is the vector sum given by

$$B = \mu_0(H + M) \tag{13}$$

where μ_0 is the permeability of free space = $4\pi \times 10^{-7}$ in SI units.

Sometimes the relative permeability of a medium, μ_r, is used. It is given by

$$\mu_r = \mu / \mu_0 \tag{14}$$

The relative permeability is closely related to the susceptibility and the following equation is always true:

$$\mu_r = \chi + 1 \tag{15}$$

Magnetization of the material, M, is generally more interesting to the material scientist because it relates how a material responds to a magnetic field. Understanding the mechanisms behind the response provides information on the physical mechanics of the material. The various different types of magnetic materials are classified according to their bulk magnetic susceptibility, χ [30]. Table 2.1 lists the observed bulk susceptibility and relative permeability of several metals.

The first group of materials for which χ is small and negative are called diamagnetic, and their magnetic response opposes the applied magnetic field. Within a diamagnetic substance, a field opposite to the applied field is created, causing the internal field to be smaller.

TABLE 2.1

SUSCEPTIBILITIES AND PERMEABILITIES OF VARIOUS ELEMENTS

		χ (1/cc)	μ_r
Diamagnets	Bi	-1.21×10^{-6}	0.99983
	Be	-1.85×10^{-6}	0.99998
	Ag	-2.02×10^{-6}	0.99997
	Au	-2.74×10^{-6}	0.99996
	Ge	-0.56×10^{-6}	0.99999
	Cu	-0.77×10^{-6}	0.99999
Paramagnets	β-Sn	0.19×10^{-6}	1.00000
	K	0.47×10^{-6}	1.00001
	Na	0.68×10^{-6}	1.00001
	Al	1.65×10^{-6}	1.00002
	W	6.18×10^{-6}	1.00008
	Pt	21.04×10^{-6}	1.00026
	Mn	66.10×10^{-6}	1.00083

If the internal field is greater, the substance is creating a magnetic field parallel to the applied magnetic field. When the magnetic field acts individually upon atoms, with no mutual interaction between them, the effect will exist only when the external magnetic field is present, and is termed paramagnetic.

The most widely recognized magnetic materials are termed ferromagnetic. Like paramagnetic solids, the magnetic field is strengthened within the substance. In a ferromagnetic substance, the magnetic moments of adjacent atoms orient themselves mutually parallel with the aid of an external magnetic field, and a magnetic order is established. As a result, ferromagnetic behavior is much stronger than paramagnetic, and permanent magnetism of the substance can result.

The magnetic properties of metals are the result of the metallic electrons which belong to the crystal as a whole, and the localized electrons on each particular ion. For a metallic specimen like an Al- 4 wt. pct. Cu alloy, the measured bulk magnetic susceptibility will be the sum of three separate contributions; orbital diamagnetism from the ion, diamagnetism, and Pauli paramagnetism from the conducting electrons [31].

2.2.1.1 Orbital Diamagnetism

All electrons below the Fermi level give rise to an orbital diamagnetism. The physical origin of diamagnetism can be seen from the classical picture of an atom as electronic charges circulating around the nucleus in definite orbits. An electric charge in a

ARTHUR LAKES LIBRARY
COLORADO SCHOOL OF MINES
GOLDEN, CO 80401

closed loop motion is known to generate a magnetic moment given by

$$\mu_m = iA \tag{16}$$

where i is the current and A is the area of the loop. For an electron in orbital motion

$$\mu_m = eA/\tau \tag{17}$$

where e is the charge on the electron and τ is the orbital period. For a circular orbital area $A=\pi r^2$ and $\tau=2\pi r/v$, where v is the instantaneous tangential velocity of the electron and r is the radius of the orbit. The magnetic moment obtained as a result of the orbital motion of an electron is then

$$\mu_m = \frac{evr}{2} \tag{18}$$

In the absence of a magnetic field the orbital moments of paired electrons within an atom will cancel. An applied magnetic field $\boldsymbol{H}$ will accelerate or decelerate the orbital motion of the electron and thereby contribute to a change in the orbital magnetic moment. The action of a magnetic field causes changes in the velocity of electrons in the atom in such a way that the induced moment opposes the field producing it. The susceptibility resulting from the magnetic field effect on the orbital electrons is given by

$$\chi = -\left(\frac{N_o \rho}{W_a}\right)\frac{(\mu_o Z e^2 r^2)}{6m} \tag{19}$$

where N_o is Avogadro's number, ρ is the density, W_a is the relative atomic mass, Z is the number of outer electrons with orbit of radius r, and m is the effective mass of an electron.

As shown by this equation, it is the electrons with large orbital radius that contribute the most to orbital diamagnetism.

2.2.1.2 Conducting Electron Diamagnetism

The magnetic susceptibilities of metals are affected by the fact that the outermost electrons are at the Fermi level and are partially freed in the solid. Calculation of the susceptibilities of the metals must therefore take account of the behavior of these electrons in the Fermi distribution. The free electrons of a metal make both diamagnetic and paramagnetic contributions to the susceptibilities, but since the paramagnetic behavior is larger, the net contribution of the free electrons is paramagnetic.

The external magnetic field effects the motion of the valence electrons and produces a diamagnetic behavior. The field produces a force on the moving electrons, causing them to move in spiral paths between collisions, rather than in straight lines. The effect is diamagnetic, and in the free electron theory, the magnitude is about 1/3 the magnitude of the Pauli paramagnetism. The quantity cannot be calculated with any accuracy in real metals, and cannot be experimentally separated from other contribution to the magnetic susceptibility.

One of the most powerful techniques for studying the electronic structure of pure metals is the de Haas van Alphen effect, which measures the oscillatory energy absorption of a metal as the magnetic field is varied [32]. Since the energy of the metal is raised by application of a magnetic field, conservation of energy requires the energy gain by the metal to be absorbed from the magnetic field. The diamagnetism resulting from the conducting electrons counteracts the energy increase. As these conducting electrons are at the Fermi level, information on the Fermi surface can be obtained. The period of oscillatory variation in the magnetic susceptibility is inversely proportional to the maximum area of the Fermi surface. The de Haas van Alphen effect does not depend on the magnitude of χ, only on the frequency and amplitude of the oscillations with magnetic field.

2.2.1.3 Pauli Paramagnetism

The electron possesses a spin defined by the spin quantum number s which has the values $\pm\frac{1}{2}$. If an electron is visualized as a rotating electric charge, it is equivalent to a circular current flow so that an electron always possesses a magnetic moment. The magnitude of this atomic magnetic moment, $\boldsymbol{\mu}_{spin}$, is found experimentally to be

$$\mu_{\text{spin}} = \frac{|e|}{m} \hbar s \tag{20}$$

In the absence of a magnetic field, a metal has a complete balance of electron spins, and the spin has no effect upon the energy.

In a magnetic field, H, the occupation of spin states is altered. An electron parallel to the field, $s = +\frac{1}{2}$, has its energy lowered by $\mu_{\text{spin}}\mu_o H$. An electron with spin anti-parallel, $s = -\frac{1}{2}$, increases in energy by the same amount. If the electron were isolated it would simply align itself parallel with the field. In a Fermi gas however almost all the electrons are in states where the opposite spin state is already occupied. The electrons near the Fermi level occupy a closely spaced set of energy levels, and $\mu_{\text{spin}}H$ is generally larger than the spacing of the energy levels. Those electrons of antiparallel spin within $2\mu_{spin}\mu_o H$ of the Fermi level can lower their total energy by reversing their spin and occupying an unfilled energy level with spins parallel to the field. When the Fermi energy of the parallel spin balances that of the anti-parallel spin, there is a net imbalance in the spins. After the field is applied and the electrons transfer, more electrons exist with spin parallel, and they create a net magnetization parallel to the field. The closer the spacing of the energy levels at the Fermi level (higher density of states) the more electrons will reverse their *s*, and the higher the paramagnetic susceptibility.

The macroscopic magnetization, *M,* is given as a product of the number of electrons which change their spin direction and twice the spin magnetic moment. This factor of 2 arises because each electron which transfers from one distribution to the other contributes twice its magnetic moment to the total magnetic moment of the system. Thus

$$M = (number\ of\ transferred\ electrons) \times 2\mu_{spin} \tag{21}$$

The total number of electrons which change their direction is equal to the density of states in one of the spin distributions times the change in energy,

$$Transferred\ electrons = N_{+}(E_F)\mu_{spin}\mu_o H \tag{22}$$

where $N_{+}(E_F)$ designates the density of states in the spin-up distribution at the Fermi level, which is one-half the total density of states. The final expression for the total paramagnetic magnetization is

$$M = N(E_F)\mu_{spin}^2\mu_o H \tag{23}$$

The magnetization is thus proportional to the external magnetic field, and so the susceptibility is proportional to the density of states times the square of the spin magnetic moment for the electrons.

Based on this expression, the paramagnetic susceptibility of the free electrons in a metal is then temperature-independent. However, an increase in temperature can have two effects on the paramagnetic susceptibility. First, electrons at the Fermi level are thermally excited to higher energy states so that the application of a magnetic field allows more electrons to reverse their spin since they can now occupy the levels vacated by the thermally excited electrons. This effect tends to increase the paramagnetic susceptibility. Secondly, the thermal energy tends to disorient those electron that have been aligned by the magnetic field and tends to decrease the susceptibility. The two effects approximately cancel in the noble and alkali metals so that the Pauli paramagnetism is approximately temperature-independent. In most of the non-magnetic transition metals, one effect dominates and the Pauli paramagnetism either increases or decreases slightly with temperature.

For most metals including aluminum, the Pauli paramagnetism is larger than both diamagnetic effects and the magnetic susceptibility is slightly positive. In metals, the magnetism is based on the paramagnetism of the free electrons which are free to move throughout space occupied by the metal. As explained previously, these electrons also provide a bonding mechanism for the metal as a whole. Therefore, a correlation between magnetism and bonding or phase stability should exist.

Not all metals are paramagnetic. Although the density of states at the Fermi level is normal, which makes paramagnetic behavior of its valence electron quite normal, Copper is diamagnetic. Copper comes at the end of the first long transition period, and it has a newly filled $3d$ shell. Since the radius of the d shell is large, the diamagnetic effect of each of these $3d$ electrons is large. The $3d$ state contains 10 electrons, and so the total diamagnetic behavior is large. These two factors - large orbit of $3d$ electrons and large number of $3d$ electrons - make the diamagnetism of the closed shells of Copper larger than the paramagnetism of the free $4s$ electron. Copper is thus weakly diamagnetic [29].

2.2.2 Hall Effect

When a conductor is placed in a magnetic field perpendicular to the direction of current flow, a voltage is developed across the specimen in the direction perpendicular to both the current and the magnetic field. The voltage is called the Hall voltage [33, 34]. It is developed because the moving charges making up the current are forced to one side by the magnetic field. The charges accumulate on a face of the specimen until the electric field associated with the accumulated charge is large enough to cancel the force exerted by the magnetic field.

The Hall potential V_H is generally given as:

$$V_H = R_0 IH/t \tag{24}$$

where t is the thickness of the sample, I the current flowing in the +x-direction, H the magnetic field in the +z-direction, V_H the potential measured in the +y-direction, and R_0 a constant of the metal called the Hall coefficient. R_0 is negative when conduction is by electrons moving in the -x-direction, and is positive when conduction is by "holes" moving the +x-direction. Table 2.2 lists the room temperature Hall coefficient of some common metals.

The interpretation of the Hall potential is divided into its two component parts, the ordinary Hall effect present in all metals and the anomalous Hall effect present only in ferromagnetic metals. When considering the ordinary Hall coefficient, the free electron theory yields a rather simple temperature-independent result for R_0 [25, 35].

$$R_0 = \frac{1}{n_0 e N_0} = \frac{1}{Ne} \tag{25}$$

where N_0 is the number of atoms per cm^3, n_0 is the number of current-carrying electrons per atom, and e is the charge on the electron. The Hall constant is negative for free electrons and the carrier concentration $N = n_0 N_0$ is the electron concentration. Measurements of R_0 for copper, silver, gold, lithium and sodium give values of n_0 between 0.75 and 1.5 and for Al a value of $n_0 = 3$ [35]. Measurements of R_0 for copper, silver, gold, lithium and sodium give values of n_0 between 0.75 and 1.5 and for Al a value of $n_0 = 3$ [35].

As the Hall measurements are primarily influenced by the electron concentration of the metallic matrix, the Hall coefficient should characterize the state of the metal matrix. As stated previously by equation 6, the electron concentration determines the Fermi level,

TABLE 2.2

ROOM TEMPERATURE VALUES OF THE HALL COEFFICIENT

Metal	R_o 10^{-11} m^3/A sec	Current Carriers per Atom (sign = carrier charge)
Li	-17.0	-0.8
Na	-24.5	-1.0
K	-42.0	-1.2
Cu	-6.0	-1.3
Al	-4.0	-2.6
Be	+24.4	+0.2
Zn	+3.3	+2.9
Ag	-8.4	-1.3
Au	-7.2	-1.5
Mg	-11.3	-1.4
Mn	+8.4	+0.9
Sn	-0.5	-40.0
W	+11.3	+0.8
Fe	+2.5	+3.0
Ni	-5.6	-1.2
Zr	+13.7	+1.1
Cr	+36.3	+0.2
Mo	+18.0	+0.5

which has been shown to influence the properties of the alloy. Comparing equation 6 with equation 11 reveals:

$$E_F \propto \frac{1}{R_0^{2/3}} \tag{26}$$

so that the Hall coefficient should be a measurement of Fermi level and therefore will be related to material properties.

2.2.3 Magnetic Phase Analysis

The nucleation and growth processes of precipitation involve the mass transport of specific elements which are responding to a chemical potential gradient. Formation of second phase will alter the composition of the matrix material [36] (at least at locations adjacent to the precipitates), change the chemical potential of the various species in the matrix, and cause changes in the electron concentration and Fermi energy level. These changes in electron concentration and Fermi energy are due to the transport of electrons as required to maintain the electron chemical potential equal between the matrix and precipitating phase. A change in the density of states will result as the Fermi level moves closer or further from the Brillouin zones. This change in the density of states should affect the Pauli paramagnetism of the alloy and therefore the bulk magnetic susceptibility. In addition, the change in electron concentration should alter the Hall coefficient of the alloy. Thus, second phase formation results in changes in the electrical and magnetic properties which could be monitored in part by magnetic susceptibility and Hall coefficient measurements.

2.3 Aluminum-Copper Alloy System

The first heat-treatable aluminum alloy was based on the Aluminum-Copper system, and wrought aluminum alloys having copper as the main alloying element are designated as 2XXX alloys using the four-digit numerical system developed by the Aluminum Association [36]. Copper is one of the most important alloying elements for aluminum because it provides solid-solution strengthening. Since the copper atom has a diameter about 11 pct. less than the aluminum atom, the cubic lattice parameter between copper and aluminum is less than that of the aluminum matrix. Therefore, the matrix is strained tetragonally. These strained sites impede dislocation movement, and cause an increase in hardening and a decrease in ductility.

In addition, suitable heat treatments of aluminum-copper alloys cause precipitate formation that produce increased strength. The maximum solid solubility of copper in aluminum is 5.65 wt. pct. at the eutectic temperature of 548 C. The solubility of copper in aluminum decreases rapidly with decreasing temperature from 5.65 wt. pct. to less than 0.1 wt. pct. at room temperature. The change in solid solubility with temperature is a primary factor in the heat treatment of aluminum-copper alloys. The thermal treatments are designed to alter the mode of occurrence or morphology of the soluble copper alloying elements. Mechanical and physical properties depend not only on whether the solute is in or out of solution but also on specific atomic arrangements, as well as on size and dispersion of any precipitated phases. In precipitation-strengthened aluminum-copper alloys, five structures can be identified: (1) supersaturated solid solution α, (2) GP1 zones, (3) GP2 zones (also called θ" phase), (4) θ', and (5) θ phase, $CuAl_2$. Not all of these phases occur from every heat treatment [36].

2.3.1 Solution Heat Treatment

As shown by Figure 2.2, regardless of the initial structure, holding a 4.0 wt. pct. Cu alloy at approximately 495 C to 570 C until equilibrium is attained causes the copper to go completely into solid solution. Holding an Al-Cu alloy in this range is generally known as "solution heat treating" [38]. If the temperature of a 4.0 wt. pct. Cu alloy is then reduced to below 495 C, the solid solution becomes supersaturated and there is a tendency for the excess solute no longer soluble to precipitate. The driving force for precipitation increases with the degree of supersaturation and, consequently, with decreasing temperature. But the precipitation rate also depends on the atom mobility, which is reduced as temperature decreases.

2.3.2 Quenching

The solid solution formed at a high temperature may be retained in a supersaturated state by rapidly cooling to some lower temperature usually near room temperature. The objective of quenching is to avoid precipitation in the intermediate temperature range, where high rates of diffusion and precipitation take place. The most important effect on mechanical properties of the aluminum-copper alloys occurs after this cooling or quenching operation. The rate of cooling from the solution treatment temperature has a

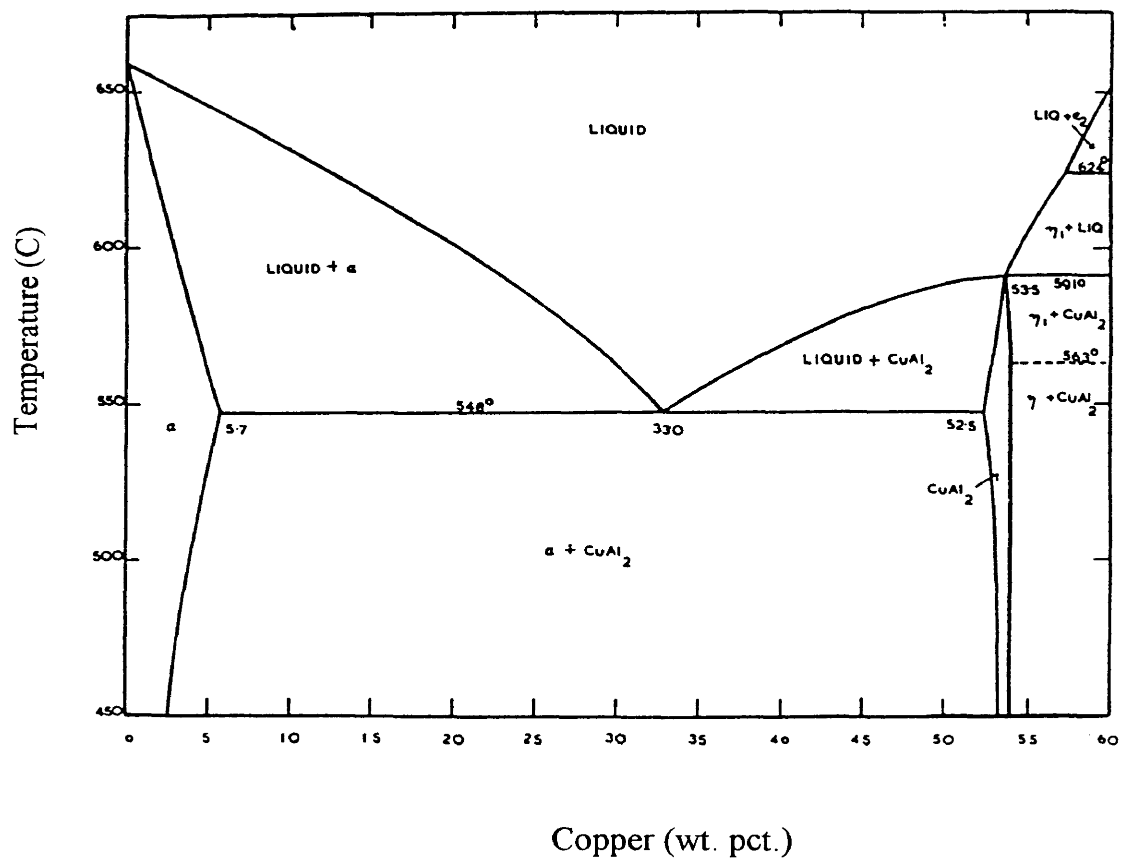

Figure 2.2: Aluminum-Copper Equilibrium Phase Diagram showing the solid solubility of copper in aluminum is 5.65 wt. pct. at the eutectic temperature of 548 C

pronounced effect on corrosion behavior and mechanical properties of the precipitation-hardenable aluminum alloys. The effects of precipitation during the quench on properties have been investigated by considering kinetics of precipitation. A method which accurately predicts the type of corrosion attack or themechanical properties from the cooling curve has been developed [39].

The precipitation can be controlled more precisely at the lower temperatures that follow the quench. The formation of precipitates requires diffusion of copper to enable nucleation and growth. Diffusion of the substitutional copper, as well as aluminum self-diffusion, is believed to occur primarily by a vacancy exchange mechanism. An atom can diffuse by moving into a vacant lattice position, leaving behind a new vacant lattice site. This mechanism of diffusion is energetically favorable to the diffusion that occurs by two atoms changing places. In addition, the substitutional copper atom is close in size to the aluminum atom so that interstitial diffusion does not happen. Therefore, the increased low-temperature solute mobility required for the high rate of precipitate formation is explained by a nonequilibrium high vacancy concentration at the low temperature. The equilibrium concentration of vacancies in aluminum increases with increasing temperature. Quenching not only retains solute copper atoms in solution, but maintains a certain minimum number of vacant lattice sites to promote the low-temperature diffusion required for precipitation nucleation and growth.

In aluminum-copper alloys, the nucleation of a new phase is greatly influenced by the existence of discontinuities in the lattice. The precipitate will strain the surrounding solid-solution matrix, and there is a driving force to minimize this lattice strain energy. Therefore, nucleation is heterogeneous and takes place preferentially at locations of greater disorder and higher energy than the solid-solution matrix. As a result, grain boundaries are preferred sites for nucleation of precipitates. Dislocations formed by condensation of vacancies or by introduction of plastic strain are also very active nucleation sites for precipitation. Variations in dislocation density resulting from different quenching rates and the degree of vacancy and solute retention achieved during the quench are factors in determining the effects of quenching rates on strengthening. The most rapid quenching rates establish conditions for more uniform precipitation throughout the alloy. More uniform precipitation provides a maximum number of strengthening units which is the most effective strengthening condition [40].

2.3.3 Aging

Most aluminum alloys exhibit property changes at room temperature after quenching. This process of change is called "natural aging," and is the result of precipitate strengthening. It may start immediately after quenching, or after an induction period. The rates vary from one aluminum alloy to another over a wide range, so that the approach to a stable condition may require only a few days or several years. In some alloys, sufficient precipitation to yield stable products with properties adequate for many application occurs in a few days at room temperature. Historically, magnesium has been added to Al-Cu alloys to improve natural aging characteristics [41].

Atomic and crystallographic structural changes occur in supersaturated solid solutions during precipitation. These changes involve a complex sequence of time-dependent and temperature-dependent steps. At relatively low temperatures and during initial periods of artificial aging at moderately elevated temperatures, the principal change is a redistribution of copper atoms within the solid-solution lattice to form clusters or zones (Guinier-Preston zones). These zones are considerably enriched in solute. This local segregation of solute atoms produces a distortion of the lattice planes, both within the zones and extending for several atom layers in the matrix. With an increase in number or density of zones, the amount of disturbance to the regularity and periodicity of the lattice increases. This increased irregularity interferes with the motion of dislocations through the lattice. Strengthening occurs by the inability of dislocations to move through the matrix to cause plastic strain.

During natural aging of Al-Cu alloys, the dissociation of the supersaturated solid solution begins by coherent precipitation of copper-rich zones only a few atoms thick (40 to 60 nm). These precipitates are two dimensional discs and are named Guinier-Preston 1 (GP1) zones. The GP1 zones form clusters on the {100} cubic planes of the aluminum solid solution matrix and are usually 300-500 nm in diameter. They stress the aluminum lattice, and because of their great number, form a dense network which impedes the movement of dislocations during deformation. The zone size does not change with aging time, but the number increases until in the average distance between zones is about 1,000 nm [37].

The effects of precipitation on mechanical properties are greatly accelerated and accentuated by reheating the quenched material to about 100 to 200°C. As aging temperatures or time are increased, the zones are either converted into or replaced by particles having a crystal structure distinct from that of the solid solution and also different from the structure of the equilibrium phase. These particles are referred to as transition precipitates. They have a specific crystallographic orientation relationship with the solid solution, such that the two phases remain coherent on certain planes by adaptation of the matrix through local elastic strain. Slowing the movement of dislocations, the lattice strains and precipitate particles create a strengthening effect. The operation of heating above room temperature to grow precipitant is called "artificial aging" or precipitation heat treating [42].

GP1 zones go back into solution in a short time at 150-200°C. This "reversion" leads to a temporary reduction in hardness, and suggests that the arrangement of the strengthening atoms, after artificial aging, is basically different from that after natural aging. Artificial aging causes new enrichment of copper atoms in Guinier-Preston 2 (GP2) zones soon after the end of the reversion. GP2 zones are sometimes referred to as θ''.

As in the case of GP1 zones, GP2 zones have a tetragonal structure and are coherent with the {100} matrix planes. The GP2 zones range in size from 100 to 400 nm thick and 1,000 to 10,000 nm in diameter. Although these precipitates are only a few atom layers in thickness, they are considered three-dimensional and have an ordered atomic arrangement.

The increase in strength continues indefinitely at room temperature, although the rate of change may be extremely slow after months or years. Aging at elevated temperatures is characterized by a different behavior, in which strength and hardness increase to a maximum and subsequently decrease. Maximum hardness and strength occur when the amount of GP2 is essentially maximum. The softening effects, observed as more complete precipitation occurs during extended isothermal aging at elevated temperatures, are referred to as "overaging" [40].

Overaging is characterized by a reduction in the hardness, tensile strength, and elongation. Softening results from changes in both type and size of the precipitated particles, and from dilution of solid solution.

As the artificial aging continues at approximately 150^{0}C, the formation of a metastable phase, θ', takes place. θ' forms after the GP2 but coexists with it over a range of time and temperature. θ' has the same composition as the equilibrium phase θ ($CuAl_2$), but has a different crystal lattice and exhibits coherency with the solid solution lattice. θ' is fully coherent with the matrix along the broad faces, and the {001} planes and <001> directions of the θ' are parallel to the {001} planes and <001> direction of the matrix. This phase nucleates heterogeneously, especially on dislocations that can act to relieve the misfit associated with the precipitate. Deformation prior to aging can accelerate the formation of θ' at the expense of the GP zones. The size of the θ' phase depends on the time and temperature of aging, and ranges from 1,000 to 60,000 nm or more in diameter with a thickness of 1,000 to 1,500 nm [38].

As the amount of θ' increases, particle growth eventually decreases the coherency strains. This loss in coherency, together with the simultaneous decrease in GP2, causes overaging. Figure 2.3 shows lattice arrangements that represent the transition from coherent to partially coherent to incoherent precipitates.

Aging at temperatures of about 190^{0}C or above for extensive times will produce the equilibrium incoherent θ phase, $CuAl_2$. This phase has a body-centered tetragonal structure. θ can form from θ' or directly from the matrix, and is present when the alloy is in a highly overaged condition. This softest, lowest-strength condition of the heat treatable alloys has the maximum amount of solute precipitated as relatively large particles, leaving the solid solution as dilute as possible.

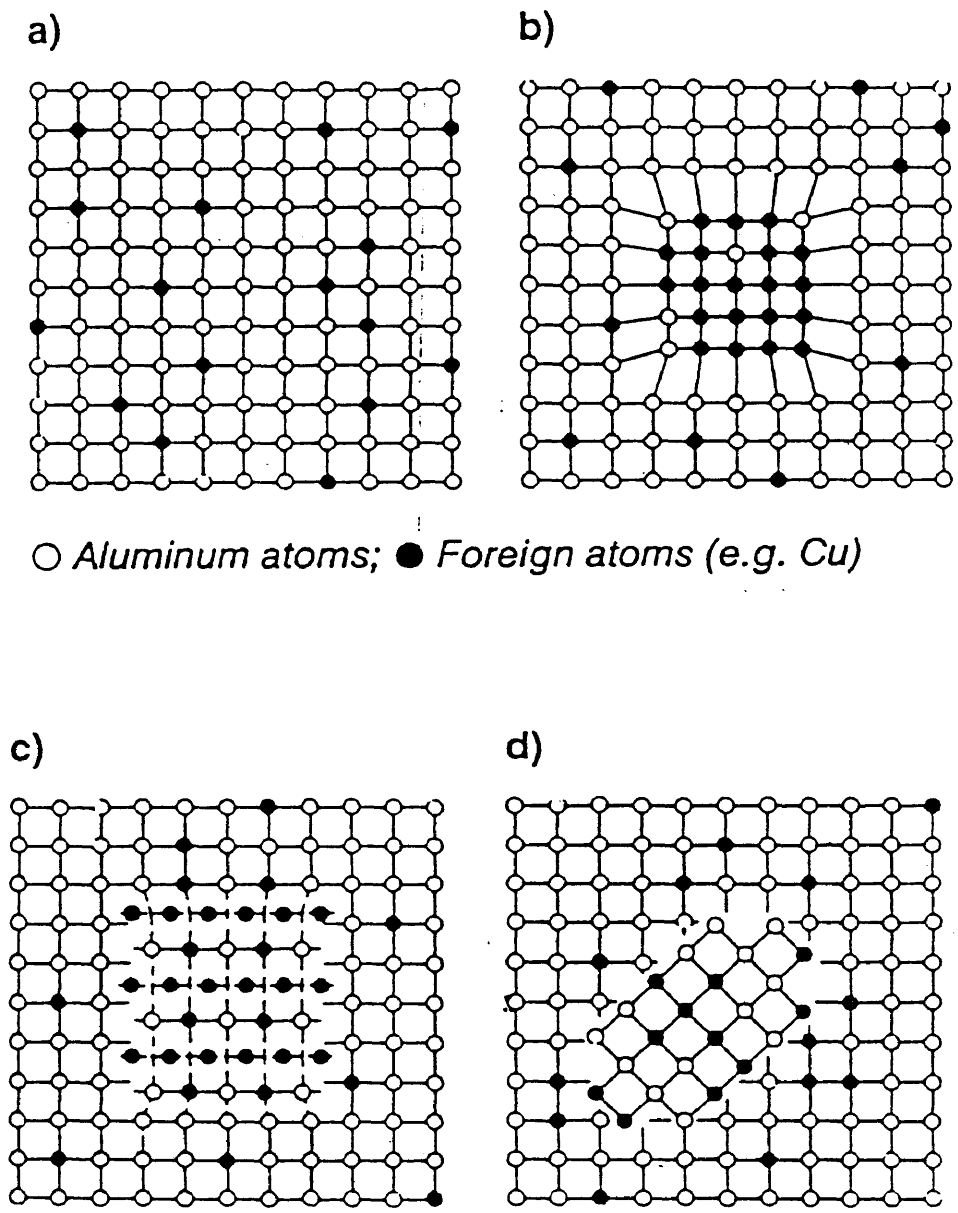

Figure 2.3: Schematic representation of (a) a solid solution with a random distribution of foreign atoms; (b) coherent precipitation; (c) a partially coherent intermediate phase in a solid solution. The vertical crystal planes are coherent, the horizontal planes incoherent; (d) an incoherent precipitate [40].

CHAPTER 3

EXPERIMENTAL PROCEDURES

3.1 Sample Preparation

Selection of an alloy system with a thoroughly studied phase stability is required to evaluate the use of electronic and/or magnetic measurements. The binary aluminum - copper system, with its phase transitions during annealing from GP1 to GP 2 to θ' to θ phase, was chosen for this investigation. These phase transitions range from pre-precipitates with coherent interfaces to incoherent stable precipitates.

A 2 kilogram ingot of 99.999 wt. pct. aluminum and 500 grams of 99.9 wt. pct. copper shot, 1 to 10 mm in diameter, were procured from the Johnson Matthey Chemical Company. Two 750 milliliter conical crucibles, two crucible covers, and one 750 milliliter rectangular back-up tray, all fabricated of alumina, were procured from Ceramicon Designs Ltd.

The aluminum ingot was cut into pieces, and 940.0 grams of aluminum along with 37.6 grams copper were charged in a alumina crucible to produce an aluminum alloy with 4 wt. pct. copper. The crucible was covered with a lid, set in the rectangular tray, and placed in the vacuum furnace. The furnace was programmed and the metal was melted according to the parameters shown in Appendix A, Figure A-1. Using a band saw, the produced ingot was then cut and the pieces mixed and place in the second conical crucible. The alloy was remelted in the vacuum furnace in the sequence indicated in Appendix A, Figure A-2.

From the resulting ingot, rectangular prisms were cut with dimensions of approximately 10 mm x 10 mm x 70 mm. Eight of these prisms were then turned on a lathe to produce 5 mm cylinders. The cylinders were cut to 10 mm lengths resulting in 32 samples being prepared.

3.2 Sample Matrix

To achieve a θ phase in a reasonable aging time, artificial aging at 200 C was selected. Using the 32 samples to cover the range of microstructures and precipitates anticipated, a matrix of aging times was developed. Samples were prepared according to the heat treatment outlined in Table 3.1.

3.3 Magnetic Susceptibility Measurement

The magnetic susceptibility measurements were performed on a Quantum Design Magnetic Property Measurement System (MPMS) at the National Institute of Standards and Technologies (NIST), Boulder, Colorado. The MPMS is a modular integration of a superconducting quantum interference device (SQUID) detection system and a precision temperature control unit residing in the bore of a superconducting magnet. The system is controlled by a computer.

The SQUID detection allows measurement of the magnetic response of a material. The SQUID consists of a superconducting ring with a small insulating layer which serves as a 'weak link', and is known as a Josephson junction [30]. The magnetic flux passing through the ring is quantized once the ring has gone superconducting but the weak link

TABLE 3.1

SAMPLE MATRIX

Sample Number	Solutionizing Temperature (C)	Solutionizing Time (hrs)	Quench Media	Aging Temperature (C)	Aging Time (hrs)
1	520	5	Water	200	2
2	520	5	Water	200	4
3	520	5	Water	200	6
4	520	5	Water	200	8
5	520	5	Water	200	10
6	520	5	Water	200	12
7	520	5	Water	200	14
8	520	5	Water	200	16
9	520	5	Water	200	18
10	520	5	Water	200	20
11	520	5	Water	200	22
12	520	5	Water	200	24
13	520	5	Water	200	28
14	520	5	Water	200	32
15	520	5	Water	200	36
16	520	5	Water	200	40
17	520	5	Water	200	44
18	520	5	Water	200	48
19	520	5	Water	200	56
20	520	5	Water	200	64
21	520	5	Water	200	72
22	520	5	Water	200	84
23	520	5	Water	200	96
24	520	5	Water	200	132
25	520	5	Water	200	168
26	520	5	Water	200	240
27	520	5	Water	200	360
28	520	5	Water	200	720
29	520	5	Water	200	1,080
30	520	5	Water	200	1,440
31	520	5	Water	200	1,800
32	520	5	Water	200	2,160

enables the flux trapped in the ring to change by discrete amounts. In the MPMS, the SQUID is placed in the superconducting magnet which is held at a constant and stable field. The material of interest is raised and lowered through the center of the SQUID ring. In response to the superconducting magnet, the material of interest is a source of a magnetic field. The magnetic field of a material will change the supercurrent of the SQUID when the material passes through the SQUID. The device can thereby be used to measure very small magnetic responses in materials in the field of the external superconducting magnet.

Measuring each sample was accomplished by following a set sequence. First, a sample was mounted to the sample rod. The rod was placed into the clamping fixture of the slide seal assembly. The airlock of the assembly was purged, a valve was opened, and the sample was lowered into the cryogenic sample chamber. Figure 3.1 shows a picture of the measuring apparatus.

Once the sample was lowered into the chamber, the sample rod was adjusted so that the sample was centered in the SQUID during the 40 mm scan length. The needed adjustment was given by running an initial measurement scan and viewing the SQUID Response Plot. The peak of the Response Plot should fall at 20 mm, which was the center of the scan length. The sample rod was raised or lowered as necessary to center the sample.

The computer was programmed to make the magnetic moment measurement. The sequence control applied magnetic fields of 6,000, 7,000, 8,000, 9,000, and 10,000 Oersteds (Oe) at 300 K. At each discrete field, the sample was raised and lowered

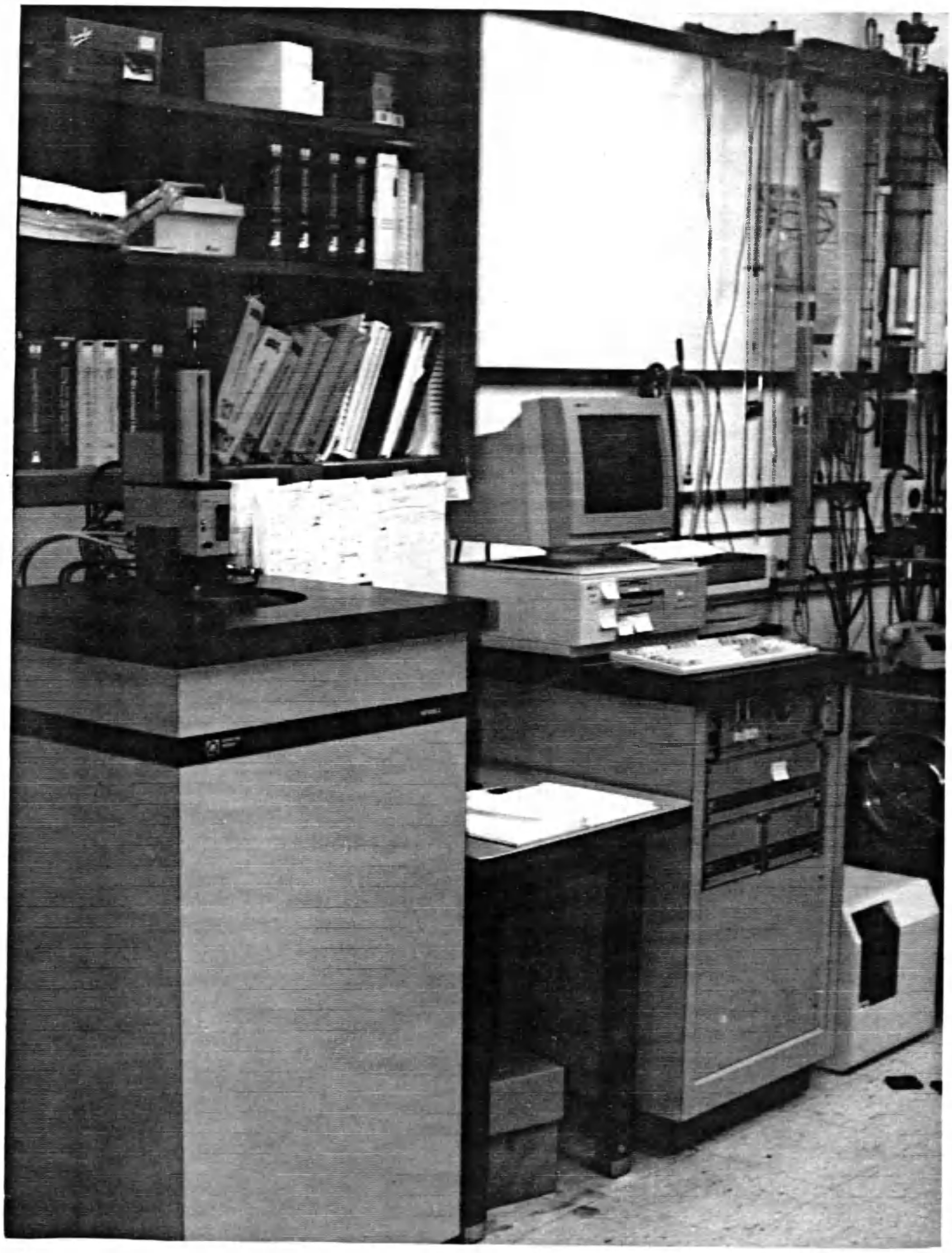

Figure 3.1: Picture of the Quantum Design Magnetic Property Measurement System at the National Institute of Standards and Technologies, Boulder, Colorado.

through the SQUID three times. The magnetic moment induced in the sample was measured in electromagnetic units (emu) and the average for the three scans was reported. Dividing the moment by the sample volume produced the magnetization (emu/cc). As expressed by equation 11, the magnetic susceptibility for each sample was given by the slope of the best fit line through the magnetization versus field data for each sample. Appendix B contains the experimental data, and Table 4.1 presents the experimentally determined magnetic susceptibility of each sample.

3.4 Analytical Techniques

To determine the copper content, each sample was analyzed on a TN Technologies Inc. alloy analyzer. Containing radioactive isotopes of iron and cadmium, the analyzer uses x-ray fluorescence to determine alloy composition. Four scans were run on different locations of each sample, and the composition was averaged. Results of these measurements have been included in Table 4.1. As shown by the results, a random variation of composition was detected (2.9 wt. pct. to 6.0 wt. pct. Cu).

To relate the mechanical properties to the magnetic susceptibility, hardness measurements were made according to the American Society for Testing and Materials (ASTM) Standard E 18-89a [43, Appendix C]. Because of the sample size and hardness, the Rockwell superficial hardness T scale was used. A minimum of five measurements were made and averaged, and the result for each sample is presented in Table 4.1.

The microstructure of several samples was examined using a transmission electron microscope (TEM). Foils for use in the microscope were prepared from the selected samples. First four disks, approximately 0.5 mm thick, were cut from the cylindrical sample using a diamond blade cutoff wheel. These disks were then thinned by hand on 320 and 600 grit sand paper to approximately 0.225 mm thick. To match the TEM sample holder, 3 mm diameter disks were then punched from the center of each disk. Using 600 grit sand paper, these disks were then thinned to 0.095 to 0.125 mm thick. Finally, the foils were electrochemically thinned to approximately 10,000 nm in a 25 pct. nitric acid in methanol etchant at -30 C. Micrographs are presented in Chapter 4.

CHAPTER 4

DISCUSSION OF RESULTS

As discussed in Chapter 3, the magnetic susceptibility, hardness, and copper concentration of each sample was measured. Table 4.1 reports all the properties gathered for each sample, and the corresponding sample number and artificial aging time at 473 K.

To investigate the correlation between magnetic susceptibility, artificial aging time and the resulting phase formation, graphic analysis was completed with the values in Table 4.1. Figure 4.1 presents the magnetic susceptibility as a function of log(aging time in hours). Scatter of the data is present, but generally, the magnetic susceptibility was found to increase with time.

The increase in magnetic susceptibility with aging time for the aluminum-copper system agrees with the predictions presented in the literature which states the copper atoms will mask the Pauli paramagnetism of the aluminum atoms associated with each copper atom [11]. The increase in magnetic susceptibility with aging time reflects an increase in the weight fraction of free aluminum, aluminum not associated with copper, which occurs as the solid solution decomposes to form phases. Every atom of dissolved copper which forms a new phase appears to lose magnetic influence over its solid solution nearest-neighbor aluminum atoms, and gain influence over those aluminum atoms associated with the phase. In the short range order of the solid solution, the copper atom will associate with twelve aluminum atoms. The number twelve is the number of nearest neighbors a copper atom would have when substituted into the face-centered cubic

TABLE 4.1

SUMMARY OF MEASURED PROPERTIES

Sample Number	Art. Aging Time (hrs @ 473 K)	Log Aging Time log(hours)	Mag. Susceptibility (10^{-6} 1/cc @ 300 K)	Hardness Rockwell 15T	wt. pct. Copper
1	2	0.301	1.051	47.2	4.15
2	4	0.602	1.026	47.9	4.88
3	6	0.778	1.041	49.2	4.96
4	8	0.903	1.042	51.8	4.30
5	10	1.000	1.038	53.7	4.51
6	12	1.079	1.074	53.5	4.35
7	14	1.146	1.079	54.8	4.43
8	16	1.204	1.138	58.2	3.71
9	18	1.255	1.158	57.6	3.34
10	20	1.301	1.162	57.6	3.32
11	22	1.342	1.128	58.8	4.07
12	24	1.380	1.140	59.3	4.05
13	28	1.447	1.177	63.2	2.87
14	32	1.505	1.141	60.2	3.28
15	36	1.556	1.156	62.8	3.42
16	40	1.602	1.150	65.4	5.19
17	44	1.644	1.173	64.1	3.38
18	48	1.581	1.115	57.6	5.96
19	56	1.748	1.193	59.6	4.01
20	64	1.806	1.226	61.7	4.07
21	72	1.857	1.203	60.2	4.41
22	84	1.924	1.231	63.3	4.22
23	96	1.982	1.263	59.6	3.50
24	132	2.121	1.260	58.6	2.89
25	168	2.225	1.206	58.5	4.92
26	241	2.382	1.172	54.8	5.51
27	480	2.681	1.245	59.3	4.39
28	744	2.872	1.277	56.1	3.72
29	1,080	3.033	1.242	53.8	3.53
30	1,536	3.186	1.261	52.6	4.36
31	1,824	3.261	1.224	51.2	4.62
32	2,184	3.339	1.234	50.5	4.05

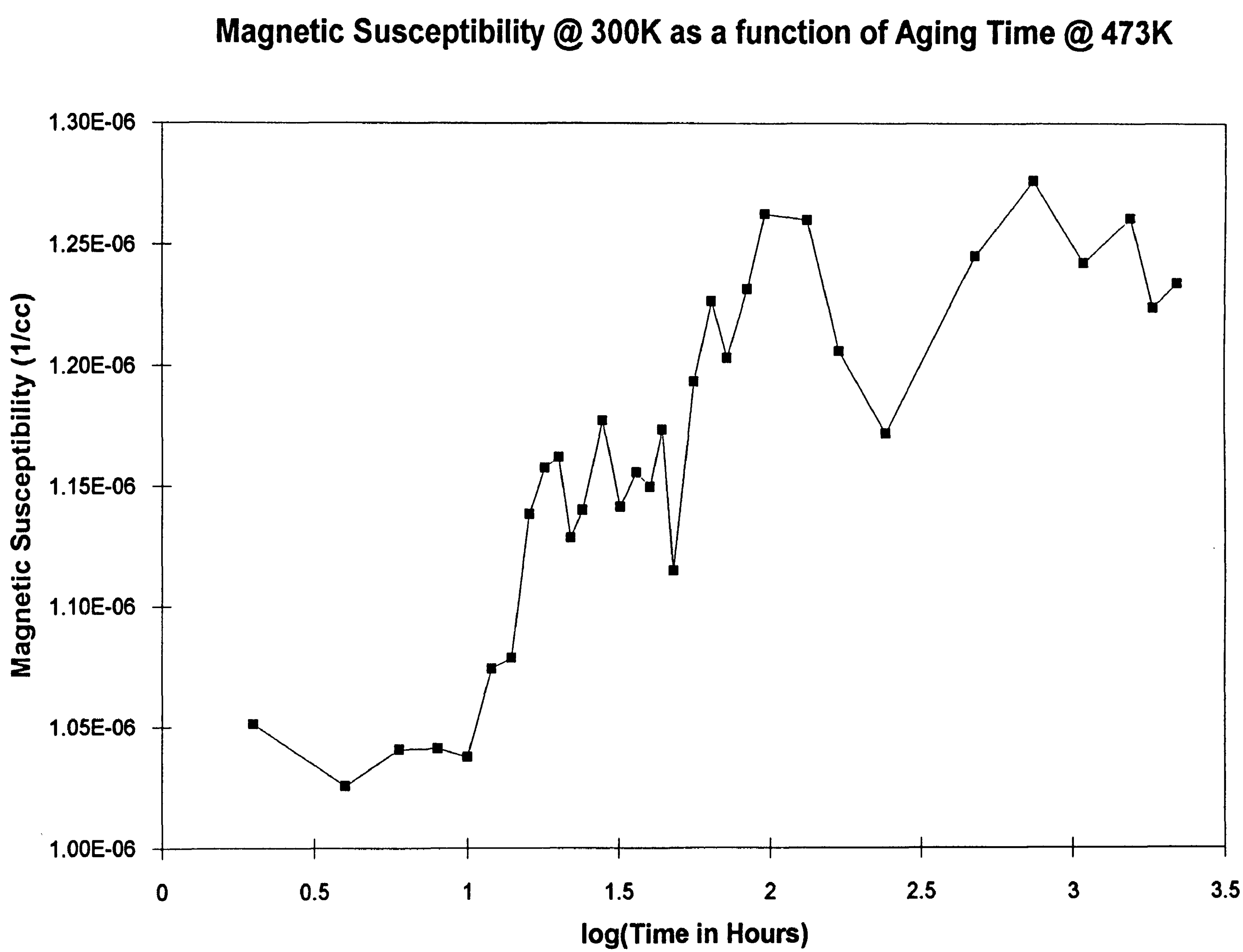

Figure 4.1: Plot showing the relationship between magnetic susceptibility @ 300K and log(aging time @473K).

lattice of aluminum. In the θ phase ($CuAl_2$) that occurs after extended artificial aging, copper atoms will associate with only two aluminum atoms. This transition, which occurs with aging, allows ten addition aluminum atoms to contribute fully to the magnetic response of the bulk alloy, resulting in the increase in magnetic susceptibility with aging time.

The scatter of Figure 4.1 is attributed to varying composition. This fact was discovered by subdividing the data to look at smaller deviations in copper concentration. Figure 4.2 presents the magnetic susceptibility as a function of log(aging time in hours) for the samples with copper concentrations between 4.0 wt. pct. and 4.4 wt. pct.. Three regions are observed in Figure 4.2. Figures 4.3 to 4.5 display the same information for samples with copper concentrations between 4.4 to 4.8 wt. pct., 4.8 to 5.2 wt. pct., and 3.8 to 4.2 wt. pct. respectively. Although data are not available at enough aging times to produce a full curve for each copper concentration range, each figure shows data in agreement with Figure 4.2, that three regions exist. For discussion in this thesis, the regions have been numbered sequentially 1, 2, and 3, starting with the region containing the samples of lowest aging times. The majority of samples fall into Region 2.

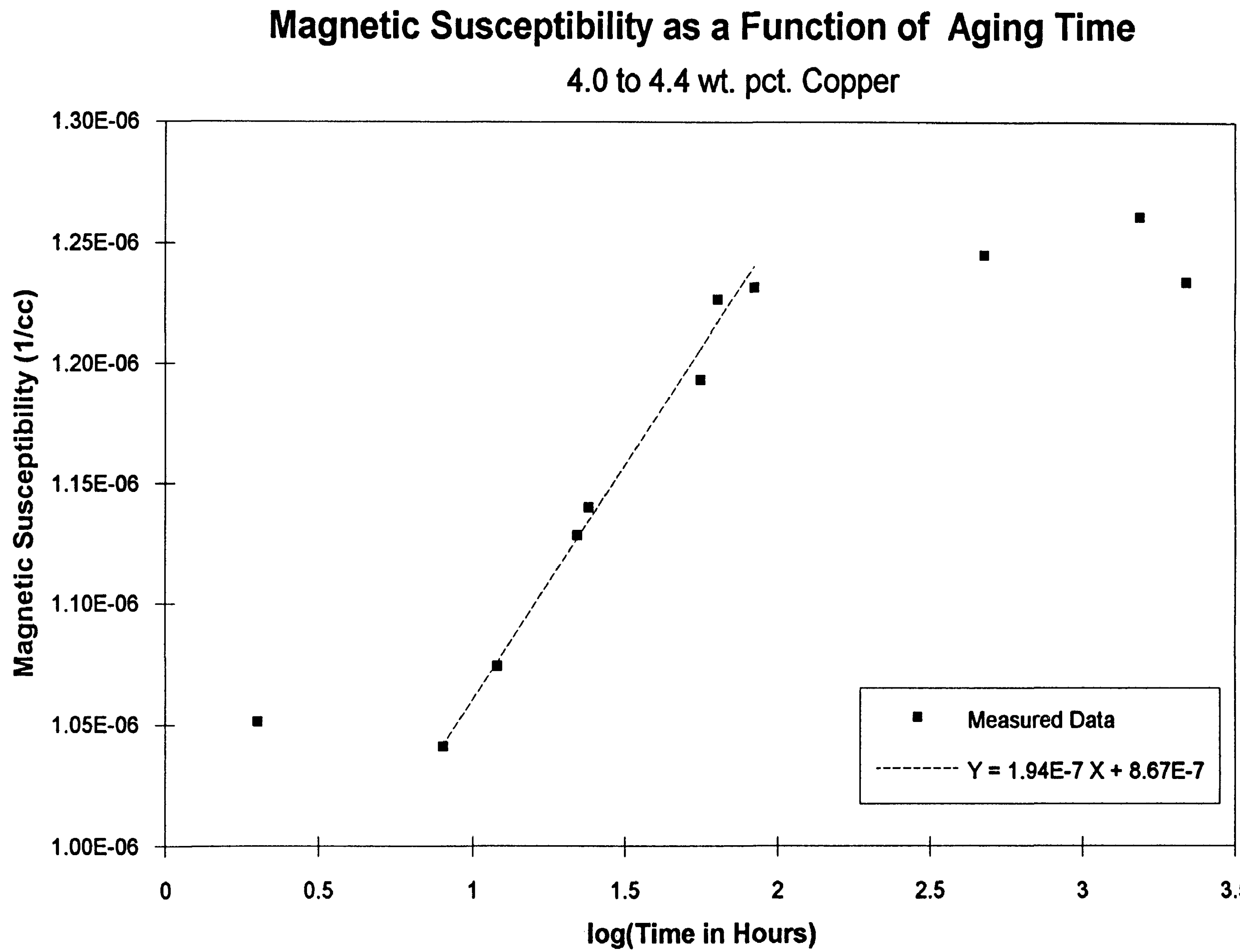

Figure 4.2: Magnetic susceptibility at 300K as a function of log(aging time at 473K) for samples with Copper between 4.0 and 4.4 wt pct.

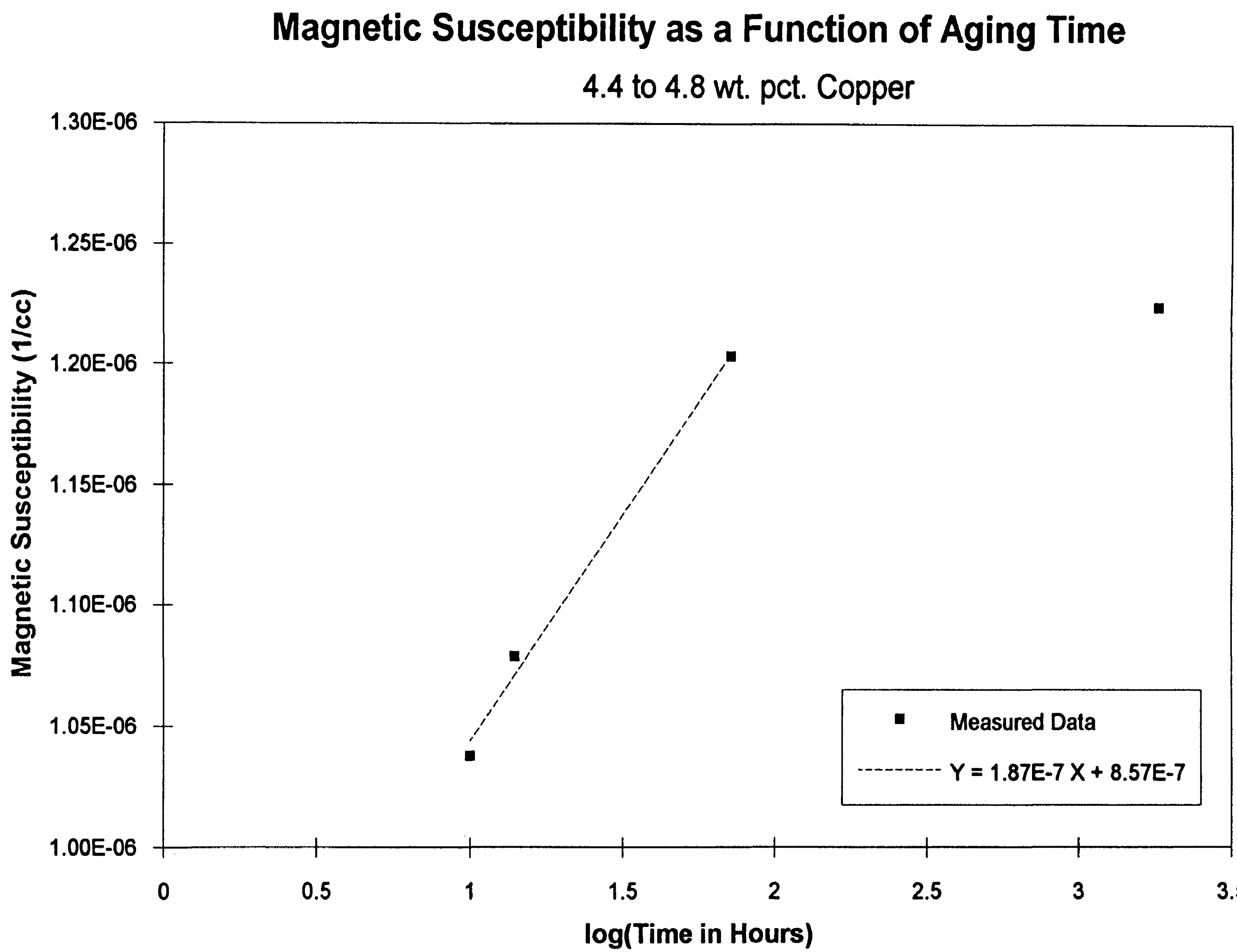

Figure 4.3: Magnetic susceptibility at 300K as a function of log(aging time at 473K) for samples with Copper between 4.4 and 4.8 wt. pct.

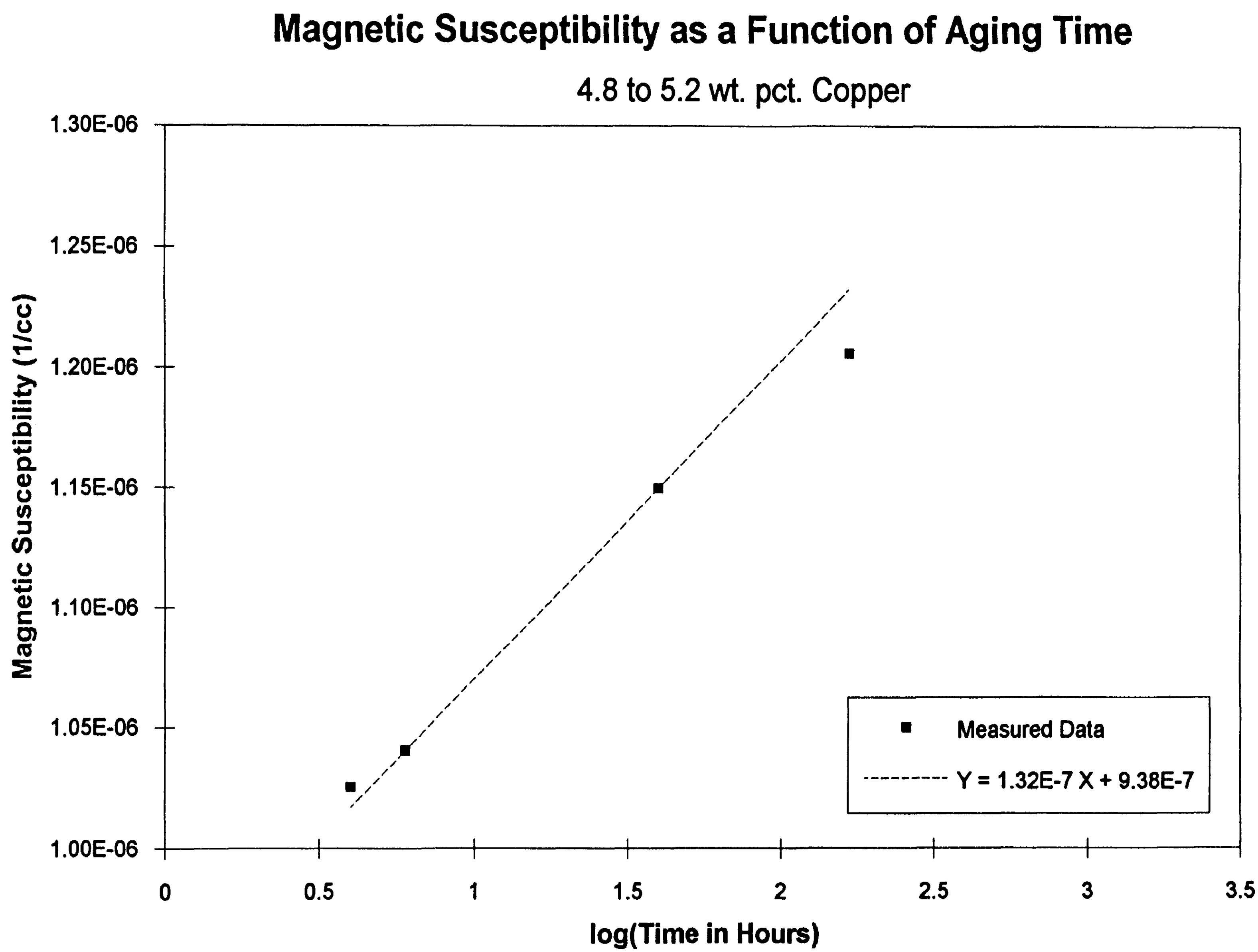

Figure 4.4: Magnetic susceptibility at 300K as a function of log(aging time at 473K) for samples with Copper between 4.8 and 5.2 wt. pct.

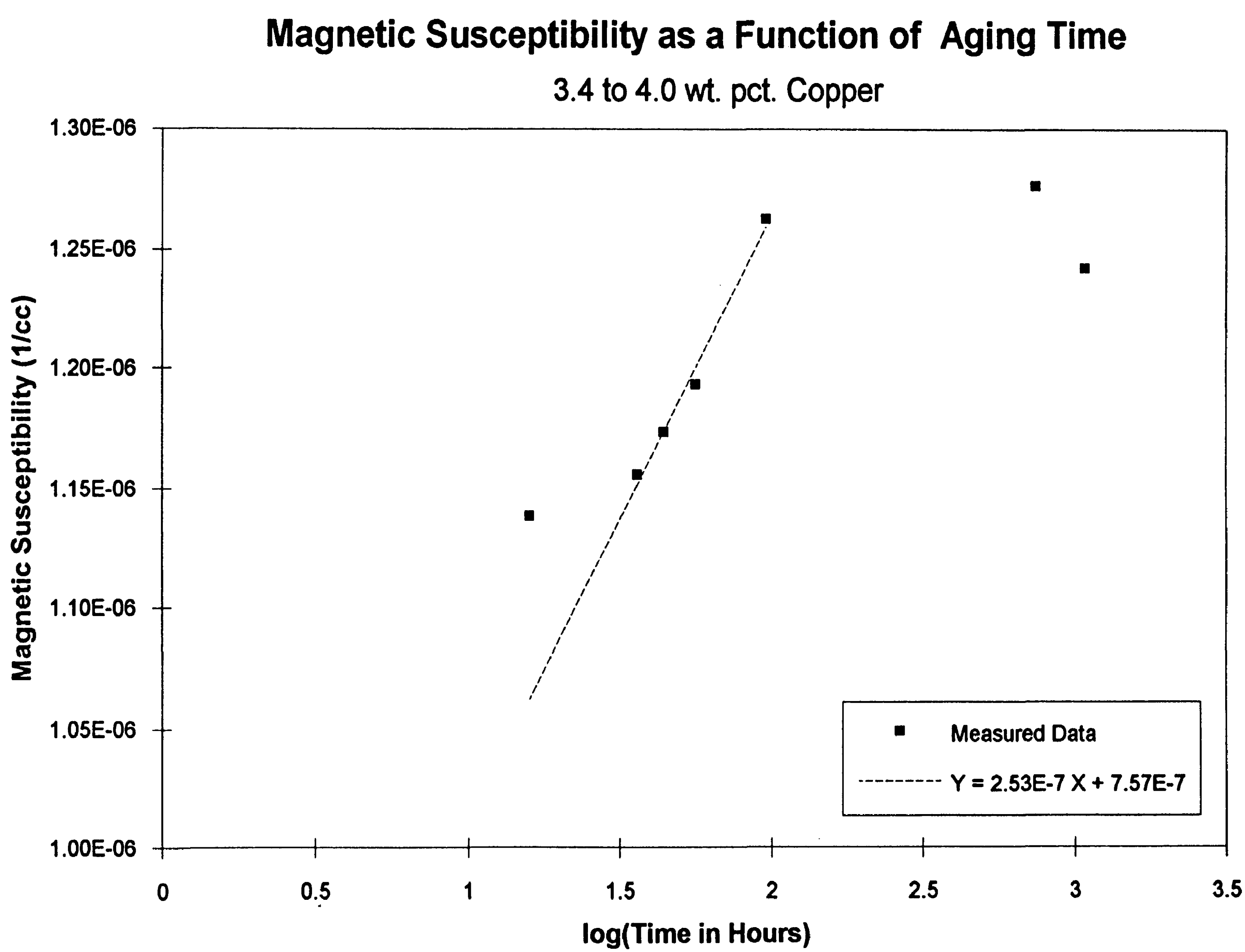

Figure 4.5: Magnetic susceptibility at 300K as a function of log(aging time at 473K) for samples with Copper between 3.4 and 4.0 wt. pct.

To describe the relationship of each region, a linear regression was performed on each of the three regions of Figure 4.1. With copper concentration and log(aging time in hours) as the independent variables and magnetic susceptibility as the dependent variable, the following equations were ascertained. In Figure 4.6, the predicted values from equations 26, 27, and 28 have been overlaid on the actual measured values.

Region 1: χ = -5.97E-9*(log (t))-1.72E-6*(wt. pct.Cu)+1.12E-6 (27)

Region 2: χ = 1.63E-7*(log (t))-2.93E-6*(wt. pct.Cu)+1.03E-6 (28)

Region 3: χ = 2.04E-8*(log (t))-3.43E-6*(wt. pct. Cu)+1.32E-6 (30)

As the α phase of the aluminum copper system only extends to 5.65 wt. pct. copper, samples with more copper will not produce a complete solid solution. Regardless of solutionizing and quenching practices, some copper will remain in precipitates. Therefore, equations 26, 27, and 28 are limited to alloys with up to 5.65 wt. pct. copper. Because its copper content exceeds the solutionizing maximum, sample 18 was excluded from the regression analysis that produced equations 26, 27, and 28. Regression analysis is included in Appendix B.

Comparison between Figures 4.2 to 4.5 reveals that with increasing copper concentration, the initiation of Region 2 is delayed and the slope of Region 2 decreases. This observation is supported by the equations for Regions 1, 2, and 3. As shown by the negative constant in front of the (wt. pct. Cu) in each of the three regions, an increase in copper concentration will lower the magnetic susceptibility at a given aging time. An

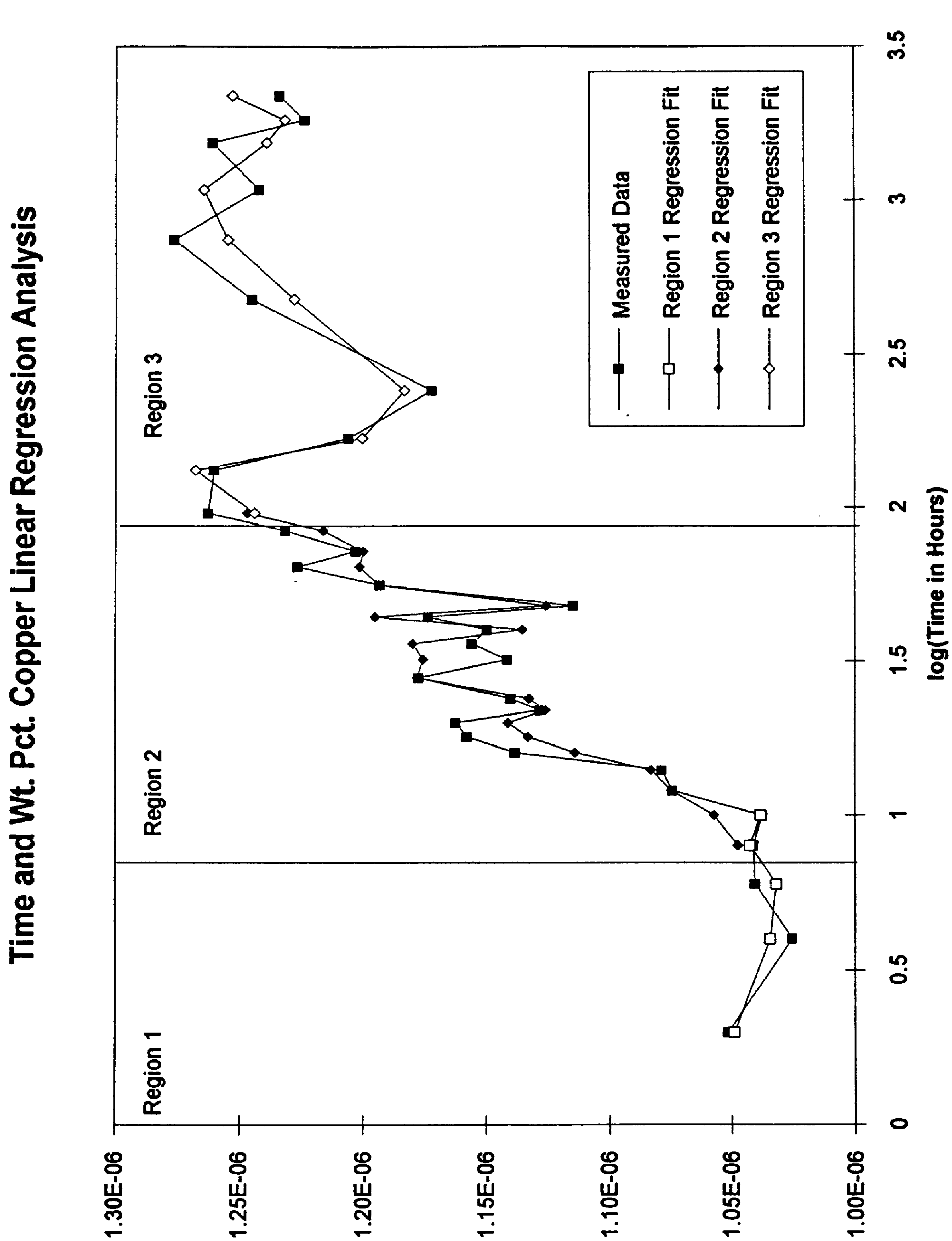

Figure 4.6: Plot showing correlation between measured and predicted magnetic susceptibility.

increased copper concentration means there are more copper atoms present to influence the aluminum atoms. These additional copper atoms will mask the Pauli paramagnetism of additional aluminum atoms, which accounts for the lower magnetic susceptibility with increasing copper concentration.

For 4.0 wt. pct. copper, the boundary between Regions 1 and 2 occurs at t = 7.1 hours, and the boundary between Regions 2 and 3 occurs at t = 88 hours (3.7 days). Figure 4.7 shows the magnetic susceptibility data again. With the copper concentration set equal to 4.0 wt. pct., the best fit line for each region is plotted through the data points. In general, data points above the best fit lines have copper concentration below 4.0 wt. pct., while those below the lines have copper concentration above 4.0 wt. pct.

To correlate the three regions found in the magnetic susceptibility as a function of aging time data to phase transformation occurring in the alloy, the hardness data were investigated and the TEM microstructures were analyzed. Figure 4.8 presents the hardness as a function of aging time curve. Once again there is some scatter attributable to varying copper concentration. However, the classical relationship was observed: an initial flat to slight increase in hardness, followed by a sharp increase in hardness to a peak hardness, then overaging and a loss in hardness. Peak hardness was observed at 40 hours (1.6 days). Figure 4.8 also displays the boundaries between the three regions, as determined from the magnetic susceptibility data.

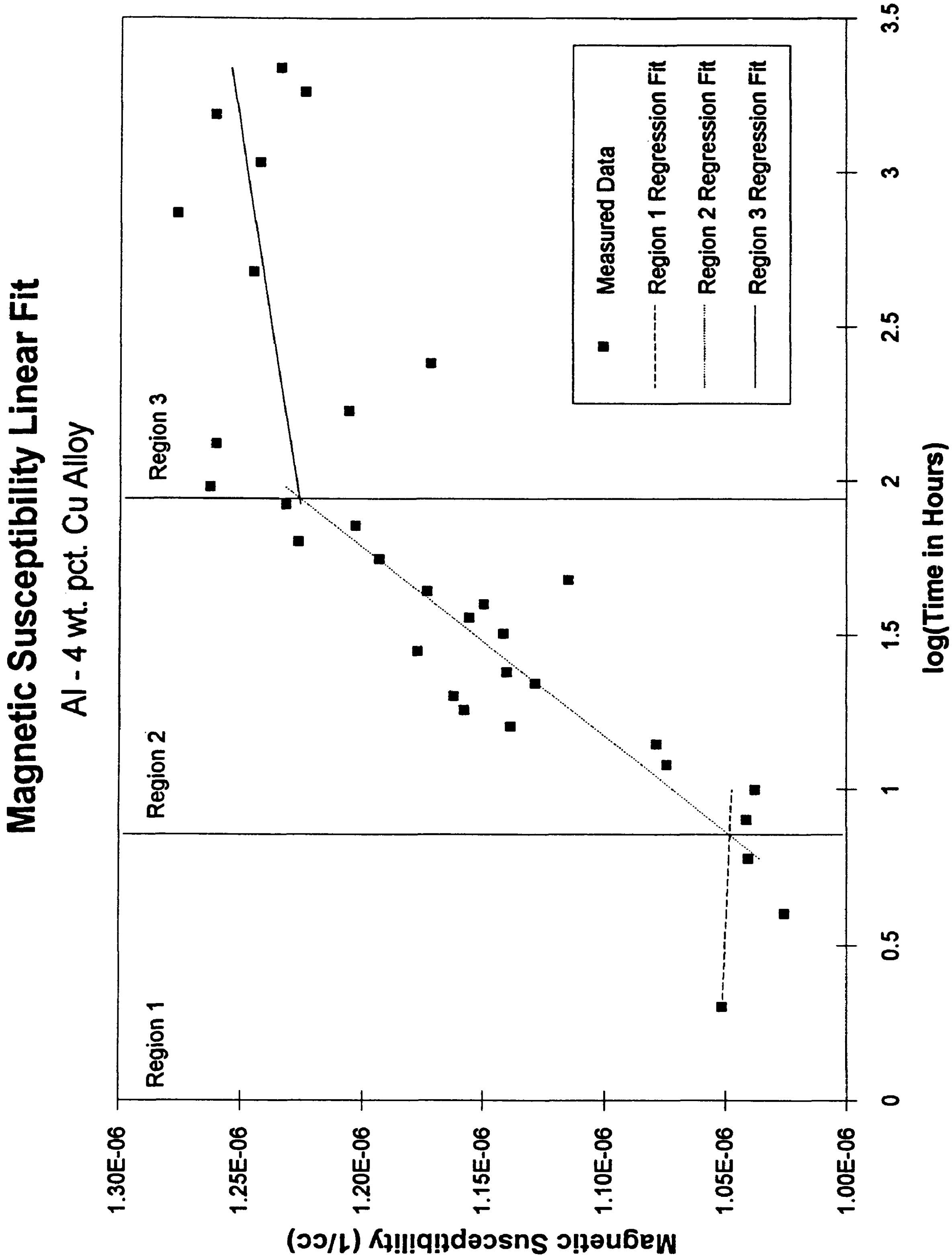

Figure 4.7 Linear regression best fit lines for Cu = 4.0 wt. pct.

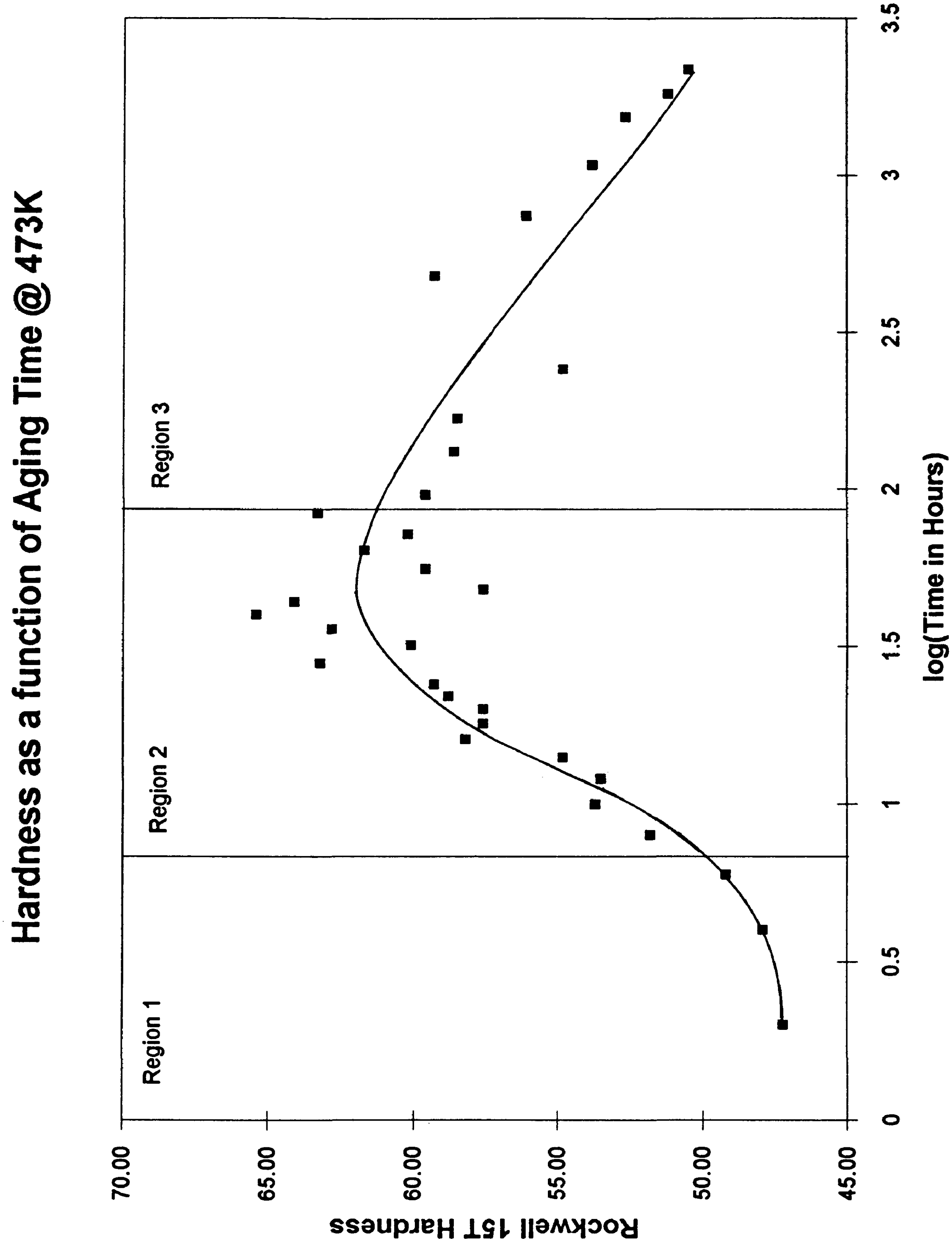

Figure 4.8: Hardness as a function of log(aging time at 473K).

4.1 Region 1

The initial flat to slight increase in hardness occurs in Region 1 of the magnetic susceptibility data and corresponds to GP1 zone refinement that occurs at the early stages of artificial aging. As indicated by a negative coefficient of log(time) in equation 26, the magnetic susceptibility for Region 1 was found to decrease with aging time. This decrease is the result of GP1 zone reversion prior to GP2 formation. The samples had naturally aged at room temperature for several days prior to the artificial aging resulting in GP1 zone formation. However, the GP1 phase is not stable at artificial aging temperatures, and GP1 zones go back into solution in a short time during artificial aging. As each copper atom dissolves into solution from the ordered atomic arrangement of GP1 zones, it will associate with additional aluminum atoms. The influence of the copper atom as it associates with additional aluminum atoms accounts for the decrease in magnetic susceptibility found in Region 1.

The TEM Micrographs shown in Figures 4.9 and 4.10 depict the microstructures of samples 1 and 4. These samples correspond to Region 1 and depict the GP1 zone refinement as aging proceeds with increasing sample number. Narrow disc shaped precipitates are observed in view (a) of both figures. These discs are oriented both in the plane of the micrograph and perpendicular to the plane such that the edges are evident. In view (b) of each figure, lattice strain is apparent along the edge of the precipitates, indicating coherency between the precipitate and matrix is intact. The precipitants

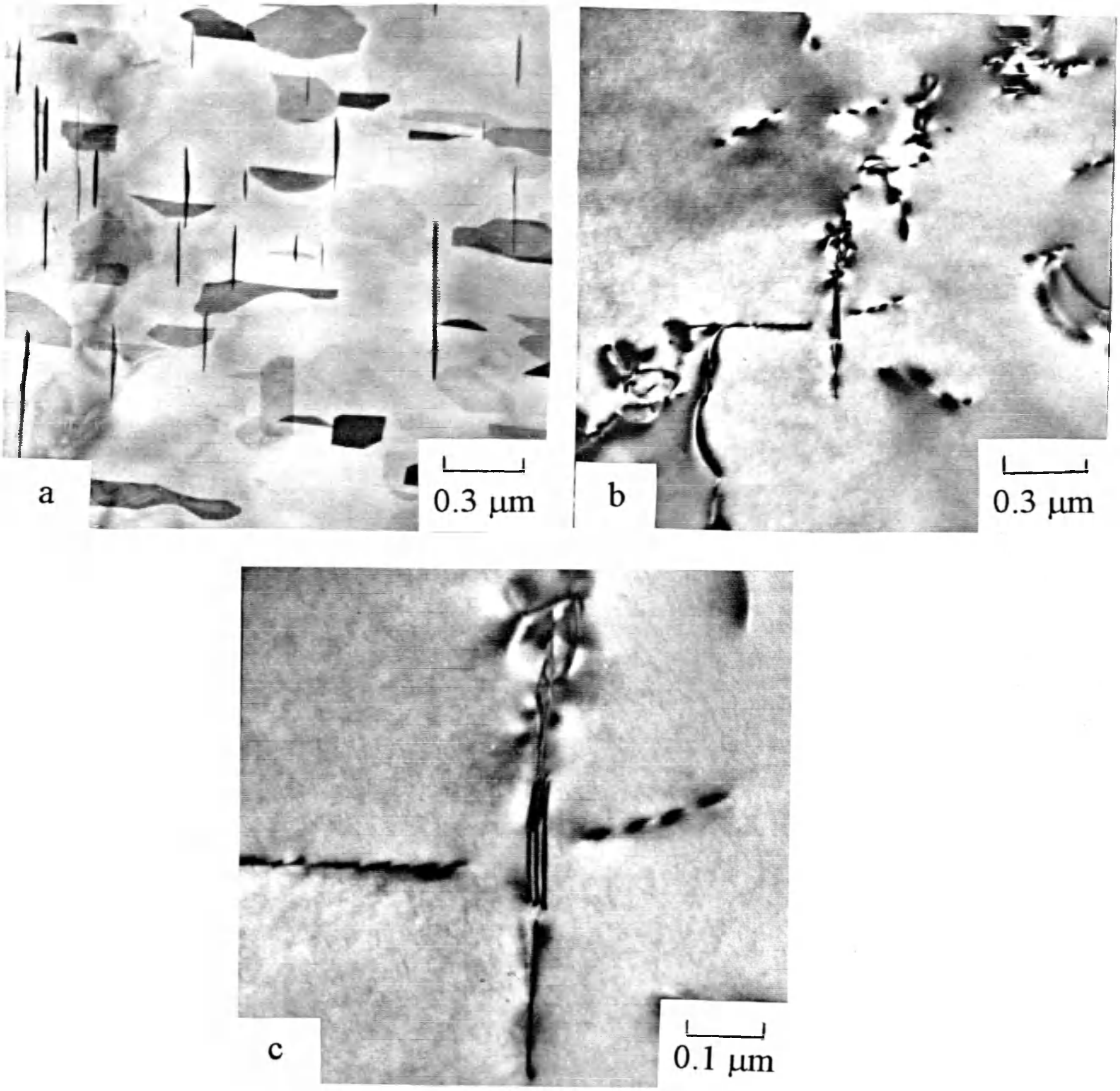

Figure 4.9: TEM micrographs of Sample 1 which was solutionized, quenched, and artificially aged at 473 K for 2 hours. a) Disc shaped precipitants observed in plane of micrograph. Edges of disc perpendicular to plane of micrograph show as lines. b and c) Strain field associated with the precipitates, indicative of coherency being maintained.

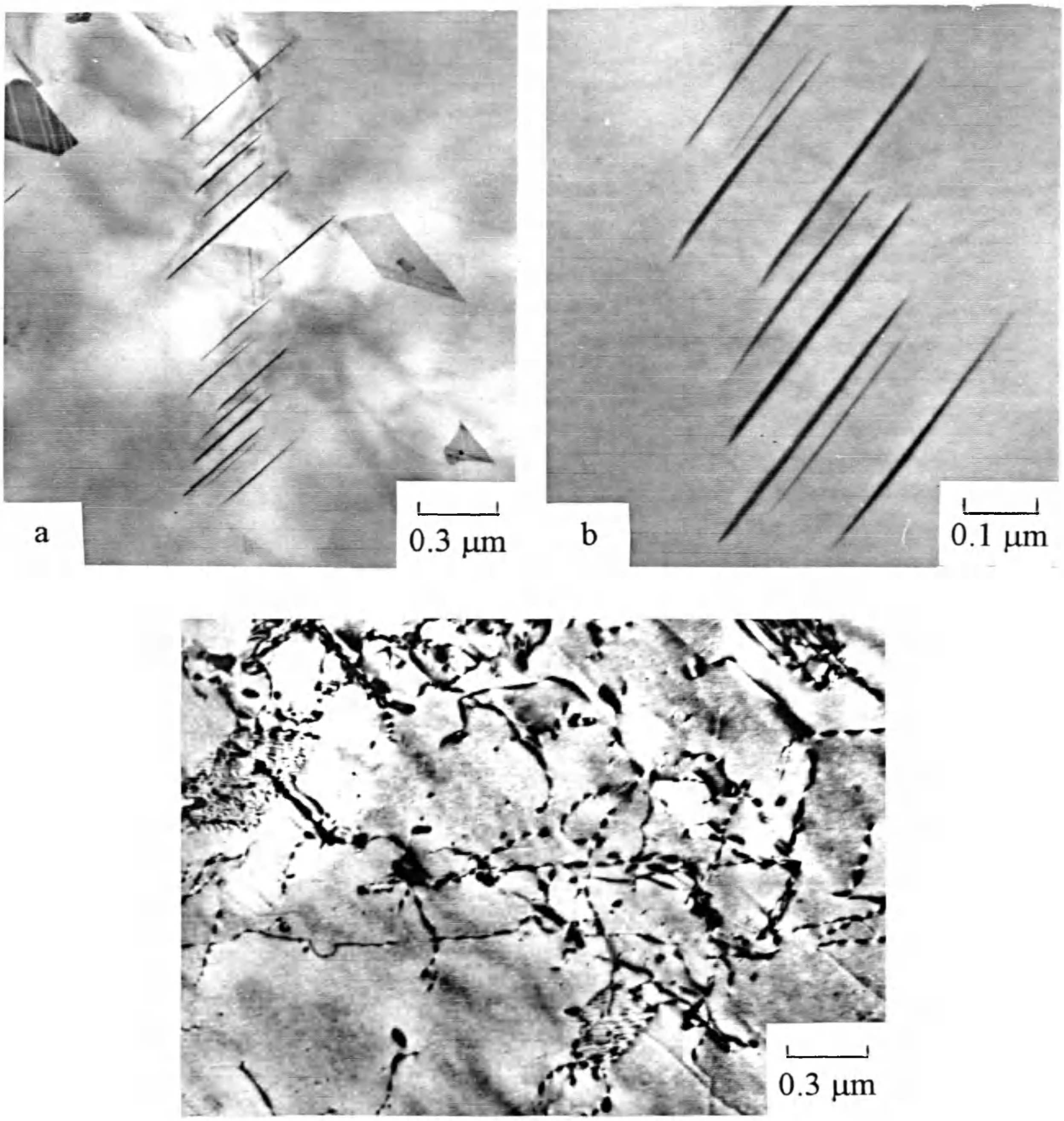

Figure 4.10: TEM micrographs of Sample 4 which was solutionized, quenched, and artificially aged at 473 K for 8 hours. a and b) Disc shaped precipitants observed in plane of micrograph. Edges of disc perpendicular to plane of micrograph show as lines. c) Strain field associated with the precipitates, indicative of coherency being maintained.

decrease in size and number between samples 1 and 4, which corresponds to GP1 zone refinement, copper returning to solution, and a decrease in magnetic susceptibility with increased aging time.

4.2 Region 2

The magnetic susceptibility increases with aging time throughout Region 2. This increase corresponds to copper leaving the solid solution to form new phases. The diamagnetic behavior of copper atoms screens the paramagnetic behavior of the aluminum atoms which bond with copper. The copper atoms associate with fewer aluminum atoms in the phases that grow out of solid solution, and additional aluminum atoms contribute their full paramagnetic response to the bulk alloy measurement.

As seen in Figure 4.8, the hardness was found to sharply increase in Region 2, which is attributable to GP2 formation. The GP2 precipitates produce the increased strength of a heat treatable Cu-Al alloy. The maximum hardness occurred in Region 2, which indicates GP2 precipitates reached a maximum. The θ' phase is not related to the GP1 or GP2 metastable phases, but nucleates heterogeneously. However, θ' phase grows at the expense of GP zones. Hardness decreases once θ' precipitation starts. Region 2 extends over the range of time that GP2 and θ' precipitants coexist. As reported in the literature, the maximum hardness for a Al - 4 wt. pct. Cu alloy is reached after artificially aging at 473 K for one day [39]. The experimental data found the maximum hardness to occur at 1.6 days. Since the maximum hardness was experimentally reached 0.6 days later than reported in the literature, the time to precipitate θ' experimentally should also be delayed. The literature states that θ' precipitates in a Al - 4 wt. pct. copper alloy after three days of artificially aging at 473 K. This fact corresponds to the boundary between Regions 2 and 3 which occurred at 3.7 days. The experimentally longer times for precipitation to occur over those reported in the literature are a result of the time required for GP1 zone refinement. The time to form precipitates reported in the literature result from artificial aging immediately following quenching, and no GP1 zones are allowed to form. As a result, refinement does not take place, Region 1 does not occur, and maximum hardness and θ' precipitates are reached earlier. The boundary between Regions 2 and 3 indicates where GP2 zones no longer exist.

Figures 4.11, 4.12, 4.13, and 4.14 display the TEM Micrographs of samples 8, 12, 16, and 22 respectively, which fall within Region 2. The precipitate are observed to grow with aging time, most noticeably in length. The density also increases, as the spacing between parallel precipitants decreases. This increase in precipitant size and density corresponds to copper leaving the solid solution and residing within the precipitants. The presence of strain fields along the long sides of the precipitates are evidence that coherency is being maintained.

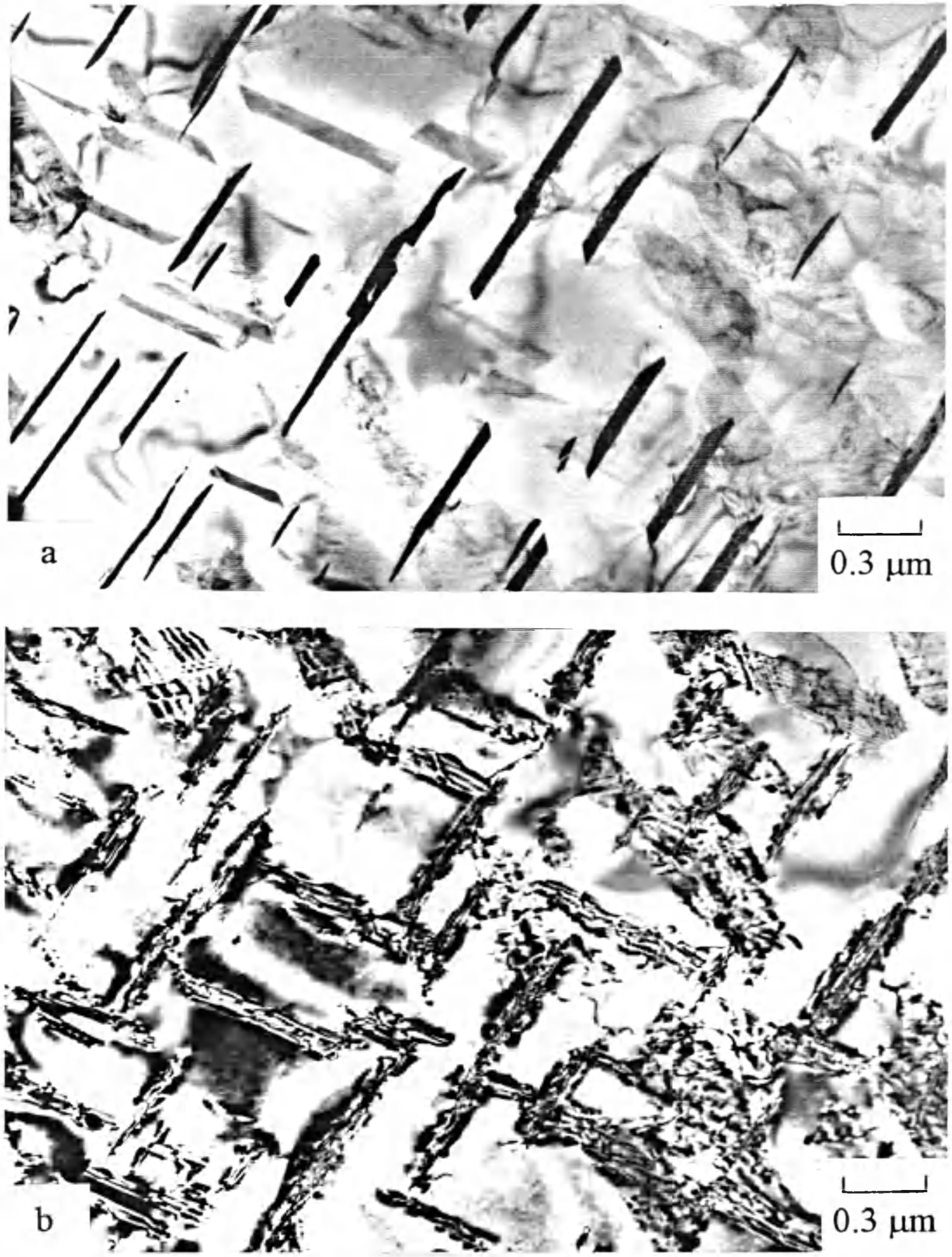

Figure 4.11: TEM micrographs of Sample 8 which was solutionized, quenched, and artificially aged at 473 K for 16 hours. a) Disc shaped precipitants observed in plane of micrograph. Edges of disc perpendicular to plane of micrograph show as lines. b) Strain field associated with the precipitates, indicative of coherency being maintained

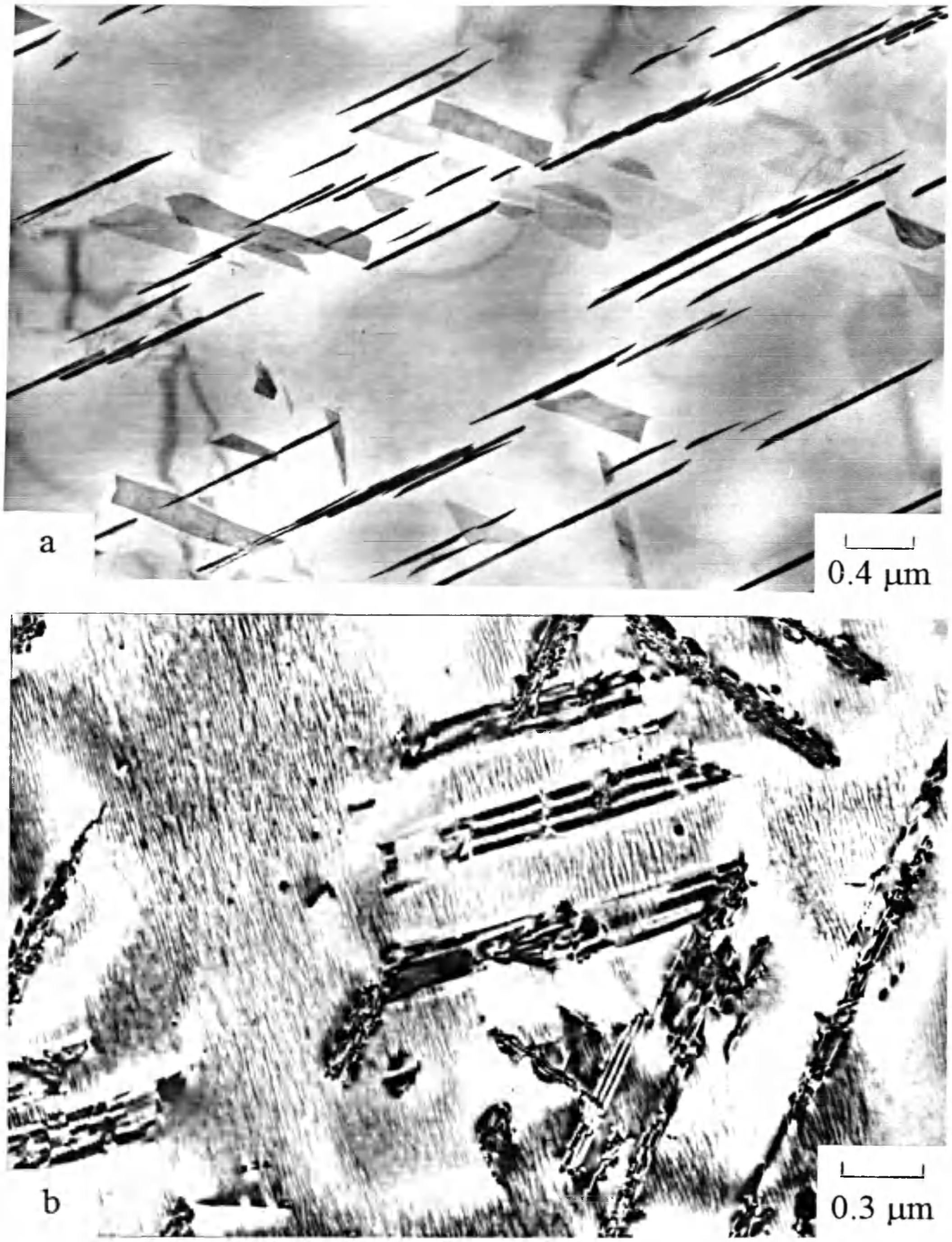

Figure 4.12: TEM micrographs of Sample 12 which was solutionized, quenched, and artificially aged at 473 K for 24 hours. a) Disc shaped precipitants observed in plane of micrograph. Edges of disc perpendicular to plane of micrograph show as lines. b) Strain field associated with the precipitates, indicative of coherency being maintained

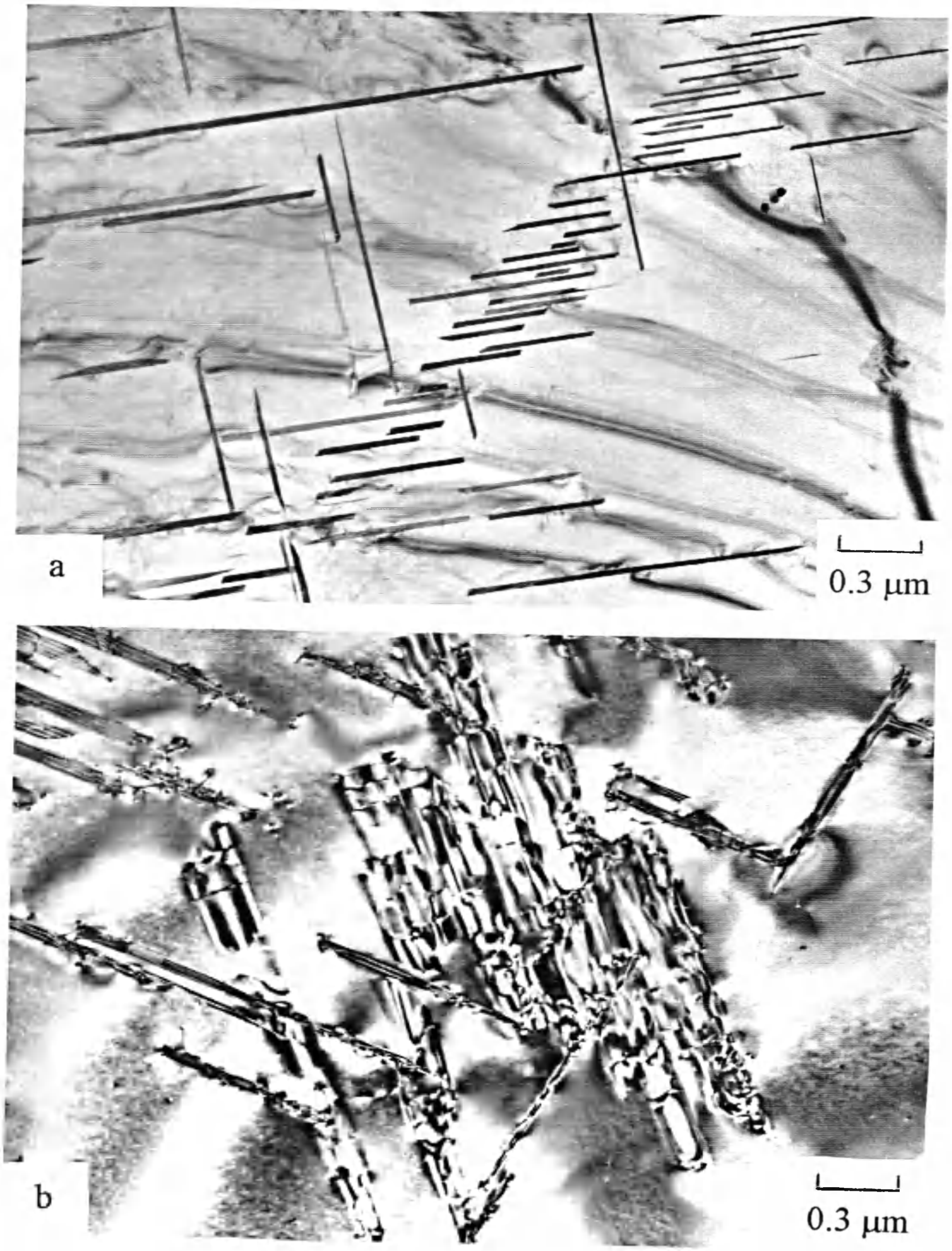

Figure 4.13: TEM micrographs of Sample 16 which was solutionized, quenched, and artificially aged at 473 K for 40 hours. a) Disc shaped precipitants observed in plane of micrograph. Edges of disc perpendicular to plane of micrograph show as lines. b) Strain field associated with the precipitates, indicative of coherency being maintained.

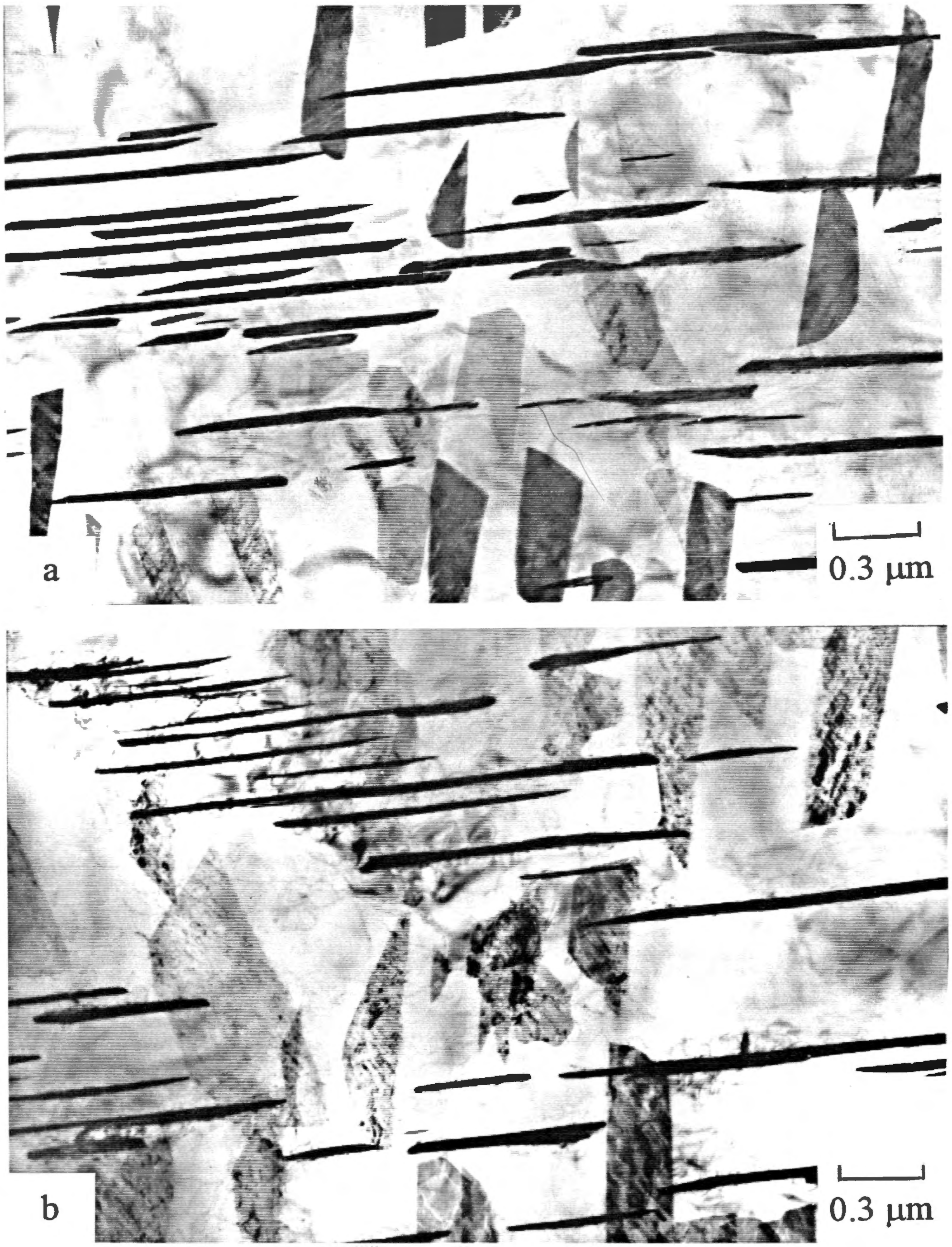

Figure 4.14: TEM micrographs of Sample 22 which was solutionized, quenched, and artificially aged at 473 K for 84 hours. a) Disc shaped precipitants observed in plane of micrograph. Edges of disc perpendicular to plane of micrograph show as lines. b) Strain field associated with the precipitates, indicative of coherency being maintained.

4.3 Region 3

As shown in Figure 4.8, the hardness decreases through Region 3, as θ' and finally θ form. The literature reports that the θ phase forms at the expense of the θ' phase, and is present in a highly overaged condition. The condition is reached by artificially aging at 473 K for approximately 2000 hours (80 days). In Region 3, the increase in magnetic susceptibility with aging time is at a lower rate indicating the majority of copper has left the solid solution and resides in phases. The increase observed is attributable to the growth of θ precipitates. The θ phase transforms from the θ' phase and coarsening occurs as smaller precipitates grow together. Additional aluminum atoms are able to contribute to the bulk magnetic response of the alloy with the transformation, but not at the rate observed when copper came out of solid solution where it associated with twelve aluminum atoms. As the precipitates coarsen, their surface area will decrease, which reduces the number of matrix aluminum atoms influenced by the copper. The loss in coherency found between the θ phase and the matrix will also free additional aluminum atoms to contribute completely to the paramagnetic behavior of the bulk alloy.

Figures 4.15 and 4.16 contain TEM Micrographs of samples 27 and 32 found in Region 3. An increase in precipitate size and thus the depletion of copper from the matrix is evident with increasing aging time through Region 3. This coarsening of precipitates corresponds to an increase in magnetic susceptibility with time, as a two phase equilibrium alloy is approached. The strain fields surrounding the precipitates are extensive and

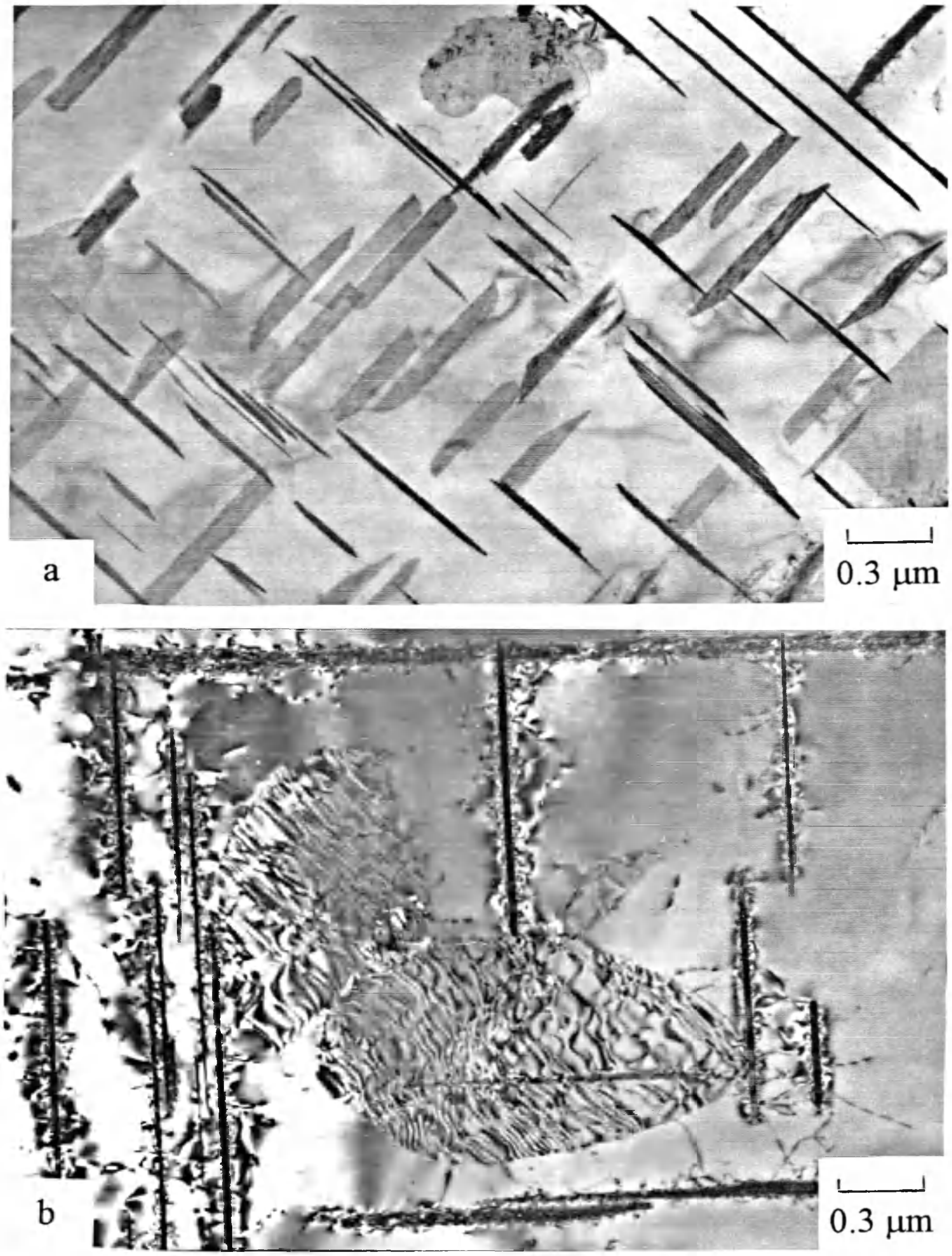

Figure 4.15: TEM micrographs of Sample 27 which was solutionized, quenched, and artificially aged at 473 K for 360 hours. a) Disc shaped precipitants observed in plane of micrograph. Edges of disc perpendicular to plane of micrograph show as lines. b) Extensive strain field associated with the precipitates as coherency is being lost.

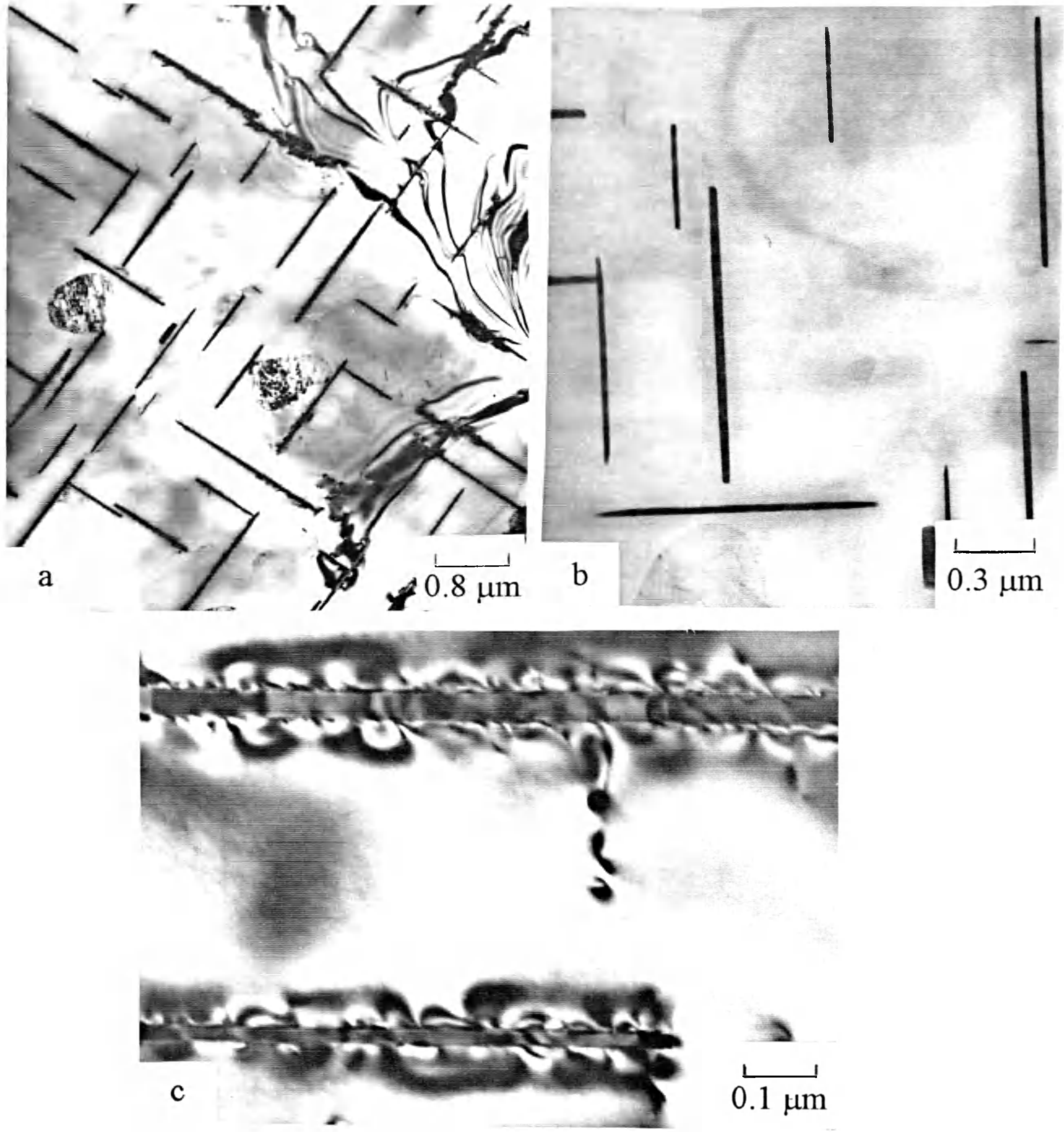

Figure 4.16: TEM micrographs of Sample 32 which was solutionized, quenched, and artificially aged at 473 K for 2,160 hours. a and b) Disc shaped precipitants observed in plane of micrograph. Edges of disc perpendicular to plane of micrograph show as lines. c) Strain field associated with the precipitates decreasing as coherency is lost.

annunciate a loss in coherency as the matrix atoms are strained to align with those in the precipitates. Because these large incoherent precipitates are less effective at impeding dislocation movement during plastic strain, a loss in strength occurs which was noticed in the decrease in hardness of Region 3 in Figure 4.8.

4.4 Statements Of Completion

The three regions observed in the magnetic susceptibility data result as the copper atoms associate with different numbers of aluminum atoms as the precipitates within the alloy transform. Region 1 saw the magnetic susceptibility decrease with aging time as the copper left the GP1 zones and returned to solution, resulting in an increase in aluminum atoms affected by the copper. Regions 2 and 3 found the magnetic susceptibility increase with aging time. This increase, although at different rates, occurs as each copper atom looses influence over aluminum atoms. The loss of influence occurs as phases develop that reduce the aluminum atoms associated with copper atoms. As a result, the change in aluminum-copper alloy microstructure, which occurs by transformation through several metastable phases, can be monitored with the bulk magnetic susceptibility measurements.

The change in magnetic susceptibility with changing microstructure is evident from this work. In addition this work confirmed that the aluminum-copper microstructure is responsible for the hardness present in the alloy. Figure 4.17 shows the Rockwell 15T hardness as a function of the magnetic susceptibility. The solid curve represents a best fit for a 4.0 wt. pct. copper concentration in the aluminum alloy. The measured data points

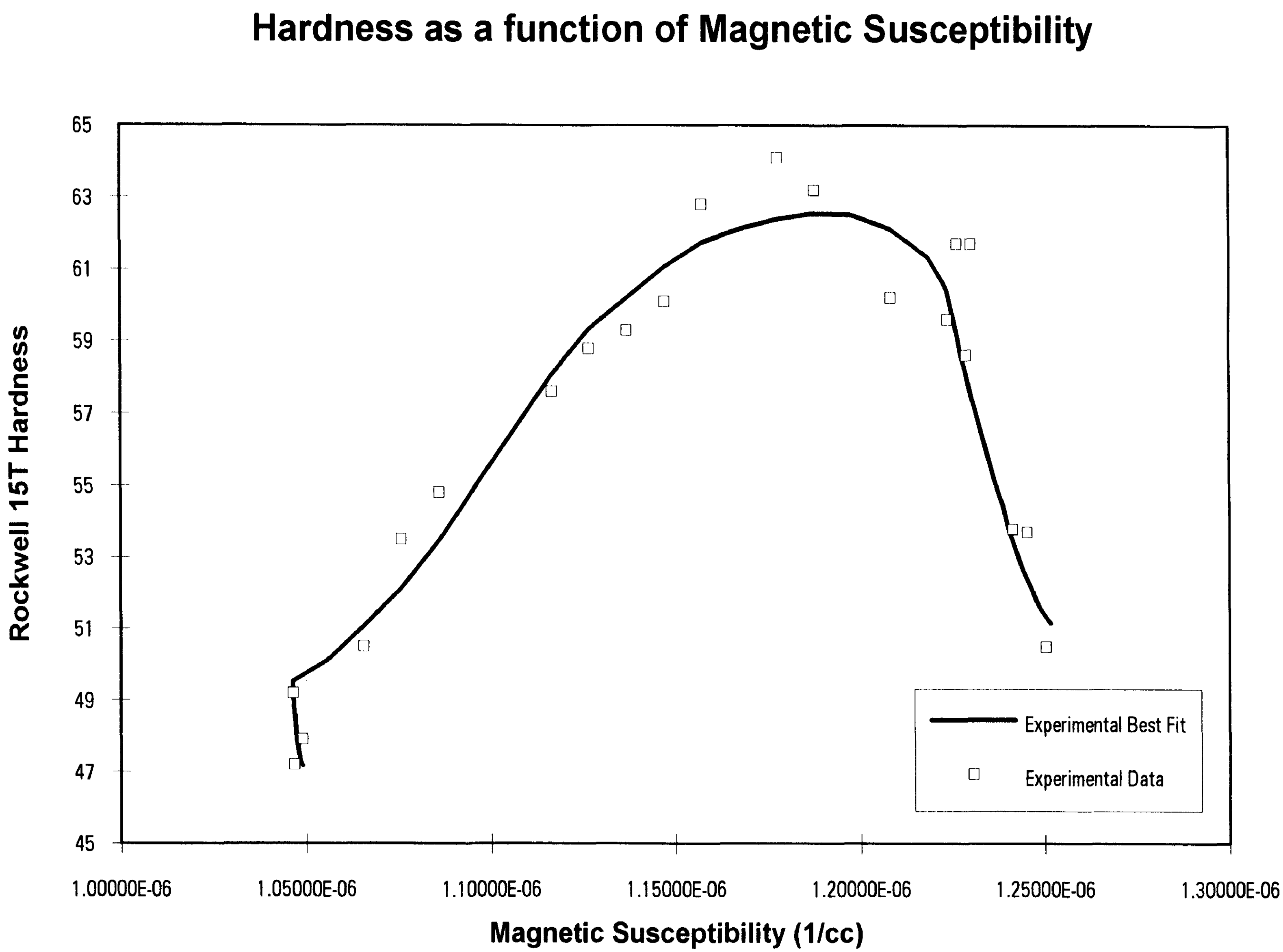

Figure 4.17: Mechanical property (hardness) correlated to an electronic measurement (magnetic susceptibility).

vary partially because their composition varies from 4.0 wt. pct. copper. Examining Figure 4.17 reveals that by measuring the magnetic susceptibility, the hardness can be predicted. This observation addresses the objective of this thesis. The results suggest that bulk electronic and magnetic measurements (magnetic susceptibility) can be used to predict properties (hardness) of alloy systems (aluminum-copper system). A secondary observation results from the curve of Figure 4.17. Because of the curvature, a hardness measurement correlates to two magnetic susceptibility. Therefore the magnetic susceptibility cannot be predict from a hardness measurement.

This thesis considered a binary alloy. Engineering alloys are typically more complicated, having several alloying elements that will contribute to the electronic measurements. To characterized these alloys may require additional analysis Two or more electronic and magnetic measurements, sensitive to different attributes of the microstructure, may provide additional insight to the alloy state. Additional bulk electronic properties (Hall Effect, electrical resistivity) will likely exhibit relationships with alloy microstructure. One measured property could be plotted on the y-axis and the second property plotted on the x-axis, for example; magnetic susceptibility as a function of Hall coefficient. The intersection of these values should identify specific locations on the plot. These locations will suggest the state of precipitation by their position relative to prior-determined, equal-phase-condition lines. In future work, a variety of different electronic and magnetic quantities could be used to develop such plots for many different alloy systems. These plots could then be used to metallurgically characterize alloy components, providing significant improvements in the nondestructive evaluation of advanced alloy properties and the prediction of service life.

The initial stages of developing the nondestructive evaluation of alloys must show that electronic and magnetic measurements are sensitive to microstructure and can be correlated to material properties. This objective is best met by preparing alloy samples to fit the requirements of existing measurement equipment. Once this fact is established, future development will adapt the measured properties to the real world. In order for this technique to be nondestructive, the measurement must conform to the geometry of fabricated parts and must be completed in field environments.

CHAPTER 5

CONCLUSION

1 The mechanical properties of alloys are often a function of the phases present and the resulting microstructure. Alloy phases are dependent on electron concentration. Electronic and magnetic measurements, which are related to electron state, can be correlated to alloy phases and the associated mechanical properties. By using nondestructive electronic and magnetic measurements, it is possible to predict alloy mechanical properties.

2 The magnetic susceptibility of heat-treatable aluminum alloys is sensitive to changes such as solution or dissolution of solute and the precipitation of new phases. The diamagnetic behavior of the copper atom was found to influence the paramagnetic behavior of the aluminum atoms associated with copper. As the number of aluminum atoms associated with a copper atom change through precipitation, a corresponding change in magnetic susceptibility was found.

3 Magnetic susceptibility measurements were used to follow phase transformation in Al-Cu alloys. The three regions found in the magnetic susceptibility data correspond to the hardness data and phases documented in the TEM micrographs. Region 1 is consistent with GP1 zone refinement, Region 2 is attributable to GP2 zone and θ' formation, and Region 3 corresponds to overaging as θ' transforms and finally θ precipitates.

REFERENCES CITED

1. A. S. Brown, 1992, "Industry Seeks Tonic for Aging Aircraft", Material Performance, 31 no. 9 (September 1992): pp. 55-58.
2. C.S. Barrett, Structure of Metals, Pergamon Press, New York, NY, pp. 223-379 (1982).
3. L. Brewer, "Viewpoint of Stability of Metallic Structures", Batelle Colloquium on Phase Stability Metals and Alloys, McGraw-Hill Book Co., New York, pp. 39-61 (1967).
4. L. Brewer, "Bonding and Structures of Transition Metals", Science 161 (12 July) pp. 115-122 (1968).
5. L. Brewer, "Nature of Bonding in Transition-Metal Aluminides", J. Phys. Chemistry 94, pp. 1196-1203 (1990).
6. Seung-Am Cho, "The Engel-Brewer Theory and Related Physical Properties of The Hume-Rothery's Class I Metals", Acta Metallurgica, 25, pp. 1085-1094 (1977).
7. D.A. Rigney and C.Y. Flynn, "Electronic Structure of Dilute Alloys", Phil. Mag. B. 15, pp. 1213-1232 (1967).
8. C.P. Flynn and D.A.R. Rigney, "Magnetic Polarization of Transitional Impurities in Aluminum", Phil. Mag. B. 15, pp. 1255-1273 (1967).
9. M.H. Cohen, "The Electronic Theory of Simple Metals and Alloys", Alloying Behavior and Effects in Concentrated Solid Solutions, 29 pp. 1-24 (1963).
10. B.L. Gyorffy, "The Electronic Structure and Phase Stabilities of Metallic Alloys", Mat. Res. Soc. Symp. "Alloy Phase Stability and Design", 186, pp. 3-31 (1991).
11. W.C. Sleppy, "Magnetic Analysis of Dilute Binary Alloys of Copper, Zinc, and Magnesium in Aluminum", TMS - AIME, 239 (May 1967): pp. 684-690.
12. J. Crangle, Solid State Magnetism, Van Nostrand Reinhold, New York, NY, pp. 1-85 (1991).
13. V.I. Prokoshin, "Behavior of the Thermo EMF and Hall Coefficient on the Plastic Deformation of Bismuth Alloyed with Lead", Fiz. Metal. Metalloved. 22 (2), pp. 199-203 (1966).
14. R.P. Vasileva, A. V. Cheremushkina. S. Yasiliyev and Y. A. Kadyrov, "Hall Effect and Electrical Resistance of Iron-Cobalt Alloys", Fiz. Metal. Metalloved. 38 (2) pp. 289-294 (1974).
15. Y.I. Kondorskiy, A.V. Cheremushkina, R.P. Yasilyeva, and Y.N. Arkipov, "The Hall and Nernst-Ettingshausen Effects in Iron and Nickel", Fix. Metal. Metalloved. 34 (2) pp. 289-294 (1974).
16. A.V. Vedyayev, A.B. Granovskiy and Y.I. Kondorskiy, "Toward a Theory of the Residual and Anomalous Hall Effect of Disordered Alloys. Weak Scattering. II", Fix. Metal. Metalloved. 40 (4), pp. 688-694 (1975).

17. L.I. Abramova and G. V. Fedorev, "The Normal Hall Effect in Palladium-Iron Alloys", Fiz Metal. Metalloved. 44 (1), pp. 179-182 (1977).
18. V.A. Matveyev and G.V. Fedorev, "Anomalous Hall Effect of Pb-Ni, Pb-Co and Pb-Fe Alloys", Fiz. Metal. Metalloved. 53 (1), pp. 34-41 (1982).
19. V.G. Dvunitkin, M.V. Vedernikov and N.I. Moreva, "Hall Constant and Resistivity of Holmium and Erbium at High Temperatures", Fiz Metal. Metalloved. 45 (4), pp. 894-896 (1978).
20. Y.I. Kondorskiy, A.V. Vedyayev and A.B. Granovskiy, "Theory of the Residual Anomalous Hall Effect of Disordered Alloys. I", Fiz. Metal. Metalloved. 40 (3), pp. 455-464 (1975).
21. Y.I. Kondorskiy, A.V. Vedyayev and A.B. Granovskiy, "On the Theory of the Residual Anomalous Hall Effect of Disordered Alloys II", Fiz. Metal. Metalloved. 40 (5), pp. 903-909 (1975).
22. D.K. Bhattacharya, S. Vaidyanathan, V. Moorthy, and B. Raj, Magnetic Barkhausen Noise Signals in Gardedned and Tempered 2.25Cr-1Mo Steel Specimens, Presented at the Indo-German seminar on non-destructive materials characteriasation, 1990, Bhabha Atomic Research Centre, Bombay, (1990).
23. D.K. Bhattacharya, S. Vaidyanathan, V. Moorthy, T. Jayakumar, and B. Raj, Magnetic Barkhausen Noise Analysis for the Assessment of Microstructures in Heat Treated 2.25Cr-1Mo and 17-4-PH Steels, Presented at the 13th World Confernence on Non-Destructive Testing, San Paulo, Brazil, October, 1992.
24. P.A. Tipler, Modern Physics, Worth Publishers, New York, NY, pp. 321-337 (1983).
25. C. Kittel, Introduction to Solid State Physics, John Wiley & Sons, New York, NY, pp. 234-346 (1956).
26. R.G. Baker and J. Nutting, "The Tempering of 2 1/4% Cr - 1% Mo Steel After Quenching and Normalizing," Journal of the Iron and Steel Institute, 192, pp.257-268 (1959).
27. J.L. Walter, M.R. Jackson and C.T. Sims, Alloying, ASM International, Materials Park, Ohio, pp. 1-103 (1988).
28. A.E. Berkowitz and E. Kneller, Magnetism and Metallurgy. Academic Press, New York, NY, pp. 331-361 (1969).
29. C.A. Wert et al., Physics of Solids, McGraw-Hill Book Company, New York, NY, pp. 422-436 (1970).
30. D. Jiles, Introduction to Magnetism and Magnetic Materials, Chapman and Hall, New York, NY, pp. 1-125 (1991).
31. P. Wilkes, Solid State Theory in Metallurgy, Cambridge University Press, New York, NY, pp. 308-331 (1973).
32. T.B. Massalski, Alloying Behavior and Effects in Concentrated Solid Solutions, Gordon and Breach Science Publishers, New York, NY, pp. 40-49 (1965).

33. C.M. Hurd, The Hall Effect in Metals and Alloys, Plenum Press, New York, NY pp. 1-44 (1972).

34. C.L. Chien and C.R. Westgate, The Hall Effect and Its Applications, Plenum Press, New York, NY pp. 1-54 (1979).

35. R.J. Weiss, Solid State Physics for Metallurgists, Pergamon Press, New York, NY, pp. 251-258 (1963).

36. R. F. Decker, "Alloy Design Using Second Phases", Met. Trans. (1973).

37. W.F. Smith, Structure and Properties of Engineering Alloys, McGraw-Hill Book Company, New York, NY, pp. 176-184 (1981).

38. K.R. Van Horn, Aluminum, Volume I. Properties, Physical Metallurgy and Phase Diagrams, American Society for Metals, Metals Park, Ohio, pp. 109-176 (1967).

39. J.W. Evancho and J.T. Staley, "Kinetics of Precipitation in Aluminum Alloys During Continuous Cooling", Metallurgical Transactions, 5 (January), pp. 43-47 (1974).

40. D. Altenpohl, Aluminum Viewed from Within, Aluminium-Verlag, Düsseldorf, West Germany, pp. 149-163 (1982).

41. A.K. Vasudevan and R.D. Doherty, Aluminum Alloys - Contemporary Research and Applications, Academic Press, Inc., San Diego, CA, pp. 1-54 (1989).

42. K.R. Van Horn, Aluminum, Volume III. Fabrication and Finishing, American Society for Metals, Metals Park, Ohio, pp. 109-176 (1967).

43. American Society for Testing and materials (ASTM), E 18-89a, Standard Test Method, Rockwell Hardness and Rockwell Superficial Hardness of Metallic Materials, 1989 revision, Philadelphia, PA.

APPENDIX A

FURNACE PARAMETERS

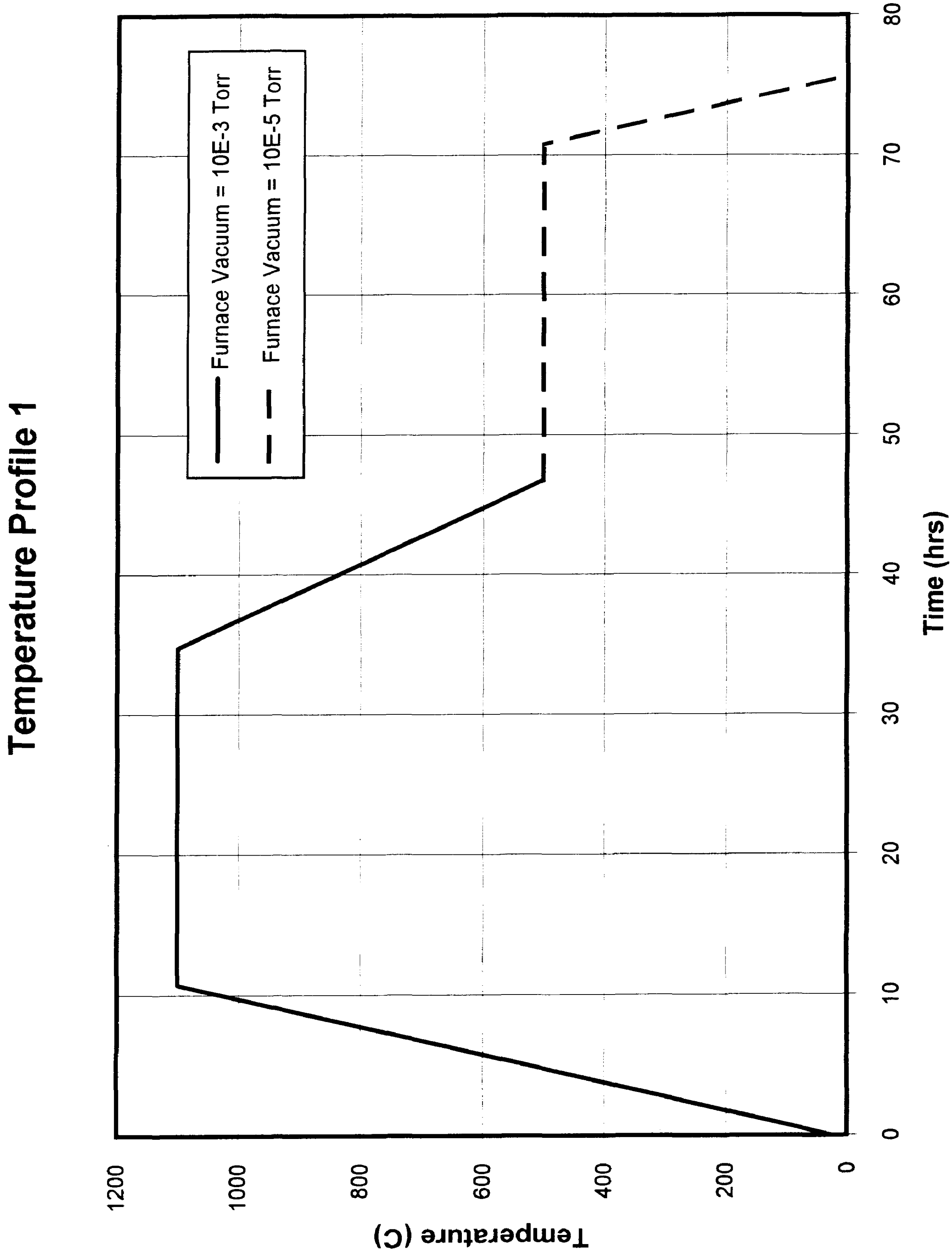

Figure A-1: First alloy melt vacuum furnace parameters.

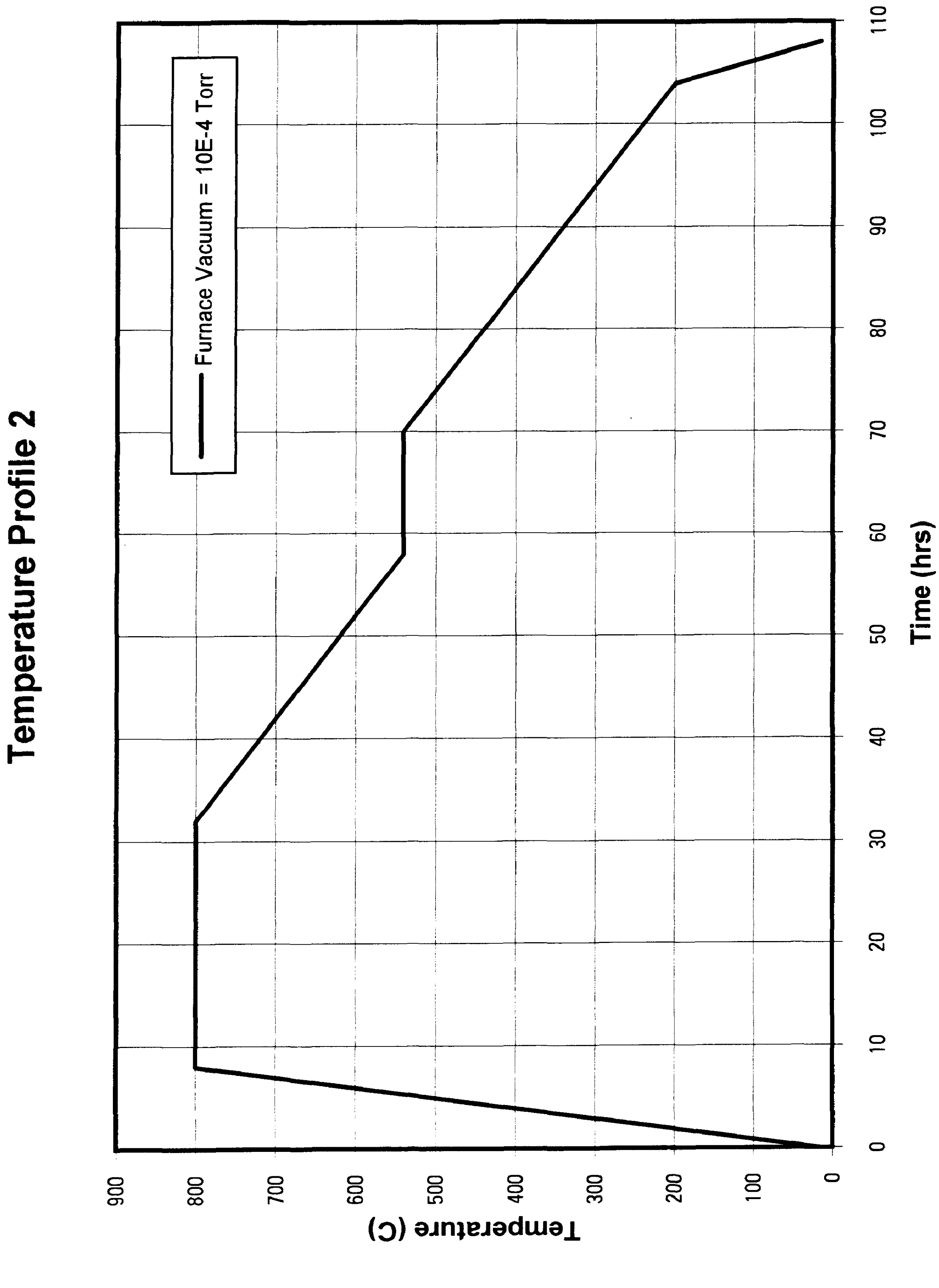

Figure A-2: Second alloy melt vacuum furnace parameters.

APPENDIX B

RAW DATA

Sample No.	Age Time hrs	Length cm	Diameter cm	Volume cc	Field Gauss	Moment emu	Magnetization emu/cc	Mag Sus 1/cc
1	2	1.1595	0.4890	0.2177	6000	1.3804E-03	6.3403E-03	1.0513E-06
					7000	1.6055E-03	7.3742E-03	
					8000	1.8326E-03	8.4173E-03	
					9000	2.0561E-03	9.4439E-03	
					10000	2.2846E-03	1.0493E-02	
2	4	1.1935	0.4902	0.2253	6000	1.3954E-03	6.1942E-03	1.0255E-06
					7000	1.6215E-03	7.1979E-03	
					8000	1.8479E-03	8.2029E-03	
					9000	2.0757E-03	9.2141E-03	
					10000	2.3049E-03	1.0232E-02	
3	6	1.1448	0.5126	0.2362	6000	1.4858E-03	6.2898E-03	1.04063E-06
					7000	1.7276E-03	7.3134E-03	
					8000	1.9687E-03	8.3341E-03	
					9000	2.2090E-03	9.3514E-03	
					10000	2.4482E-03	1.0364E-02	
4	8	1.2339	0.5118	0.2539	6000	1.5935E-03	6.2770E-03	1.04114E-06
					7000	1.8544E-03	7.3047E-03	
					8000	2.1126E-03	8.3218E-03	
					9000	2.3757E-03	9.3582E-03	
					10000	2.6397E-03	1.0398E-02	
5	10	1.1709	0.5072	0.2366	6000	1.4847E-03	6.2747E-03	1.03759E-06
					7000	1.7245E-03	7.2881E-03	
					8000	1.9642E-03	8.3011E-03	
					9000	2.2051E-03	9.3192E-03	
					10000	2.4480E-03	1.0346E-02	
6	12	1.1664	0.5024	0.2312	6000	1.5011E-03	6.4918E-03	1.07437E-06
					7000	1.7451E-03	7.5470E-03	
					8000	1.9876E-03	8.5957E-03	
					9000	2.2330E-03	9.6570E-03	
					10000	2.4761E-03	1.0708E-02	
7	14	1.1577	0.5037	0.2307	6000	1.4998E-03	6.5016E-03	1.07881E-06
					7000	1.7433E-03	7.5572E-03	
					8000	1.9909E-03	8.6306E-03	
					9000	2.2378E-03	9.7009E-03	
					10000	2.4855E-03	1.0775E-02	
8	16	1.1427	0.4905	0.2159	6000	1.5036E-03	6.9640E-03	1.13829E-06
					7000	1.7370E-03	8.0450E-03	
					8000	1.9699E-03	9.1237E-03	
					9000	2.2025E-03	1.0201E-02	
					10000	2.4341E-03	1.1274E-02	

Sample No.	Age Time hrs	Length cm	Diameter cm	Volume cc	Field Gauss	Moment emu	Magnetization emu/cc	Mag Sus 1/cc
9	18	1.2141	0.5004	0.2388	6000	1.6985E-03	7.1140E-03	1.15772E-06
					7000	1.9550E-03	8.1883E-03	
					8000	2.2153E-03	9.2786E-03	
					9000	2.4748E-03	1.0365E-02	
					10000	2.7344E-03	1.1453E-02	
10	20	1.1156	0.5009	0.2198	6000	1.5612E-03	7.1022E-03	1.16207E-06
					7000	1.8033E-03	8.2035E-03	
					8000	2.0462E-03	9.3085E-03	
					9000	2.2894E-03	1.0415E-02	
					10000	2.5333E-03	1.1524E-02	
11	22	1.1839	0.4940	0.2269	6000	1.5488E-03	6.8247E-03	1.12837E-06
					7000	1.7977E-03	7.9215E-03	
					8000	2.0484E-03	9.0262E-03	
					9000	2.2987E-03	1.0129E-02	
					10000	2.5551E-03	1.1259E-02	
12	24	1.0739	0.4877	0.2006	6000	1.3710E-03	6.8345E-03	1.13991E-06
					7000	1.5909E-03	7.9308E-03	
					8000	1.8310E-03	9.1277E-03	
					9000	2.0610E-03	1.0274E-02	
					10000	2.2900E-03	1.1416E-02	
13	28	1.1791	0.4966	0.2283	6000	1.6340E-03	7.1559E-03	1.17724E-06
					7000	1.8927E-03	8.2888E-03	
					8000	2.1522E-03	9.4253E-03	
					9000	2.4120E-03	1.0563E-02	
					10000	2.6731E-03	1.1706E-02	
14	32	1.1758	0.4821	0.2146	6000	1.4802E-03	6.8968E-03	1.14137E-06
					7000	1.7210E-03	8.0188E-03	
					8000	1.9628E-03	9.1455E-03	
					9000	2.2015E-03	1.0258E-02	
					10000	2.4393E-03	1.1366E-02	
15	36	1.1410	0.4839	0.2098	6000	1.4771E-03	7.0403E-03	1.1557E-06
					7000	1.7156E-03	8.1770E-03	
					8000	1.9578E-03	9.3314E-03	
					9000	2.1199E-03	1.0104E-02	
					10000	2.4403E-03	1.1631E-02	
16	40	1.2167	0.4953	0.2344	6000	1.6334E-03	6.9678E-03	1.14971E-06
					7000	1.8948E-03	8.0829E-03	
					8000	2.1571E-03	9.2018E-03	
					9000	2.4200E-03	1.0323E-02	
					10000	2.6839E-03	1.1449E-02	

Sample No.	Age Time hrs	Length cm	Diameter cm	Volume cc	Field Gauss	Moment emu	Magnetization emu/cc	Mag Sus 1/cc
17	44	1.1621	0.4953	0.2239	6000	1.5897E-03	7.1001E-03	1.17338E-06
					7000	1.8447E-03	8.2390E-03	
					8000	2.1018E-03	9.3873E-03	
					9000	2.3612E-03	1.0546E-02	
					10000	2.6181E-03	1.1693E-02	
18	48	1.1737	0.5032	0.2334	6000	1.5770E-03	6.7567E-03	1.11452E-06
					7000	1.8297E-03	7.8394E-03	
					8000	2.0822E-03	8.9213E-03	
					9000	2.3357E-03	1.0007E-02	
					10000	2.5893E-03	1.1094E-02	
19	56	1.1511	0.5004	0.2264	6000	1.6372E-03	7.2325E-03	1.19325E-06
					7000	1.8997E-03	8.3921E-03	
					8000	2.1622E-03	9.5517E-03	
					9000	2.4238E-03	1.0707E-02	
					10000	2.6904E-03	1.1885E-02	
20	64	1.1501	0.5070	0.2322	6000	1.7197E-03	7.4069E-03	1.22635E-06
					7000	1.9997E-03	8.6128E-03	
					8000	2.2803E-03	9.8214E-03	
					9000	2.5584E-03	1.1019E-02	
					10000	2.8377E-03	1.2222E-02	
21	72	1.1300	0.4958	0.2182	6000	1.5852E-03	7.2656E-03	1.20303E-06
					7000	1.8436E-03	8.4499E-03	
					8000	2.1004E-03	9.6270E-03	
					9000	2.3572E-03	1.0804E-02	
					10000	2.6183E-03	1.2001E-02	
22	84	1.1552	0.4933	0.2208	6000	1.6427E-03	7.4413E-03	1.23132E-06
					7000	1.9098E-03	8.6512E-03	
					8000	2.1759E-03	9.8566E-03	
					9000	2.4414E-03	1.1059E-02	
					10000	2.7096E-03	1.2274E-02	
23	96	1.0795	0.4958	0.2084	6000	1.5897E-03	7.6274E-03	1.26268E-06
					7000	1.8486E-03	8.8696E-03	
					8000	2.1073E-03	1.0111E-02	
					9000	2.3637E-03	1.1341E-02	
					10000	2.6235E-03	1.2588E-02	
24	132	1.1435	0.5017	0.2260	6000	1.6964E-03	7.5058E-03	1.26011E-06
					7000	1.9700E-03	8.7164E-03	
					8000	2.2426E-03	1.0147E-02	
					9000	2.5148E-03	1.1379E-02	
					10000	2.7890E-03	1.2620E-02	

Sample No.	Age Time hrs	Length cm	Diameter cm	Volume cc	Field Gauss	Moment emu	Magnetization emu/cc	Mag Sus 1/cc
25	168	1.1654	0.5090	0.2371	6000	1.7220E-03	7.2614E-03	1.20579E-06
					7000	2.0064E-03	8.4607E-03	
					8000	2.2883E-03	9.6495E-03	
					9000	2.5716E-03	1.0844E-02	
					10000	2.8534E-03	1.2032E-02	
26	241	1.1476	0.5052	0.2300	6000	1.6270E-03	7.0726E-03	1.17188E-06
					7000	1.8926E-03	8.2272E-03	
					8000	2.1579E-03	9.3805E-03	
					9000	2.4224E-03	1.0530E-02	
					10000	2.6887E-03	1.1688E-02	
27	480	1.1029	0.5093	0.2247	6000	1.6936E-03	7.5388E-03	1.245E-06
					7000	1.9648E-03	8.7460E-03	
					8000	2.2384E-03	9.9639E-03	
					9000	2.5125E-03	1.1184E-02	
					10000	2.7863E-03	1.2403E-02	
28	744	1.1610	0.5009	0.2288	6000	1.7670E-03	7.7236E-03	1.27657E-06
					7000	2.0531E-03	8.9742E-03	
					8000	2.3390E-03	1.0224E-02	
					9000	2.6245E-03	1.1472E-02	
					10000	2.9071E-03	1.2707E-02	
29	1080	1.1628	0.4933	0.2222	6000	1.6659E-03	7.4969E-03	1.24219E-06
					7000	1.9421E-03	8.7399E-03	
					8000	2.2183E-03	9.9829E-03	
					9000	2.4730E-03	1.1129E-02	
					10000	2.7496E-03	1.2374E-02	
30	1536	1.1341	0.4851	0.2096	6000	1.5942E-03	7.6044E-03	1.26085E-06
					7000	1.8550E-03	8.8484E-03	
					8000	2.1163E-03	1.0095E-02	
					9000	2.3764E-03	1.1335E-02	
					10000	2.6360E-03	1.2574E-02	
31	1824	1.2167	0.4851	0.2249	6000	1.6599E-03	7.3805E-03	1.22354E-06
					7000	1.9324E-03	8.5922E-03	
					8000	2.2029E-03	9.7949E-03	
					9000	2.4733E-03	1.0997E-02	
					10000	2.7439E-03	1.2200E-02	
32	2184	1.1890	0.5027	0.2360	6000	1.7533E-03	7.4308E-03	1.2338E-06
					7000	2.0425E-03	8.6565E-03	
					8000	2.3294E-03	9.8724E-03	
					9000	2.6189E-03	1.1099E-02	
					10000	2.9046E-03	1.2310E-02	

Region 1 Regression Analysis

Regression Statistics	
Multiple R	0.723258523
R Square	0.523102891
Adjusted R Square	0.046205782
Standard Error	9.03584E-09
Observations	5

Analysis of Variance

	df	*Sum of Squares*	*Mean Square*	*F*	*Significance F*
Regression	2	1.79114E-16	8.95569E-17	1.096888367	0.476897109
Residual	2	1.63293E-16	8.16464E-17		
Total	4	3.42407E-16			

	Coefficients	*Standard Error*	*t Statistic*	*P-value*	*Lower 95%*	*Upper 95%*
Intercept	1.12207E-06	5.8434E-08	19.20235779	4.33433E-05	8.7065E-07	1.37349E-06
Wt. Pct. Cu Coeff	-1.72281E-06	1.31725E-06	-1.307887921	0.261011335	-7.39047E-06	3.94485E-06
log(Time) Coeff	-5.96819E-09	1.6884E-08	-0.353481294	0.741571126	-7.86144E-08	6.6678E-08

Region 2 Regression Analysis

Regression Statistics

Multiple R	0.941537691
R Square	0.886493224
Adjusted R Square	0.871358987
Standard Error	1.88527E-08
Observations	18

Analysis of Variance

	df	*Sum of Squares*	*Mean Square*	*F*	*Significance F*
Regression	2	4.16382E-14	2.08191E-14	58.57535028	8.17831E-08
Residual	15	5.33136E-15	3.55424E-16		
Total	17	4.69695E-14			

	Coefficients	*Standard Error*	*t Statistic*	*P-value*	*Lower 95%*	*Upper 95%*
Intercept	1.02616E-06	3.27227E-08	31.3592657	1.74175E-16	9.56413E-07	1.09591E-06
Wt. Pct. Cu Coeff	-2.92814E-06	6.11186E-07	-4.790916226	0.000170094	-4.23085E-06	-1.62543E-06
log(Time) Coeff	1.63003E-07	1.62378E-08	10.03848775	1.46347E-08	1.28393E-07	1.97613E-07

Region 3 Regression Analysis

Regression Statistics	
Multiple R	0.818781505
R Square	0.670403153
Adjusted R Square	0.610476453
Standard Error	1.86129E-08
Observations	14

Analysis of Variance

	df	*Sum of Squares*	*Mean Square*	*F*	*Significance F*
Regression	2	7.75127E-15	3.87563E-15	11.18705281	0.002233093
Residual	11	3.81083E-15	3.46439E-16		
Total	13	1.15621E-14			

	Coefficients	*Standard Error*	*t Statistic*	*P-value*	*Lower 95%*	*Upper 95%*
Intercept	1.3236E-06	3.86143E-08	34.27740586	3.91887E-14	1.23861E-06	1.40859E-06
Wt. Pct. Cu Coeff	-3.42866E-06	7.99378E-07	-4.289165002	0.000880784	-5.18808E-06	-1.66924E-06
log(Time) Coeff	2.0381E-08	8.82018E-09	2.310720184	0.037897089	9.67873E-10	3.97941E-08

APPENDIX C

ASTM STANDARD

Designation: E 18 – 92

Standard Test Methods for Rockwell Hardness and Rockwell Superficial Hardness of Metallic Materials[1,2]

This standard is issued under the fixed designation E 18; the number immediately following the designation indicates the year of original adoption or, in the case of revision, the year of last revision. A number in parentheses indicates the year of last reapproval. A superscript epsilon (ε) indicates an editorial change since the last revision or reapproval.

This standard has been approved for use by agencies of the Department of Defense to replace method 243.1 of Federal Test Method Standard No. 151b. Consult the DoD Index of Specifications and Standards for the specific year of issue which has been adopted by the Department of Defense.

1. Scope

1.1 These test methods cover the determination of the Rockwell hardness and the Rockwell superficial hardness of metallic materials, including methods for the verification of machines for Rockwell hardness testing (Part B) and the calibration of standardized hardness test blocks (Part C).

1.2 Values stated in inch-pound units are to be regarded as the standard. SI units are provided for information only.

1.3 *This standard does not purport to address all of the safety problems, if any, associated with its use. It is the responsibility of the user of this standard to establish appropriate safety and health practices and determine the applicability of regulatory limitations prior to use.* (See Note 4.)

2. Referenced Documents

2.1 *ASTM Standards:*

A 370 Test Methods and Definitions for Mechanical Testing of Steel Products[3]
B 19 Specification for Cartridge Brass Sheet, Strip, Plate, Bar, and Disks (Blanks)[4]
B 36 Specification for Brass Plate, Sheet, Strip, and Rolled Bar[4]
B 96 Specification for Copper-Silicon Alloy Plate, Sheet, Strip, and Rolled Bar for General Purposes and Pressure Vessels[4]
B 97 Specification for Copper-Silicon Alloy Plate, Sheet, Strip, and Rolled Bar for General Purposes[5]
B 103 Specification for Phosphor Bronze Plate, Sheet, Strip, and Rolled Bar[4]
B 121 Specification for Leaded Brass Plate, Sheet, Strip, and Rolled Bar[4]
B 122 Specification for Copper-Nickel-Tin Alloy, Copper-Nickel-Zinc Alloy (Nickel Silver), and Copper-Nickel Alloy Plate, Sheet, Strip, and Rolled Bar[4]
B 130 Specification for Commercial Bronze Strip for Bullet Jackets[4]
B 134 Specification for Brass Wire[4]
B 152 Specification for Copper Sheet, Strip, Plate, and Rolled Bar[4]
B 291 Specification for Copper-Zinc-Manganese Alloy (Manganese Brass) Sheet and Strip[4]
B 370 Specification for Copper Sheet and Strip for Building Construction[4]
E 4 Practices of Load Verification of Testing Machines[6]
E 6 Terminology Relating to Methods of Mechanical Testing[6]
E 29 Practice for Using Significant Digits in Test Data to Determine Conformance with Specifications[7]
E 140 Standard Hardness Conversion Tables for Metals (Relationship Between Brinell Hardness, Vickers Hardness, Rockwell Hardness, Rockwell Superficial Hardness, and Knoop Hardness)[6]

3. Terminology

3.1 *Rockwell hardness test*—an indentation hardness test using a verified machine to force a diamond spheroconical indenter (diamond indenter), or hard steel ball indenter under specified conditions, into the surface of the material under test in two operations, and to measure the difference in depth of the indentation under the specified conditions of preliminary and total test forces (minor and major loads, respectively).

3.2 *Rockwell superficial hardness test*—same as the Rockwell hardness test except that smaller preliminary and total test forces are used.

3.3 *Rockwell hardness number, HR*—a number derived from the net increase in the depth of indentation as the force on an indenter is increased from a specified preliminary test force to a specified total test force and then returned to the preliminary test force.

3.3.1 *Discussion: Indenters*—Indenters for the Rockwell hardness test include a diamond spheroconical indenter and steel ball indenters of several specified diameters.

3.3.2 *Discussion*—Rockwell hardness numbers are always quoted with a scale symbol representing the indenter and forces used. The hardness number is followed by the symbol HR and the scale designation.

Examples: 64 HRC = Rockwell hardness number of 64 on Rockwell

---

[1] These test methods are under the jurisdiction of ASTM Committee E-28 on Mechanical Testing and are the direct responsibility of Subcommittee E28.06 on Indentation Hardness Testing.

Current edition approved Jan. 15, 1992. Published March 1992. Originally published as E 18 – 32 T. Last previous edition E 18 – 89a.

[2] In this test method, the term Rockwell refers to an internationally recognized type of indentation hardness test as defined in Section 3, and not to the hardness testing equipment of a particular manufacturer.

[3] *Annual Book of ASTM Standards*, Vols 01.01-01.05, and 03.01.

[4] *Annual Book of ASTM Standards*, Vol 02.01.

[5] Discontinued, see *1981 Annual Book of ASTM Standards*, Part 6.

[6] *Annual Book of ASTM Standards*, Vol 03.01.

[7] *Annual Book of ASTM Standards*, Vols 02.03, 03.0[illegible], and 14.02.

C scale. 81 HR30N = Rockwell superficial hardness number of 81 on Rockwell 30N scale.

3.4 *verification*—checking or testing to assure conformance with the specification.

3.5 *calibration*—determination of the values of the significant parameters by comparison with values indicated by a reference instrument or by a set of reference standards.

4. Significance and Use

4.1 The Rockwell hardness test is an empirical indentation hardness test. Rockwell hardness tests provide useful information about metallic materials. This information may correlate to tensile strength, wear resistance, ductility, and other physical characteristics of metallic materials, and may be useful in quality control and selection of materials.

4.2 Rockwell hardness testing at a specific location on a part may not represent the physical characteristics of the whole part or end product.

4.3 Rockwell hardness tests are considered satisfactory for acceptance testing of commercial shipments, and have been used extensively in industry for this purpose.

A. GENERAL DESCRIPTION AND TEST PROCEDURE FOR ROCKWELL HARDNESS AND ROCKWELL SUPERFICIAL HARDNESS TESTS

5. Apparatus

5.1 *General Principles*—The general principles of the Rockwell hardness test are illustrated in Fig. 1 (diamond indenter) and Fig. 2 (ball indenters) and the accompanying Tables 1 and 2. In the case of the Rockwell superficial test the general principles are illustrated in Fig. 3 (diamond indenter) and Fig. 4 (ball indenter) and the accompanying Tables 3 and 4.

5.1.1 See *Equipment Manufacturer's Instruction Manual* for a description of the machine's characteristics, limitations, and respective operating procedures. Typical applications of the various hardness scales are shown in Tables 5 and 6. Rockwell hardness values are usually determined and reported in accordance with one of these standard scales. An indenter (diamond cone or steel ball) is forced into the surface of a test piece in two steps under specified conditions (see Section 7) and the difference in depth of indentation is measured as *e*.

5.1.2 The unit measurement for *e* is 0.002 mm and 0.001 mm for the Rockwell hardness test and Rockwell superficial hardness test, respectively. From the value of *e*, a number known as the Rockwell hardness is derived. There is no Rockwell hardness value designated by a number alone because it is necessary to indicate which indenter and force have been employed in making the test (see Tables 5 and 6).

5.2 *Description of Machine and Method of Test*—The tester for making Rockwell hardness determinations is a machine that measures hardness by determining the difference in penetration depths of an indenter under two specified forces, called preliminary and total test forces.

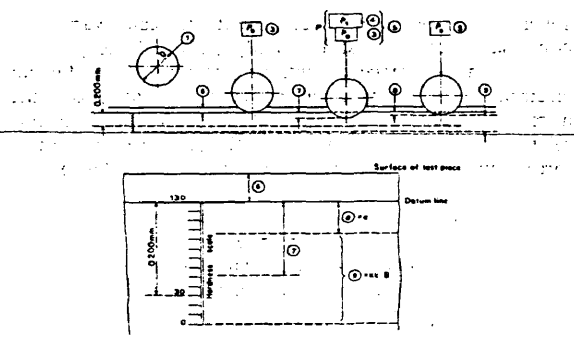

FIG. 2 Rockwell Hardness Test with Steel Ball Indenter (Rockwell B Example) (Table 2)

5.2.1 There are two general classifications of the Rockwell test: the Rockwell hardness test and the Rockwell superficial hardness test.

5.2.2 In the Rockwell hardness test the preliminary test force is 10 kgf (98 N). Total test forces are 60 kgf (589 N), 100 kgf (981 N) and 150 kgf (1471 N). In the Rockwell superficial hardness test the preliminary test force is 3 kgf (29 N) and total test forces are 15 kgf (147 N), 30 kgf (294 N), and 45 kgf (441 N). The indenter for either test shall be of a

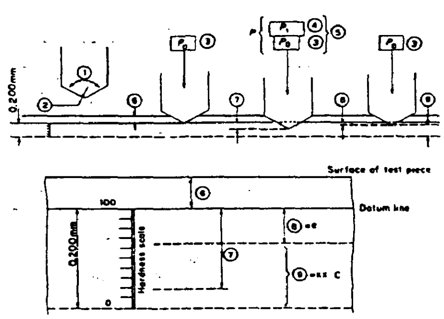

FIG. 1 Rockwell Hardness Test with Diamond Indenter (Rockwell C Example) (Table 1)

TABLE 1 Symbols and Designations Associated with Fig. 1

Number	Symbol	Designation
1	...	Angle at the top of the diamond indenter (120°)
2	...	Radius of curvature at the tip of the cone (0.200 mm)
3	P_0	Preliminary Test Force = 10 kgf (98 N)
4	P_1	Additional Force = 90 or 140 kgf (883 or 1373 N)
5	P	Total Test Force = $P_0 + P_1$ = 10 + 140 = 150 kgf (147 N)
6	...	Depth of penetration under test force before application of additional load
7	...	Increase in depth of penetration under additional load
8	e	Permanent increase in depth of penetration under preliminary test force after removal of additional force, the increase being expressed in units of 0.002 mm
9	xx HRC	Rockwell C hardness = 100 − e

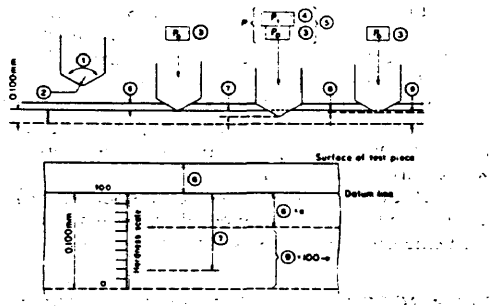

FIG. 3 Rockwell Superficial Hardness Test with Diamond Indenter (Rockwell 30N Example) (Table 3)

spheroconical or spherical configuration. Scales vary by a combination of total test force and type of indenter.

5.2.3 The difference in depth is normally measured by an electronic device or by a dial indicator. The hardness value, as read from the instrument, is an arbitrary number which is related to the difference in the depths produced by the two forces; and since the scales are reversed, the higher the number the harder the material.

5.2.4 In accordance with the operating procedures recommended by the manufacturer of the hardness tester, the test is started by applying the preliminary test force causing an initial penetration of the specimen. Since measurement of the difference in depth starts after the preliminary force has been applied, the dial gage pointer is set to zero if the instrument is a dial indicator model. On a digital readout instrument, the zero point is captured by the electronics automatically. The instrument shall be designed to eliminate the effect of impact in applying the preliminary test force.

5.2.5 The additional force is applied for the required dwell time and then removed. The return to the preliminary test force position holds the indenter at the point of deepest penetration yet allows elastic recovery to occur and the stretch of the frame to be factored out. The test result is displayed by the testing machine.

5.3 *Indenters*:

5.3.1 The standard indenters, as have been mentioned in 3.3, are the diamond spheroconical indenter and steel ball

TABLE 2 Symbols and Designations Associated with Fig. 2.

Number	Symbol	Designation
1	D	Diameter of ball = 1/16 in. (1.588 mm)
3	P_0	Preliminary Test Force = 10 kgf (98 N)
4	P_1	Additional force = 90 kgf (883 N)
5	P	Total Test Force = $P_0 + P_1$ = 10 + 90 = 100 kgf (981 N)
6	...	Depth of penetration under preliminary test force before application of additional force
7	...	Increase in depth of penetration under additional force
8	e	Permanent increase in depth of penetration under preliminary test force after removal of the additional force, the increase being expressed in units of 0.002 mm
9	xx HRB	Rockwell B hardness = 130 − e

TABLE 3 Symbols and Designations Associated with Fig. 3

Number	Symbol	Designation
1	...	Angle at the tip of the diamond indenter (120°)
2	...	Radius of curvature at the tip of the cone (0.200 mm)
3	P_0	Preliminary Test Force = 3 kgf (29 N)
4	P_1	Additional force = 27 kgf (265 N)
5	P	Total Test Force = $P_0 + P_1$ = 3 + 27 = 30 kgf (294 N)
6	...	Depth of penetration under preliminary test force before application of additional force
7	...	Increase in depth of penetration under additional force
8	e	Permanent increase in depth of penetration under preliminary test force after removal of additional force, the increase being expressed in units of 0.001 mm
9	xx HR30N	Rockwell 30N hardness = 100 − e

indenters 1/16, 1/8, 1/4, and 1/2 in. (1.588, 3.175, 6.350, and 12.70 mm) in diameter.

5.3.2 The diamond indenter shall conform to the requirements prescribed in 13.1.2.1.

5.3.3 The steel balls shall conform to the requirements prescribed in 13.1.2.2.

5.3.4 Dust, dirt, grease, and scale shall not be allowed to accumulate on the indenter as this will affect the test results.

5.4 *Anvils*—When required, an anvil shall be used that is suitable for the specimen to be tested. Cylindrical pieces shall be tested with a V-grooved anvil that will support the specimen with the axis of the V-groove directly under the indenter or on hard, parallel, twin cylinders properly posi-

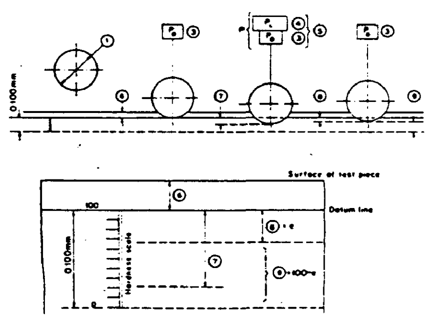

FIG. 4 Rockwell Superficial Hardness Test with Steel Ball Indenter (Rockwell 30T Example) (Table 4)

TABLE 4 Symbols and Designations Associated with Fig. 4

Number	Symbol	Designation
1	D	Diameter of ball = 1/16 in. (1.588 mm)
3	P_0	Preliminary Test Force = 3 kgf (29 N)
4	P_1	Additional force = 27 kgf (265 N)
5	P	Total Test Force = $P_0 + P_1$ = 3 + 27 = 30 kgf (294 N)
6	...	Depth of penetration under preliminary test force before application of additional force
7	...	Increase in depth of penetration under additional force
8	e	Permanent increase in depth of penetration under preliminary test force after removal of the additional force, the increase being expressed in units of 0.001 mm
9	xx HR15T xx HR30T xx HR45T	Rockwell 15T hardness = 100 − e Rockwell 30T hardness = 100 − e Rockwell 45T hardness = 100 − e

TABLE 5 Rockwell Hardness Scales

Scale Symbol	Indenter	Total Test Force, kgf	Dial Figures	Typical Applications of Scales
B	1/16-in. (1.588-mm) ball	100	red	Copper alloys, soft steels, aluminum alloys, malleable iron, etc.
C	diamond	150	black	Steel, hard cast irons, pearlitic malleable iron, titanium, deep case hardened steel, and other materials harder than B 100.
A	diamond	60	black	Cemented carbides, thin steel, and shallow case-hardened steel.
D	diamond	100	black	Thin steel and medium case hardened steel, and pearlitic malleable iron.
E	1/8-in. (3.175-mm) ball	100	red	Cast iron, aluminum and magnesium alloys, bearing metals.
F	1/16-in. (1.588-mm) ball	60	red	Annealed copper alloys, thin soft sheet metals.
G	1/16-in. (1.588-mm) ball	150	red	Malleable irons, copper-nickel-zinc and cupro-nickel alloys. Upper limit G 92 to avoid possible flattening of ball.
H	1/8-in. (3.175-mm) ball	60	red	Aluminum, zinc, lead.
K	1/8-in. (3.175-mm) ball	150	red	Bearing metals and other very soft or thin materials. Use smallest ball and heaviest load that does not give anvil effect.
L	1/4-in. (6.350-mm) ball	60	red	
M	1/4-in. (6.350-mm) ball	100	red	
P	1/4-in. (6.350-mm) ball	150	red	
R	1/2-in. (12.70-mm) ball	60	red	
S	1/2-in. (12.70-mm) ball	100	red	
V	1/2-in. (12.70-mm) ball	150	red	

TABLE 6 Rockwell Superficial Hardness Scales

Total Test Force, kgf (N)	Scale Symbols				
	N Scale, Diamond Indenter	T Scale, 1/16-in. (1.588-mm) Ball	W Scale, 1/8-in. (3.175-mm) Ball	X Scale, 1/4-in. (6.350-mm) Ball	Y Scale, 1/2-in. (12.70-mm) Ball
15 (147)	15N	15T	15W	15X	15Y
30 (294)	30N	30T	30W	30X	30Y
45 (441)	45N	45T	45W	45X	45Y

tioned and clamped in their base. Flat pieces shall be tested on a flat anvil that has a smooth, flat bearing surface whose plane is perpendicular to the axis of the indenter. For thin materials or specimens that are not perfectly flat, an anvil having an elevated, flat "spot" about 1/4 in. (6 mm) in diameter shall be used. This spot shall be polished smooth and flat and shall have a Rockwell hardness of at least 60 HRC. The seating and supporting surfaces of all anvils shall be clean and smooth and shall be free from pits, heavy scratches, dust, dirt, and grease. If the provisions of 6.3 on thickness of the test piece are compiled with, there will be no danger of indenting the anvil, but, if it is so thin that the impression shows through on the under side, the anvil may be damaged. Damage may also occur from accidental contacting of the anvil by the indenter. If the anvil is damaged from any cause, it shall be replaced. Anvils showing the least perceptible dent will give inaccurate results on thin material. Very soft material should not be tested on the "spot" anvil because the applied load may cause the penetration of the anvil into the under side of the specimen regardless of its thickness.

5.5 *Test Blocks*—Test blocks meeting the requirements of Part C shall be used to periodically verify the hardness tester.

6. Test Piece

6.1 The test shall be carried out on a smooth, even surface that is free from oxide scale, foreign matter, and, in particular, completely free from lubricants (except for reactive metals, such as titanium where lubrication such as kerosene is required).

6.2 Preparation shall be carried out in such a way that any alteration of the surface hardness (for example, due to heat or cold-working) is minimized.

6.3 The thickness of the test piece or of the layer under test should be as dictated in Tables 7, 8, 9, and 10 and as presented graphically in Figs. 5 and 6. As a general rule, the thickness should exceed 10 times the depth of the indentation. As a rule, no deformation should be visible on the back of the test piece after the test although not all such marking is indicative of a bad test.

6.4 For tests on convex cylindrical surfaces the corrections

TABLE 7 A Minimum Thickness Guide for Selection of Scales Using the Diamond Indenter (see Fig. 6)

NOTE—For any given thickness, the indicated Rockwell hardness is the minimum value acceptable for testing. For a given hardness, material of any greater thickness than that corresponding to that hardness can be tested on the indicated scale.

Minimum Thickness		Rockwell Scale		
		A		C
in.	mm	Hardness Reading	Approximate Hardness C-Scale[A]	Dial Reading
0.014	0.36	...	...	...
0.016	0.41	86	69	...
0.018	0.46	84	65	...
0.020	0.51	82	61.5	...
0.022	0.56	79	56	69
0.024	0.61	76	50	67
0.026	0.66	71	41	65
0.028	0.71	67	32	62
0.030	0.76	60	19	57
0.032	0.81	...	...	52
0.034	0.86	...	...	45
0.036	0.91	...	...	37
0.038	0.96	...	...	28
0.040	1.02	...	...	20

[A] These approximate hardness numbers are for use in selecting a suitable scale and should not be used as hardness conversions. If necessary to convert test readings to another scale, refer to Hardness Conversion Tables E 140 (Relationship Between Brinell Hardness, Vickers Hardness, Rockwell Hardness, Rockwell Superficial Hardness, and Knoop Hardness).

TABLE 8 A Minimum Thickness Guide for Selection of Scales Using the 1/16-in. (1.588-mm) Diameter Ball Indenter (see Fig. 7)

NOTE—For any given thickness, the indicated Rockwell hardness is the minimum value acceptable for testing. For a given hardness, material of any greater thickness than that corresponding to that hardness can be tested on the indicated scale.

Minimum Thickness		Rockwell Scale		
		F		B
in.	mm	Hardness Reading	Approximate Hardness B-Scale[A]	Hardness Reading
0.022	0.56	...	...	...
0.024	0.61	98	72	94
0.026	0.66	91	60	87
0.028	0.71	85	49	80
0.030	0.76	77	35	71
0.032	0.81	69	21	62
0.034	0.86	...	...	52
0.036	0.91	...	...	40
0.038	0.96	...	...	28
0.040	1.02	...	...	...

[A] These approximate hardness numbers are for use in selecting a suitable scale and should not be used as hardness conversions. If necessary to convert test readings to another scale refer to Hardness Conversion Tables E 140 (Relationship Between Brinell Hardness, Vickers Hardness, Rockwell Hardness, Rockwell Superficial Hardness and Knoop Hardness).

given in Tables 11, 12, 13, and 14 shall be applied. Corrections for tests on spherical and concave surfaces should be the subject of special agreement. When testing cylindrical specimens, the accuracy of the test will be seriously affected by alignment of elevating screw, V-anvil, indenters, surface finish, and the straightness of the cylinder.

6.5 *Precautions for materials having excessive, time-dependent plasticity (indentation creep)*: In the case of materials exhibiting plastic flow after application of the total test force, the indenter will continue to move. The total test force should be removed after the specified dwell time, and the time recorded after the test results (that is, 65 HRF, 4 s) if longer than 3 s. When materials require the use of a dwell time greater than 3 s, this should be specified in the product specification.

7. Procedure

7.1 The test is normally carried out at ambient temperature within the limits of 50 to 95°F (10 to 35°C). Tests carried out under controlled conditions shall be made at a temperature of 73 ± 9°F (23 ± 5°C).

7.2 The test piece shall be supported rigidly so that no effects of displacement occur during the test.

7.3 Bring the indenter into contact with the test surface and apply the preliminary test force P_0 (minor load) of 10 kgf (98 N) for the Rockwell hardness test or 3 kgf (29 N) for Rockwell superficial hardness test in a direction perpendicular to the surface without shock or vibration. (See Table 15 for tolerances of test forces.) The dwell time for the preliminary test force shall not exceed 3 s.

7.4 Establish the reference position (see *Manufacturer's Instruction Manual*) and increase the force, without shock or vibration, over a period of 1 to 8 s by the value of the additional test force, P_1 (additional load) needed to obtain the required total test force P for a given hardness scale (see Tables 5 and 6).

7.5 While maintaining the preliminary test force P_0, remove the additional test force P_1 in accordance with the following:

7.5.1 For materials which, under the conditions of the test, show no time-dependent plasticity, remove P_1 within 3 s after the total test force is applied.

7.5.2 For materials which, under the conditions of the test, show some time-dependent plasticity, remove P_1 within 5 to 6 s when using diamond cone indenter and within 6 to 8 s when using steel ball indenter after the application of the total test force begins.

7.5.3 In special cases where the material, under the conditions of the test, shows considerable time-dependent plasticity, remove P_1 within 20 to 25 s after the application of the total test force begins.

7.5.4 When materials require the use of a dwell time greater than 3 s, this shall be specified in the product specification, and the dwell time shall be recorded.

TABLE 9 A Minimum Thickness Guide for Selection of Scales Using the Diamond Indenter (see Fig. 6)

NOTE—For any given thickness, the indicated Rockwell hardness is the minimum value acceptable for testing. For a given hardness, material of any greater thickness than that corresponding to that hardness can be tested on the indicated scale

Minimum Thickness		Rockwell Superficial Scale					
		15N		30N		45N	
in.	mm	Hardness Reading	Approximate Hardness C-Scale[A]	Hardness Reading	Approximate Hardness C-Scale[A]	Hardness Reading	Approximate Hardness C-Scale[A]
0.006	0.15	92	65	...	...	...	...
0.008	0.20	90	60	...	...	...	...
0.010	0.25	88	55	...	...	...	...
0.012	0.30	83	45	82	65	77	69.5
0.014	0.36	76	32	78.5	61	74	67
0.016	0.41	68	18	74	56	72	65
0.018	0.46	...	...	66	47	68	61
0.020	0.51	...	...	57	37	63	57
0.022	0.56	...	...	47	26	58	52.5
0.024	0.61	...	...	...	...	51	47
0.026	0.66	...	...	...	...	37	35
0.028	0.71	...	...	...	...	20	20.5
0.030	0.76	...	...	...	...	...	...

[A] These approximate hardness numbers are for use in selecting a suitable scale, and should not be used as hardness conversions. If necessary to convert test readings to another scale, refer to Hardness Conversion Tables E 140 (Relationship Between Brinell Hardness, Vickers Hardness, Rockwell Hardness, Rockwell Superficial Hardness and Knoop Hardness).

TABLE 10 A Minimum Thickness Guide for Selection of Scales Using the 1/16 in. (1.588 mm) Diameter Ball Indenter (see Fig. 7)

NOTE—For any given thickness, the indicated Rockwell hardness is the minimum value acceptable for testing. For a given hardness, material of any greater thickness than that corresponding to that hardness can be tested on the indicated scale.

Minimum Thickness		Rockwell Superficial Scale					
		15T		30T		45T	
in.	mm	Hardness Reading	Approximate Hardness B-Scale[A]	Hardness Reading	Approximate Hardness B-Scale[A]	Hardness Reading	Approximate Hardness B-Scale[A]
0.010	0.25	91	93	...	...	...	...
0.012	0.30	86	78	...	...	...	...
0.014	0.36	81	62	80	96	...	...
0.016	0.41	75	44	72	84	71	99
0.018	0.46	68	24	64	71	62	90
0.020	0.51	...	...	55	58	53	80
0.022	0.56	...	...	45	43	43	70
0.024	0.61	...	...	34	28	31	58
0.026	0.66	...	...	...	...	18	45
0.028	0.71	...	...	...	...	4	32
0.030	0.76	...	...	...	...	...	...

[A] These approximate hardness numbers are for use in selecting a suitable scale, and should not be used as hardness conversions. If necessary to convert test readings to another scale refer to Hardness Conversion Tables E 140 (Relationship Between Brinell Hardness, Vickers Hardness, Rockwell Hardness, Rockwell Superficial Hardness and Knoop Hardness).

7.6 Throughout the test, the apparatus shall be protected from shock or vibration.

7.7 The Rockwell hardness number is derived from the differential increase in depth of indentation *e* and is usually read directly. The derivation of the Rockwell hardness number is illustrated in Figs. 1 through 4.

7.8 After each change, or removal and replacement, of the indenter or the anvil, it shall be ascertained that the new indenter (or the new anvil) is correctly mounted in its housing.

7.8.1 The first two readings after a new indenter or anvil has been mounted shall be disregarded, and the operation of the machine checked with the appropriate standardized hardness test block.

NOTE 1—It is recognized that appropriate standardized test blocks are not available for all geometric shapes, or materials, or both.

7.9 The distance between the center of two adjacent indentations shall be at least three times the diameter of the indentation.

7.9.1 The distance from the center of any indentation to an edge of the test piece shall be at least two and a half times the diameter of the indentation.

7.10 Unless otherwise specified, all readings are to be reported to the nearest whole number, rounding in accordance with Practice E 29.

8. Conversion to Other Hardness Scales or Tensile Strength Values

8.1 There is no general method of accurately converting the Rockwell hardness numbers on one scale to Rockwell hardness numbers on another scale, or to other types of hardness numbers, or to tensile strength values. Such conversions are, at best, approximations and, therefore, should be avoided except for special cases where a reliable basis for the approximate conversion has been obtained by comparison tests.

NOTE 2—The Standard Hardness Conversion Tables E 140, for Metals, give approximate conversion values for specific materials such as steel, austenitic stainless steel, nickel and high-nickel alloys, cartridge brass, copper alloys, and alloyed white cast irons.

NOTE 3—ASTM Specifications giving approximate hardness-tensile strength relationships are listed in Appendix X1.

9. Report

9.1 The report shall include the following information:

9.1.1 The Rockwell hardness number (see 3.3.2).

9.1.1.1 All reports of Rockwell hardness test readings shall indicate the scale used. Unless otherwise specified, all readings are to be reported to the nearest whole number, rounding to be in accordance with Practice E 29.

9.1.2 The time of application of the total test force if greater than 3 s.

10. Precision and Bias

10.1 *Precision*—An interlaboratory test program is now in progress. When completed, it will be the basis of a statement on precision.

10.2 *Bias*—There is no basis for defining the bias for this method.

B. VERIFICATION OF MACHINES FOR ROCKWELL HARDNESS AND ROCKWELL SUPERFICIAL HARDNESS TESTING

11. Scope

11.1 Part B covers two procedures for the verification of machines for Rockwell hardness and Rockwell superficial hardness testing and a procedure which is recommended for use to confirm that the machine is operating satisfactorily in the intervals between the periodical routine checks made by the user. The two methods of verification are:

11.1.1 Separate verification of test force, indenter, and the depth measuring device followed by a performance test (13.2). This method shall be used for new and rebuilt machines.

11.1.2 Verification by standardized test block method.

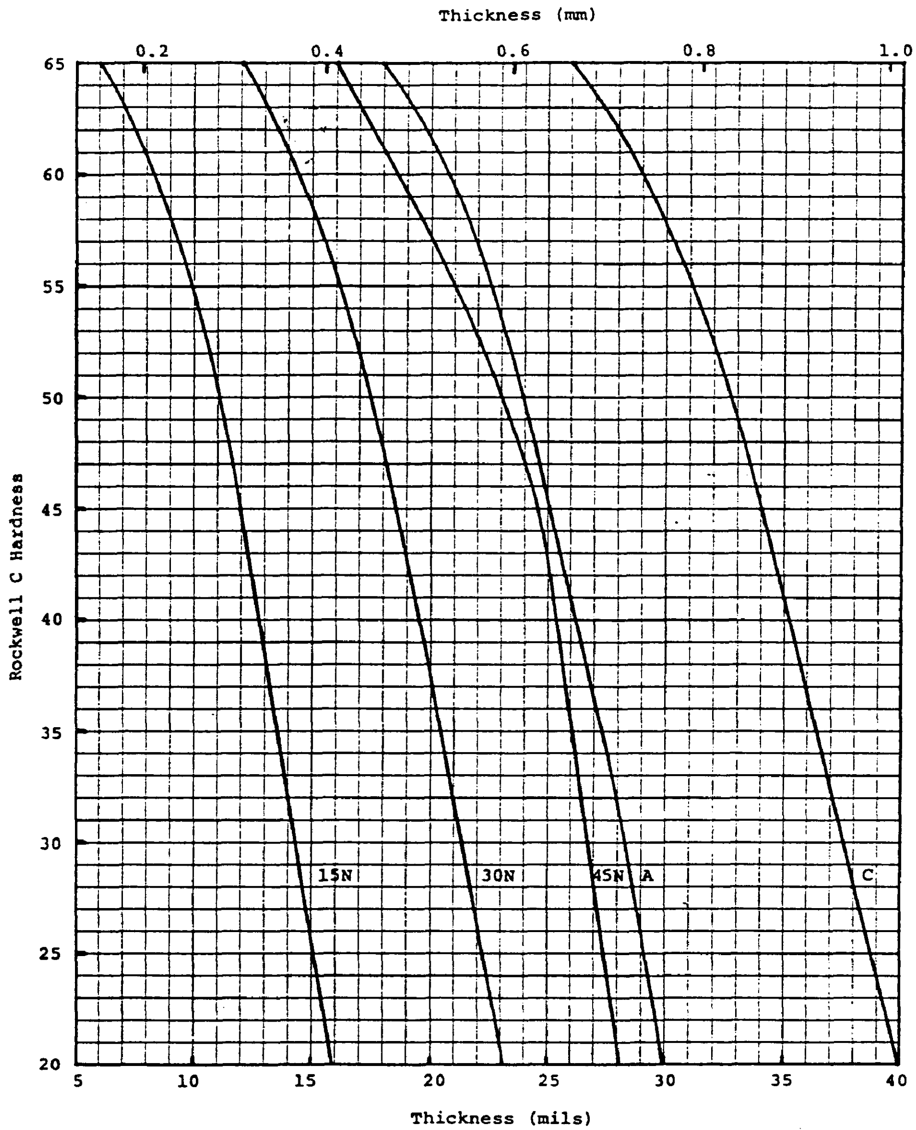

NOTE—Locate a point corresponding to the thickness-hardness combination to be tested. Only scales falling to the left of this point may be used to test this combination.

FIG. 5 Thickness Limits for Rockwell Hardness Testing Using the Diamond Indenter

This method shall be used in referee, laboratory, or routine testing to assure the operator that the machine for Rockwell hardness testing is operating properly (see 13.2).

12. General Requirements

12.1 Before a Rockwell hardness testing machine is verified, it shall be checked to ensure that:

12.1.1 The machine is properly set up.

12.1.2 The indenter-holder is properly seated in the plunger.

12.1.3 When the indenter is a steel ball, the holder is fitted with a new ball that complies with 13.1.2.2.

12.1.4 When the indenter is a diamond indenter, it must be free from defects which may affect the accuracy of the test (See 13.1.2.1).

12.1.5 The test force can be applied and removed without shock or vibration and in such a manner that the readings are not influenced.

12.1.6 The readings are not affected by deformations of the frame.

13. Verification

13.1 Direct Verification—Direct verification involves verification of the test force, verification of the indenter, and verification of the measuring device.

13.1.1 *Verification of the Test Force*:

E 18

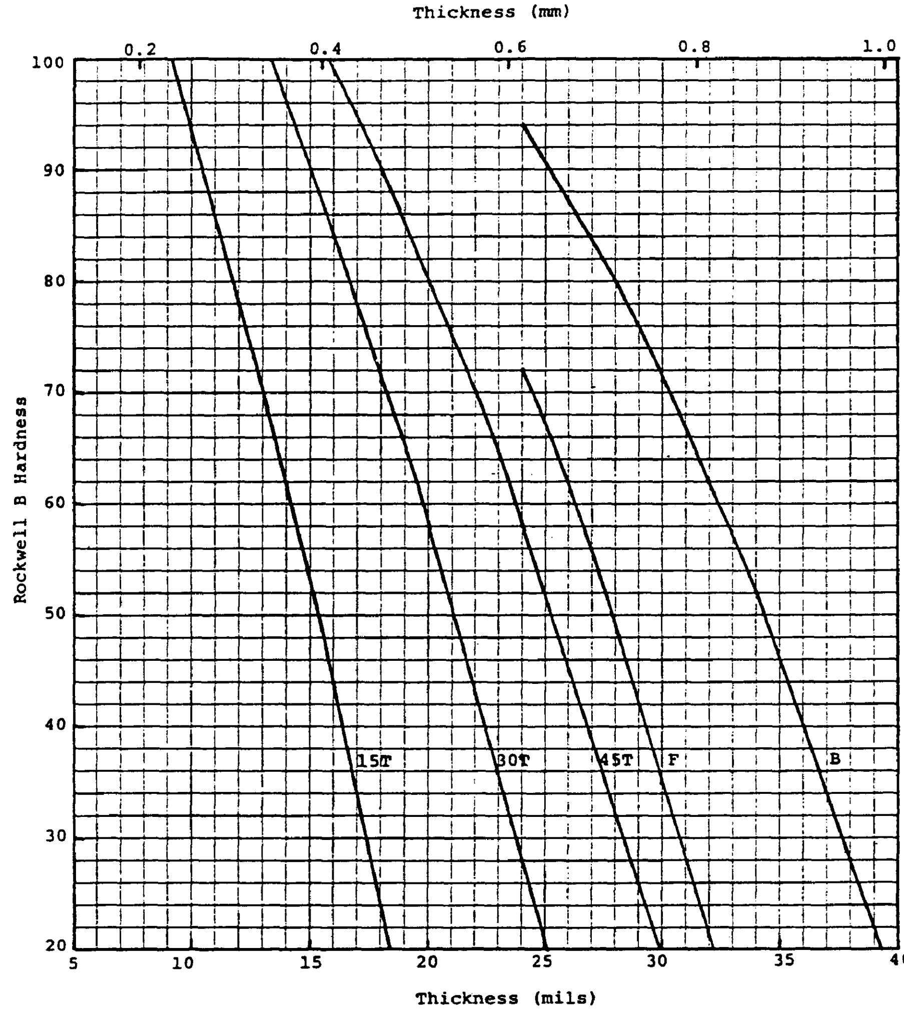

NOTE—Locate a point corresponding to the thickness-hardness combination to be tested. Only scales falling to the left of this point may be used to test this combination.

FIG. 6 Thickness Limits for Rockwell Hardness Testing Using the 1/16-in. (1.588-mm) Diameter Ball Indenter

13.1.1.1 The preliminary test force P_0 and each total test force P used (see Table 15) shall be measured, and this shall be done at not less than three positions of the plunger uniformly spaced throughout its range of movement during testing.

13.1.1.2 The forces shall be measured by one of the following two methods described in Practices E 4.

(a) Measuring by means of an elastic proving device previously calibrated to Class A accuracy of ±0.25 %, or

(b) balancing against a force, accurate to ±0.25 % applied by means of standardized masses with mechanical advantage.

13.1.1.3 Three readings shall be taken for each force at each position of the plunger. Immediately before each reading is taken, the plunger shall have been moved in the same direction as during testing.

13.1.1.4 Each measurement of the preliminary test force before application and after removal of the additional test force and each measurement of the total force shall be within the tolerances given in Table 15.

13.1.2 Verification of the indenter.

13.1.2.1 *Diamond Indenter.*

(a) The diamond indenter shall be free from surface defects (cracks, chips, pits, etc.) and polished to such an extent that no unpolished part of its surface makes contact with the test piece when the indenter penetrates to a depth of 0.3 mm for Rockwell hardness testing and 0.2 mm for Rockwell superficial hardness testing.

(b) The verification of the shape of the indenter can be made by direct measurement or by measurement of its projection on a screen. The verification shall be made at not less than four approximately equally spaced sections.

(c) The diamond indenter shall have an included angle of 120° ± 0.35°.

(d) The angle between the axis of the diamond indenter

TABLE 11 Corrections to Be Added to Rockwell C, A, and D Values Obtained on Convex Cylindrical Surfaces[A] of Various Diameters

Dial Reading	Diameters of Convex Cylindrical Surfaces								
	1/4 in. (6.4 mm)	3/8 in. (10 mm)	1/2 in. (13 mm)	5/8 in. (16 mm)	3/4 in. (19 mm)	7/8 in. (22 mm)	1 in. (25 mm)	1 1/4 in. (32 mm)	1 1/2 in. (38 mm)
	Corrections to be Added to Rockwell C, A, and D Values[B]								
20	6.0	4.5	3.5	2.5	2.0	1.5	1.5	1.0	1.0
25	5.5	4.0	3.0	2.5	2.0	1.5	1.0	1.0	1.0
30	5.0	3.5	2.5	2.0	1.5	1.5	1.0	1.0	0.5
35	4.0	3.0	2.0	1.5	1.5	1.0	1.0	0.5	0.5
40	3.5	2.5	2.0	1.5	1.0	1.0	1.0	0.5	0.5
45	3.0	2.0	1.5	1.0	1.0	1.0	0.5	0.5	0.5
50	2.5	2.0	1.5	1.0	1.0	0.5	0.5	0.5	0.5
55	2.0	1.5	1.0	1.0	0.5	0.5	0.5	0.5	0
60	1.5	1.0	1.0	0.5	0.5	0.5	0.5	0	0
65	1.5	1.0	1.0	0.5	0.5	0.5	0.5	0	0
70	1.0	1.0	0.5	0.5	0.5	0.5	0.5	0	0
75	1.0	0.5	0.5	0.5	0.5	0.5	0	0	0
80	0.5	0.5	0.5	0.5	0.5	0	0	0	0
85	0.5	0.5	0.5	0	0	0	0	0	0
90	0.5	0	0	0	0	0	0	0	0

[A] When testing cylindrical specimens, the accuracy of the test will be seriously affected by alignment of elevating screw, V-anvil, indenters, surface finish, and the straightness of the cylinder.
[B] These corrections are approximate only and represent the averages to the nearest 0.5 Rockwell number, of numerous actual observations.

TABLE 12 Corrections to Be Added to Rockwell B, F, and G Values Obtained on Convex Cylindrical Surfaces[A] of Various Diameters

Hardness Reading	Diameters of Convex Cylindrical Surfaces						
	1/4 in. (6.4 mm)	3/8 in. (10 mm)	1/2 in. (13 mm)	5/8 in. (16 mm)	3/4 in. (19 mm)	7/8 in. (22 mm)	1 in. (25 mm)
	Corrections to be Added to Rockwell B, F, and G Values[B]						
0	12.5	8.5	6.5	5.5	4.5	3.5	3.0
10	12.0	8.0	6.0	5.0	4.0	3.5	3.0
20	11.0	7.5	5.5	4.5	4.0	3.5	3.0
30	10.0	6.5	5.0	4.5	3.5	3.0	2.5
40	9.0	6.0	4.5	4.0	3.0	2.5	2.5
50	8.0	5.5	4.0	3.5	3.0	2.5	2.0
60	7.0	5.0	3.5	3.0	2.5	2.0	2.0
70	6.0	4.0	3.0	2.5	2.0	2.0	1.5
80	5.0	3.5	2.5	2.0	1.5	1.5	1.5
90	4.0	3.0	2.0	1.5	1.5	1.5	1.0
100	3.5	2.5	1.5	1.5	1.0	1.0	0.5

[A] When testing cylindrical specimens, the accuracy of the test will be seriously affected by alignment of elevating screw, V-anvil, indenters, surface finish, and the straightness of the cylinder.
[B] These corrections are approximate only and represent the averages to the nearest 0.5 Rockwell number, of numerous actual observations.

and the axis of the indenter holder (normal to the seating surface) shall not exceed 0.5°.

(e) The spherical tip of the diamond cone shall have a mean radius of 0.200 ± 0.010 mm. In each measured section the radius shall be 0.200 ± 0.015 mm and local deviations from a true radius shall not exceed 0.002 mm. The surfaces of the cone and spherical tip shall blend in a truly tangential manner.

(f) The hardness values given by the testing machine do not depend only on the dimensions given in 13.1.2.1 (c-e), but also on the surface roughness and the position of the crystallographic axis of the diamond and the seating of the diamond in its holder. For this reason, a performance test is considered necessary. The indenter shall be used in a standardizing machine in which the test force applied and the measuring device can be verified by fundamental measurement. Tests shall be made on a minimum of two standardized blocks, one from each of the minimum and maximum ranges specified in Table 16. Three test impressions shall be made on each of these blocks. The mean of these readings shall not differ from the value of the standardized test block by more than the amount shown in Table 17.

13.1.2.2 *Steel Balls:*

NOTE 4: **Caution**—Only steel balls should be used. Balls made out of other hard materials such as tungsten carbide may give different results.

(a) For the purpose of verifying the size and the hardness of the indenter, it is considered sufficient to test a sample selected at random from a batch. The ball(s) verified for hardness shall be discarded.

(b) The ball shall be polished and free from surface defects.

(c) The user shall either measure the balls to ensure that they meet the following requirements, or he shall obtain balls from a supplier who can certify that the following conditions are met. The diameter, when measured at not less than three positions, shall not differ from the nominal diameter by more than the tolerance given in Table 18. The hardness shall not be less than 850 HV 10. Mean diagonals of Vickers impressions corresponding to this hardness level are given in Table 19.

13.1.3 *Verification of the Measuring Device:*

13.1.3.1 The depth-measuring device shall be verified over not less than three intervals, including the intervals

TABLE 13 Corrections to Be Added to Rockwell Superficial 15N, 30N, and 45N Values Obtained on Convex Cylindrical Surfaces of Various Diameters[A]

Hardness Reading	Diameters of Convex Cylindrical Surfaces					
	1/8 in. (3.2 mm)	1/4 in. (6.4 mm)	3/8 in. (10 mm)	1/2 in. (13 mm)	3/4 in. (19 mm)	1 in. (25 mm)
	Corrections to be Added to Rockwell Superficial 15N, 30N, and 45N Values[B]					
20	6.0	3.0	2.0	1.5	1.5	1.5
25	5.5	3.0	2.0	1.5	1.5	1.0
30	5.5	3.0	2.0	1.5	1.0	1.0
35	5.0	2.5	2.0	1.5	1.0	1.0
40	4.5	2.5	1.5	1.5	1.0	1.0
45	4.0	2.0	1.5	1.0	1.0	1.0
50	3.5	2.0	1.5	1.0	1.0	0.5
55	3.5	2.0	1.5	1.0	0.5	0.5
60	3.0	1.5	1.0	1.0	0.5	0.5
65	2.5	1.5	1.0	0.5	0.5	0.5
70	2.0	1.0	1.0	0.5	0.5	0.5
75	1.5	1.0	0.5	0.5	0.5	0
80	1.0	0.5	0.5	0.5	0	0
85	0.5	0.5	0.5	0.5	0	0
90	0	0	0	0	0	0

[A] When testing cylindrical specimens the accuracy of the test will be seriously affected by alignment of elevating screw, V-anvil, indenters, surface finish, and the straightness of the cylinder.

[B] These corrections are approximate only and represent the averages, to the nearest 0.5 Rockwell superficial number, of numerous actual observations.

TABLE 14 Corrections to Be Added to Rockwell Superficial 15T, 30T, and 45T Values Obtained on Convex Cylindrical Surfaces[A] of Various Diameters

Hardness Reading	Diameters of Convex Cylindrical Surfaces						
	1/8 in. (3.2 mm)	1/4 in. (6.4 mm)	3/8 in. (10 mm)	1/2 in. (13 mm)	5/8 in. (16 mm)	3/4 in. (19 mm)	1 in. (25 mm)
	Corrections to be Added to Rockwell Superficial 15T, 30T, and 45T Values[B]						
20	13.0	9.0	6.0	4.5	4.5	3.0	2.0
30	11.5	7.5	5.0	3.5	3.5	2.5	2.0
40	10.0	6.5	4.5	3.5	3.0	2.5	2.0
50	8.5	5.5	4.0	3.0	2.5	2.0	1.5
60	6.5	4.5	3.0	2.5	2.0	1.5	1.5
70	5.0	3.5	2.5	2.0	1.5	1.0	1.0
80	3.0	2.0	1.5	1.5	1.0	1.0	0.5
90	1.5	1.0	1.0	0.5	0.5	0.5	0.5

[A] When testing cylindrical specimens, the accuracy of the test will be seriously affected by alignment of elevating screw, V-anvil, indenters, surface finish, and the straightness of the cylinder.

[B] These corrections are approximate only and represent the averages, to the nearest 0.5 Rockwell superficial number, of numerous actual observations.

corresponding to the lowest and highest hardnesses for which the scales are normally used by making known incremental movements of the indenter.

13.1.3.2 The instrument used to verify the depth measuring device shall have an accuracy of 0.0002 mm.

13.1.3.3 The depth-measuring device shall correctly indicate within ±0.5 of Rockwell unit, over each interval. This corresponds to ±0.001 mm for regular Rockwell ranges and ±0.0005 mm on Rockwell superficial ranges.

13.2 *Indirect Verification*—Indirect verification may be carried out by means of standardized blocks calibrated in accordance with Part C.

13.2.1 *Procedure*:

13.2.1.1 For the indirect verification of a testing machine, the following procedures shall be applied: The testing machine shall be verified for each scale to be used. For each scale standardized, at least three blocks within the hardness ranges given in Table 16 shall be tested. The machine shall not be adjusted between tests made on the three blocks.

13.2.1.2 In accordance with Part A of this Method, make at least five indentations on each standardized block, distributed uniformly over the block's surface to record the hardness values to within 0.2 of a Rockwell unit. Before making these indentations, at least two indentations shall be made to ensure that the machine is workly freely and that the standardized block, the indenter, and the anvil are seating correctly. The results of these preliminary indentations shall be ignored.

13.2.1.3 For each standardized test block, let R_1, R_2 ... R_5 be the hardness readings of the 5 indentations arranged in increasing order of magnitude.

13.2.2 *Repeatability*:

13.2.2.1 The repeatability of the testing machine under the particular verification conditions is determined by the following quantity:

$$R_5 - R_1$$

13.2.2.2 The repeatability of the testing machine verified is considered satisfactory if it satisfies the conditions given in Table 20.

13.2.3 *Error*:

13.2.3.1 The error of the testing machine under the particular verification conditions is expressed by the following quantity:

TABLE 15 Tolerances on Applied Forces

Load, kgf (N)	Tolerance, kgf (N)
10 (98)	±0.20 (±1.96)
60 (589)	±0.45 (±4.41)
100 (981)	±0.65 (±4.57)
150 (147)	±0.90 (±8.83)
3 (29)	±0.060 (±0.589)
15 (147)	±0.100 (±0.981)
30 (294)	±0.200 (±1.961)
45 (441)	±0.300 (±2.943)

TABLE 16 Hardness Ranges Used in Verification by Standardized Test Block Method

Rockwell Scale	Hardness Ranges
C	20 to 30 35 to 55 59 to 65
B	40 to 59 60 to 79 80 to 100
30N	40 to 50 55 to 73 75 to 80
30T	43 to 56 57 to 70 incl over 70 to 82

TABLE 17 Allowable Deviation in Hardness Readings for Verified Diamond Indenters

For Hardness Readings in Range of:	Allowable Deviation, Rockwell Units
C 63	±0.5
C 25	±1.0
30N 80	±0.5
30N 45	±1.0

TABLE 18 Tolerances for Rockwell Hardness Ball Indenters

Diameter of Ball		Tolerance[A]	
in.	mm	in.	mm
1/16	1.588	±0.0001	±0.0025
1/8	3.175	±0.0001	±0.0025
1/4	6.350	±0.0001	±0.0025
1/2	12.700	±0.0001	±0.0025

[A] For balls in the range of diameters specified, these tolerances and the permissible variation in the diameter of any one ball, as specified in 19.1.3, are met by Grade 25 steel balls of the Anti-Friction Bearing Manufacturers' Association (AFBMA).

TABLE 19 Maximum Mean Diagonal of Vickers Hardness Indentation on Rockwell Hardness Balls

Ball Diameters		Maximum Mean Diagonal of Indentation on the Ball Made with Vickers Indenter Under 10-kgf (98-N) Load, mm
in.	mm	
1/16	1.588	0.141
1/8	3.175	0.144
1/4	6.350	0.145
1/2	12.700	0.147

TABLE 20 Repeatability of Machines

Range of Standardized Hardness Test Blocks	The Repeatability[A] of the Machine Shall Be Not Greater Than:
Rockwell C Scale:	
25 to 30	2.0
35 to 55	1.5
59 to 65	1.0
Rockwell B Scale:	
40 to 59	2.5
60 to 79	2.0
80 to 100	2.0
Rockwell 30N Scale:	
40 to 50	2.0
55 to 73	1.5
75 to 80	1.0
Rockwell 30T Scale:	
43 to 56	2.5
57 to 70, incl	2.0
Over 70 to 82	2.0

[A] The repeatability of machines on Rockwell or Rockwell superficial hardness scales other than those given in Table 20 shall be the equivalent converted difference in hardness for those scales, except for the 15N and 15T scales. In the case of the 15N and 15T scales, the repeatability shall be no greater than 1.0 for all ranges.

Example—At C 60, typical readings of a series of indentations might range from 59 to 60, 59.5 to 60.5, 60 to 61, etc. Thus, converted A-scale values corresponding to C 59 to 60 (see Table II of Standard Tables E 140) would be A 80.7 to 81.2 and the repeatability for the A-scale would be 0.5.

TABLE 21 Tolerance Values for Standardized Test Blocks

Nominal Hardness of Standardized Test Block	Tolerance Values of the Test Block Shall Not Be Greater Than
C Scale[A]	
60 and Greater	±0.5
Below 60	±1.0
A Scale	
80 and Greater	±0.5
Below 80 to 60.5, incl	±1.0
15N Scale	
90 and Greater	±0.7
Below 90 to 69.4, incl	±1.0
30N Scale	
77.5 and Greater	±0.7
Below 77.5 to 41.5, incl	±1.0
45N Scale	
66.5 and Greater	±0.7
Below 66.5 to 19.6, incl	±1.0
B Scale[B]	
45 and Greater	±1.0
Below 45 to 1.5, incl	±1.5
F Scale	
99.6 to 57.0, incl	±1.0
15T Scale	
75.3 and Greater	±1.0
Below 75.3 to 60.5, incl	±1.5
30T Scale	
46.2 and Greater	±1.0
Below 46.2 to 15.0, incl	±1.5
45T Scale	
17.6 and Greater	±1.0
Below 17.6 to 1.0, incl	±1.5

[A] All other scales on steel blocks of the equivalent converted values are as follows: 70.0 HRC to 60.0 HRC = ±0.5 and 59.9 HRC to 20.0 HRC = ±1.0.

[B] All other scales on brass blocks of the equivalent converted values are as follows: 100.0 HRB to 1.0 HRB = ±1.0.

$$\bar{R} - R$$

where:

$\bar{R} = \frac{R_1 + R_2 + \ldots R_5}{5}$, and

R = stated hardness of the standardized test block used.

13.2.3.2 The mean hardness value for the five tests shall not differ from the mean corresponding to the hardness of the standardized test block by more than the tolerance of the latter (shown in Table 21).

13.3 It should be understood that hardness test blocks, diamond indentors, and machine designs vary between manufacturers and that if all parameters are met under 13.1, it is possible that change of one or more of the parameters may be needed to meet indirect verification on test blocks. Consult manufacturer's instructions on the proper method to make corrections *within the tolerances specified in this method.*

13.4 *Time Interval Between Verifications*—It is recommended that testing machines be verified annually or more frequently if required. In no case shall the time interval between verifications exceed 18 months.

13.5 *Verification Report*:

13.5.1 The verification report shall include the following information:

13.5.1.1 Reference to this ASTM Test Method,

13.5.1.2 Method of verification (direct or indirect),

13.5.1.3 Identification data of the hardness testing machine,

13.5.1.4 Means of verification (test blocks, elastic proving devices, etc.)

13.5.1.5 The Rockwell hardness scale(s) verified,

13.5.1.6 The result obtained,

13.5.1.7 Date of verification and reference to the verifying agency, and

13.5.1.8 Signature of verifying agency representative.

14. Procedure for Periodic Checks by the User

14.1 Verification by the standardized test block method (13.2) is too lengthy for daily use. Instead, the following is recommended:

14.1.1 Make at least one routine check each day that the testing machine is used.

14.1.2 Before making the check, make at least two preliminary indentations to ensure that the hardness testing machine is working freely and that the test block, indenter, and anvil are seated correctly. The results of these preliminary indentations should be ignored.

14.1.3 Make at least three hardness readings on a standardized hardness test block on the scale and at the hardness level at which the machine is being used. If the mean of these values falls within the tolerances marked on the standardized hardness test block, the machine may be regarded as satisfactory. If not, the machine should be verified as described in 13.2.

C. CALIBRATION OF STANDARDIZED TEST BLOCKS FOR MACHINES USED FOR ROCKWELL AND ROCKWELL SUPERFICIAL HARDNESS TESTING

15. Scope

15.1 Part C specifies a method for the calibration of standardized blocks to be used in Rockwell hardness testing machines for the indirect verification of these machines as described in Part B.

16. Manufacture

16.1 The attention of the manufacturer of the block is drawn to the need to use a manufacturing process which will give the necessary homogeneity, stability of structure, and uniformity of surface hardness.

16.2 Each metal block to be standardized shall be of a thickness not less than ¼ in. (6.4 mm).

16.3 The area of the test surface of the block shall not be more than 4 in.^{2} (2581 mm^2).

16.4 The standardized block shall be free of magnetism. It is recommended that the manufacturer ensure that the blocks, if of steel, have been demagnetized at the end of the manufacturing process.

16.5 The maximum deviation in flatness of the surfaces shall not exceed 0.0002 in. (0.005 mm).

16.6 The maximum error in parallelism shall not exceed 0.0002 in. per in. (mm per mm).

16.7 The test surface shall be free from scratches which interfere with the measurement of the indentation. The mean surface roughness (R_a) shall not exceed 12 µin. (0.0003 mm) center line average.

16.8 The bottom surface shall have a fine ground finish.

16.9 To assure that material is not removed from the test surface, its thickness at the time of standardization (to the nearest ±0.005 in. (0.1 mm)) shall be marked on the block or an identifying mark shall be made on the test surface. Resurfacing of a test block for reuse is not recommended; however, if a standard test block is reconditioned, the new test surface must be recalibrated in accordance with this section.

17. Standardizing Machine

17.1 In addition to fulfilling the general requirements specified in Sections 12 and 13, the standardizing machine shall also meet the following requirements:

17.1.1 The machine shall be verified directly. Direct verification involves the following:

17.1.1.1 Verification of the test force (see 13.1.1),

17.1.1.2 Verification of the indenter (see 13.1.2), and

17.1.1.3 Verification of the measuring device (see 13.1.3).

17.1.2 Each preliminary test force shall be correct to within ±0.5 %. Each total test force shall be correct to within ±0.25 %.

17.1.3 The verification of the shape of the indenter can be made by direct measurement or by measurement of its projection on a screen. The verification shall be made at not less than eight approximately equally spaced sections.

17.1.4 The diamond indenter shall have an included angle of 120° ±0.1°.

17.1.5 The angle between the axis of the diamond indenter and the axis of the indenter holder (normal to the seating surface) shall not exceed 0.3°.

17.1.6 The tip of the diamond indenter shall be spherical with a mean radius of 0.200 ±0.005 mm. In each measured section the radius shall not exceed 0.200 ±0.007 mm and local deviations from a true radius shall not exceed 0.002 mm. The surface of the cone and spherical tip shall blend in a truly tangential manner.

17.1.7 The diameter of the steel ball shall be within the tolerance of 0.001 mm.

17.1.8 The measuring device shall be capable of accurately measuring vertical displacements corresponding to ±0.1 of a regular Rockwell unit and ±0.1 for a superficial Rockwell unit.

18. Standardizing Procedure

18.1 The standardized test blocks shall be calibrated in a standardizing machine as described in Section 17 at a temperature of 73°F ± 5°F (23°C ± 2°C) using the general test procedure described in Part A.

19. Number of Indentations

19.1 In accordance with Part A of this Method, make at least five indentations on each standardized block, distributed uniformly over the block's surface.

20. Uniformity of Hardness

20.1 Let R_1, R_2 ... R_5 be the measured values in Rockwell units arranged in increasing order of magnitude.

20.2 The nonuniformity of the block under the particular conditions of standardization is characterized by $R_5 - R_1$.

20.3 The nonuniformity of the block must satisfy the conditions of Table 22.

21. Marking and Certification Requirements

21.1 Each standardized test block shall be marked with the following:

21.1.1 Arithmetic mean of the hardness values found in the standardizing test reported to the nearest tenth, for example: 66.3 HRC,

21.1.2 Tolerance value (see Table 21),

21.1.3 Name or mark of the supplier,

21.1.4 Unique serial number,

21.1.5 Name or mark of the calibrating agency if different from supplier,

TABLE 22 Maximum Nonuniformity of Standardized Test Blocks

Nominal Hardness of Standardized Test Block	Nonuniformity of the Test Block Shall Not Be Greater Than
C Scale[A]	
60 and Greater	0.5
Below 60	1.0
A Scale	
80 and Greater	0.5
Below 80 to 60.5, incl	1.0
15N Scale	
90 and Greater	0.7
Below 90 to 69.4, incl	1.0
30N Scale	
77.5 and Greater	0.7
Below 77.5 to 41.5, incl	1.0
45N Scale	
66.5 and Greater	0.7
Below 66.5 to 19.6, incl	1.0
B Scale[B]	
45 and Greater	1.0
Below 45 to 1.5, incl	1.5
F Scale	
99.6 to 57.0, incl	1.0
15T Scale	
75.3 and Greater	1.0
Below 75.3 to 60.5, incl	1.5
30T Scale	
46.2 and Greater	1.0
Below 46.2 to 15.0, incl	1.5
45T Scale	
17.6 and Greater	1.0
Below 17.6 to 1.0, incl	1.5

[A] All other scales on steel blocks of the equivalent converted values are as follows: 70.0 HRC to 60.0 HRC = 0.5 and 59.9 HRC to 20.0 HRC = 1.0.

[B] All other scales on brass blocks of the equivalent converted values are as follows: 100.0 HRB to 1.0 HRB = 1.0.

21.1.6 Thickness of the block or an identifying mark on the test surface, and

21.1.7 Year of calibration.

21.2 Any mark put on the side of the block shall be upright when the test surface is the upper face.

21.3 Each block shall be supplied with a certificate showing the results of the individual standardizing tests and the arithmetic mean of those tests, including the following:

21.3.1 Date of standardization,

21.3.2 Serial number of block, and

21.3.3 Name of manufacturer or mark of supplier.

22. Keywords

22.1 Rockwell Hardness; metallic

APPENDIX

(Nonmandatory Information)

X1. LIST OF ASTM SPECIFICATIONS GIVING HARDNESS VALUES CORRESPONDING TO TENSILE STRENGTH

X1.1 The following ASTM standards give approximate Rockwell hardness or Rockwell superficial hardness values corresponding to the tensile strength values specified for the materials covered: Test Methods and Definitions A 370 and Specifications B 19, B 36, B 96, B 97, B 103, B 121, B 122, B 130, B 134, B 152, B 291, and B 370.